

AFRL-ML-TY-TR-2000-4568



**The Effect of Heating During In Situ Remediation on the Dynamics and
Activity of Soil Microorganisms**

Schimmel, Keith A.

**North Carolina Agricultural and Technical State University
Division of Research
1601 East Market Street
Greensboro, NC 27411**

Approved for Public Release; Distribution Unlimited

**AIR FORCE RESEARCH LABORATORY
MATERIALS & MANUFACTURING DIRECTORATE
AIR EXPEDITIONARY FORCES TECHNOLOGIES DIVISION
139 BARNES DRIVE, STE 2
TYNDALL AFB FL 32403-5323**

NOTICES

USING GOVERNMENT DRAWINGS, SPECIFICATIONS, OR OTHER DATA INCLUDED IN THIS DOCUMENT FOR ANY PURPOSE OTHER THAN GOVERNMENT PROCUREMENT DOES NOT IN ANY WAY OBLIGATE THE US GOVERNMENT. THE FACT THAT THE GOVERNMENT FORMULATED OR SUPPLIED THE DRAWINGS, SPECIFICATIONS, OR OTHER DATA DOES NOT LICENSE THE HOLDER OR ANY OTHER PERSON OR CORPORATION; OR CONVEY ANY RIGHTS OR PERMISSION TO MANUFACTURE, USE, OR SELL ANY PATENTED INVENTION THAT MAY RELATE TO THEM.

THIS REPORT IS RELEASABLE TO THE NATIONAL TECHNICAL INFORMATION SERVICE
5285 PORT ROYAL RD.

SPRINGFIELD VA 22 161

TELEPHONE 703 487 4650; 703 4874639 (TDD for the hearing-impaired)

E-MAIL orders@ntis.fedworld.gov

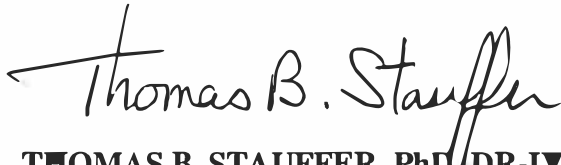
WWW <http://www.ntis.gov/index.html>

AT NTIS, IT WILL BE AVAILABLE TO THE GENERAL PUBLIC, INCLUDING FOREIGN NATIONS.

THIS TECHNICAL REPORT HAS BEEN REVIEWED AND IS APPROVED FOR PUBLICATION.



Larry N. Cook Jr., 1st Lt., USAF
Program Manager



THOMAS B. STAUFFER, PhD, DR-IV, DAF
Chief, Weapons Systems Logistics Branch



RANDY L. GROSS, Col, USAF, BSC
Chief, Air Expeditionary Forces Technologies Division

Do not return copies of this report unless contractual obligations or notice on a specific document requires its return.

REPORT DOCUMENTATION PAGE

Form Approved
OMB No. 0704-0188

Public reporting burden for this collection of information is estimated to average 1 hour per response, including the time for reviewing instructions, searching existing data sources, gathering and maintaining the data needed, and completing and reviewing the collection of information. Send comments regarding this burden estimate or any other aspect of this collection of information, including suggestions for reducing this burden, to Washington Headquarters Services, Directorate for Information Operations and Reports, 1215 Jefferson Davis Highway, Suite 1204, Arlington, VA 22202-4302, and to the Office of Management and Budget, Paperwork Reduction Project (0704-0188), Washington, DC 20503.

1. AGENCY USE ONLY (Leave blank)		2. REPORT DATE October 2000	3. REPORT TYPE AND DATES COVERED Final Report 15 May 98 – 14 May 99	
4. TITLE AND SUBTITLE The Effect of Heating During In Situ Remediation on the Dynamics and Activity of Soil Microorganisms			5. FUNDING NUMBERS F41624-98-1-0003 1900B 58B	
6. AUTHORS Keith A. Schimmel, Ph.D.				
7. PERFORMING ORGANIZATION NAME(S) AND ADDRESS(ES) North Carolina Agricultural and Technical State University Division of Research 1601 East Market Street Greensboro, NC 27411			8. PERFORMING ORGANIZATION REPORT NUMBER	
8. SPONSORING/MONITORING AGENCY NAME(S) AND ADDRESS(ES) U.S. AF, AF Material Command AFRL R&D Contracting Division/HSC/PKRC AEF Technologies Division 7909 Lindbergh Drive 139 Barnes Drive, Suite 2 Brooks AFB, TX 78235-5353 Tyndall AFB, FL 32403-5323			10. SPONSORING/MONITORING AGENCY REPORT NUMBER AFRL-ML-TY-TR-2000-4568	
11. SUPPLEMENTARY NOTES Project Officer: Larry N. Cook Jr., 1st Lt, USAF AFRL/MLQL, Tyndall AFB FL				
12a. DISTRIBUTION/AVAILABILITY STATEMENT Approved for Public Release, Distribution Unlimited			12b. DISTRIBUTION CODE "A"	
13. ABSTRACT (Maximum 200 words) The primary objective of this study was to advance knowledge regarding the microbial ecology associated with in situ resistive heating remediation technologies. After being unable to identify a cooperating remediation site using resistive heating, the study focussed on understanding the microbial ecology at the lab-scale. Experiments were performed in three insulated boxes (0.5 m x 0.5 m x 0.1 m) containing medium sand soil heated to just below 100°C. After heating for 20 hours, cooling to room temperature, and remaining at room temperature for one week, three different amendments were tested: organic media, inorganic media, and sterile water. Acridine Orange Direct Counts (AODC) and Phospholipid Fatty Acid Analysis (PLFA) one week after the nutrient addition indicated that the microbial numbers for the organic treatment were highest, but only half the initial count. The primary features of the community structure changes from the initial soil were small increases in gram positive bacteria and small decreases in eukaryotes. Heating and cooling 2-dimensional temperature profiles measured during the experiments were compared to profiles generated from mathematical models. This study provides helpful groundwork for future resistive heating microbial ecology studies at the field scale.				
14. SUBJECT TERMS resistive heating, microbial ecology, microorganisms, lab-scale, heat transfer, modeling			15. NUMBER OF PAGES 129	
			16. PRICE CODE	
17. SECURITY CLASSIFICATION OF REPORT Unclassified	18. SECURITY CLASSIFICATION OF THIS PAGE Unclassified	19. SECURITY CLASSIFICATION OF ABSTRACT Unclassified	20. LIMITATION OF ABSTRACT UL	

NOTICES

This report was prepared as an account of work sponsored by an agency of the United States Government. Neither the United States Government nor any agency thereof, nor any employees, nor any of their contractors, or their employees, make any warranty, expressed or implied, or assume any legal liability or responsibility for the accuracy, completeness, or usefulness of any privately owned rights. Reference herein to any specific commercial products, process, or service by trade name, trademark, manufacturer, or otherwise, does not necessarily constitute or imply its endorsement, recommendation, or favoring by the United States Government or any agency, contractor, or subcontractor thereof.

When Government drawings, specifications, or other data are used for any purpose other than in connection with a definitely Government-related procurement, the United States Government incurs no responsibility or any obligation whatsoever. The fact that the Government may have formulated or in any way supplied the said drawings, specifications, or other data, is not to be regarded by implication, or otherwise in any manner construed, as licensing the holder or any other person or corporation, or as conveying any rights or permission to manufacture, use, or sell patented invention that may in any way be related thereto.

This technical report has been reviewed by the Public Affairs Office (PA) and is released to the National Technical Information Service, where it will be available to the general public, including foreign nationals.

This report has been reviewed and is approved for publication.

PREFACE

This report summarizes research activities conducted by North Carolina A&T State University (NCA&TSU) for the AFRL/MLQE, Air Force Material Command, USAF, under grant no. F41624-98-1-0003, "The Effect of Heating During In Situ Remediation on the Dynamics and Activity of Soil Microorganisms," during the performance period May 14, 1998 through May 13, 1999. The use of facilities of the Air Force FAST Center for Environmental Remediation, Fate and Transport of Hazardous Wastes at NCA&TSU is acknowledged. Support of the Dover national test site, a national environmental technology test site program funded by the Strategic Environmental Research and Development Program (SERDP) is acknowledged.

The work summarized in this report has been conducted by Keith A. Schimmel (Associate Professor, Chemical Engineering), Lisa Carmichael (Post-doctoral Research Associate Civil/Chemical Engineering), Vinod Jayaraman Narayanan (M.S. Graduate Student, Thesis Defended July, 1999, Chemical Engineering), Rhea Powell-Jones (M.S. Graduate Student, Thesis Defended October, 1999, Civil Engineering), Devang Panchigar (Graduate Research Assistant, Chemical Engineering), Shakahn Gamble (Undergraduate Research Assistant, B.S.C.E., 1999), Tangela McDuffie (Undergraduate Research Assistant B.S.C.E., 1999), Tomeka Terry (Undergraduate Research Assistant B.S.C.E., 1999), and Lt. Larry N. Cook, Jr. of AFRL Airbase and Environmental Technology Division was the Project Manager.

The address of the organization performing this work, and the technical contact is:

North Carolina A&T State University
Department of Chemical Engineering
Greensboro, NC 27411
Contact: Keith A. Schimmel
Telephone: (336) 334-7564
Telefax: (336) 334-7904
E-mail: schimmel@ncat.edu

(The reverse of this page is blank)

EXECUTIVE SUMMARY

OBJECTIVES

The goal of this project was to increase the understanding of microbial ecology during and after the application of resistive heating remediation technologies. The specific objectives of the project were:

1. develop analytical methods to count soil microorganisms during lab-scale resistive heating experiments;
2. design and construct three lab-scale resistive heating soil boxes that allow soil samples and temperature measurements to be made throughout the boxes;
3. determine the short term repopulation rates of the soil boxes after resistive heating when only sterile nutrients are added to the boxes;
4. use Phospholipid Fatty Acid Analysis (PLFA) to determine changes in the community structure in the boxes;
5. use the computational fluid dynamics software package FLUENT[®] to construct a 2-dimensional, single phase mathematical model of the temperature distribution in the soil boxes both during the heating phase and cooling phase;
6. determine the sensitivity of the FLUENT[®] model to physical properties;
7. determine multiphase effects on the FLUENT[®] model;
8. determine physical property values that provide good agreement between predicted temperature profiles and experimental temperature profiles;
9. use the results of the lab-scale experiments and mathematical modeling to provide some guidelines for designing field-scale microbial ecology studies during resistive heating treatments;
10. compare lab-scale microbial population changes measured with PLFA to field-scale changes.

A. BACKGROUND

Resistive heating of soils is a heating method in which electrodes are placed in a contaminated site and may increase the subsurface temperature to over 100° C. Under this high temperature, the target contaminants are solubilized and oxidized. It has been successfully used for the in situ remediation of contaminated sub-surface sites that have a large fraction of dense non-aqueous phase liquids (DNAPLs) and low permeability soils. The high temperatures, however, may have an adverse effect on the stability of microbial populations in the subsurface.

It is currently not clear what the short term and long term effects of resistive heating technologies are on the soil microbe population characteristics of a treated site. Lacking this information, one is unable to make predictions as to the timetable for remediation of residual contaminants via natural attenuation after resistive heating. Improved mathematical models of temperature profiles both during the heating and cooling phases of resistive heating would allow remediation to be carried out at temperatures no higher than what are needed for the desired remediation. This will help to minimize the effect of resistive heating treatments on soil microbial ecology.

B. SCOPE

This report encompasses work conducted by North Carolina A&T State University during the period May 14, 1998 through May 13, 1999. Lab-scale objectives were accomplished. Comparison of lab-scale to field-scale microbial characterizations was not accomplished as after much effort, a suitable field demonstration partner could not be found for the project timeframe.

C. METHODOLOGY

To study the microbial ecology associated with resistive heating, lab-scale pan studies were first carried out using Dover AFB National Test Site soil. Experiments were then performed in insulated Lexan® boxes (0.5 m H x 0.5 m W X 0.1 m H) containing soil from the Piedmont region of North Carolina (Medium sand). Nine soil sampling ports were located uniformly throughout each box. Microbial activity in soils before and after heating was obtained by means of most probable number counts (MPN), plate

counts (CFU), Acridine Orange Direct Counts (AODC), and Phospholipid Fatty Acid Analysis (PLFA). The PLFA analysis was performed by The Center for Environmental Biotechnology at the University of Tennessee.

The heating and cooling temperature profiles generated during the box experiments were determined by continuously recording the temperature at eleven points in each box. These temperature profiles were compared to those generated from mathematical heat transfer models using the computational fluid dynamics (CFD) software package FLUENT®. Single-phase and multiphase models were set up in a 2-dimensional grid with porous media properties and appropriate boundary conditions. The multiphase model was used to study the evaporation-condensation of water at elevated temperatures. Sensitivity of the single-phase model to different values of soil and fluid properties was analyzed for adiabatic and non-adiabatic cases.

D. TEST DESCRIPTION

A lab-scale box experiment was begun by simultaneously heating soil collected and processed at the same time in each of three boxes. Each box was heated to a temperature just below 100°C over a period of about ten hours. The temperature was maintained at 100°C for about 4 hours. The power source to the heater was then turned off. The boxes cooled back down to room temperature after about 20 hours. After the boxes remained at room temperature for a week, a different nutrient media addition was made to each of the three boxes - organic media, inorganic media, and sterile water (baseline). Microbial characterization was performed on initial soil samples, samples during heating, samples during cooling, samples one week after cooling, and samples one week after nutrient addition.

E. RESULTS

Resistive heating at temperatures between 60°C and 100 °C affects the microbial community by causing a decrease in population or microbial activity. This was exhibited in both the oven heating experiments and the resistive heating experiments. Microbial counts as high as 9,152 microorganisms/g (AODC) pre-heating were reduced to no detectable counts after the heating event.

Three lab-scale resistive heating soil boxes were successfully constructed that allowed soil samples and temperature measurements to be made throughout the boxes. These boxes allowed the determination of the short-term repopulation rates of the soil boxes after resistive heating when only sterile nutrients were added to the boxes. Three runs were made with each box. PFLA analysis was done on just one of these runs. AODC analysis was performed on two of the runs. Temperature measurements were obtained for all three runs. When ambient temperatures returned to normal after a heating event, and given some time, small-scale population recovery occurred. After a period of one week, population recovery began, but counts did not reach those of the pre-heating samples. Amending heated soils with nutrients aided in microbial population recovery with the organic amendment resulting in a microbial count after one week that was about half of the initial count. The nutrients that were added affected the community structure of the soil. The primary features of the community structure changes from the initial soil were small increases in gram positive bacteria and small decreases in eukaryotes.

The computational fluid dynamics software package FLUENT[®] was used to construct a 2-dimensional, single-phase mathematical model of the temperature distribution in the soil boxes both during the heating phase and cooling phase. A technique was developed that allowed within FLUENT[®] the final results of the heating calculation to be used as the starting point for the cooling calculation. Successful runs were made to determine the sensitivity of the FLUENT[®] model to physical properties. The temperature profile modeling results indicated that by using typical soil properties and values of the convective heat transfer coefficient, good agreement could be reached between the experimental and theoretical temperature profiles. Better agreement between the experimental and theoretical temperature profiles is obtained by allowing the density to vary with temperature. Preliminary work was accomplished in determining multiphase effects on the FLUENT[®] model. Methods were developed to compare the temperature profiles of the model and experiments by comparing averages of the temperatures.

F. CONCLUSIONS

The results of the lab-scale experiments and mathematical modeling provide helpful background for attempting field-scale microbial ecology studies during resistive heating treatments. The combined results of the experimental and theoretical work indicate that the key to minimizing the impact of resistive heating on microbial ecology is to keep the temperature as low as possible while still achieving the desired contaminant removal. An essential element to this strategy is to have a mathematical model that accurately predicts the effect of soil water content on mass and energy transport.

RECOMMENDATIONS

Based on the experiments and modeling studies conducted, it is recommended that this work be continued both at the lab scale and field scale. At the lab scale, additional replicate box experiments should be performed in which more soil samples are analyzed for moisture content and longer times are monitored for repopulation characteristics. Somewhat higher temperatures ($>100^{\circ}\text{C}$) and longer heating periods should also be studied. Additional lab-scale multiphase modeling work needs to be done. At the field scale, the mathematical model should be extended to include three dimensions and soil samples should be collected and analyzed using PLFA and AODC or CFU.

TABLE OF CONTENTS

LIST OF FIGURES.....	xiv
LIST OF TABLES.....	xviii
LIST OF SYMBOLS.....	xix
CHAPTER 1. INTRODUCTION.....	1
CHAPTER 2. BACKGROUND.....	4
2.1 Soil Remediation Techniques.....	4
2.1.1 Soil Vapor Extraction.....	4
2.1.2 Air Sparging.....	5
2.1.3 Bioventing.....	6
2.2 Biodegradation.....	7
2.3 Soil Heating Technologies.....	8
2.3.1 Radio-Frequency Thermal Decontamination.....	10
2.3.2 Resistive-Heating.....	10
2.3.3 Six Phase Soil Heating.....	11
2.4 Microbial Response to Heat.....	12
2.5 Microbial Modeling.....	20
2.6 Multiphase Flow and Heat Transfer in Porous Media.....	21
2.6.1 Models Ignoring Moisture Movement in Porous Media.....	24
2.6.2 Models for Thermal Driven Heat and Moisture Transport in Soils.....	24
2.7 Objectives of this Study.....	28
CHAPTER 3. THEORY.....	29

3.1 Problem Solving Steps in FLUENT.....	29
3.2 Overview of Geometry and Grid Definition Options.....	30
3.3 The Equation set for Single-Phase Model.....	32
3.3.1 The Mass Conservation Equation.....	33
3.3.2 Momentum Conservation Equation.....	33
3.3.3 Energy Conservation Equation.....	34
3.3.4 Summary of the Single-Phase Equations Solved.....	36
3.4 Fluid Properties and Equation of State.....	36
3.4.1 Equation of State for Density.....	37
3.4.2 Viscosity.....	37
3.4.3 Thermal Conductivity and Specific Heat.....	38
3.5 Heat Transfer.....	38
3.5.1 Defining Thermal Boundary Conditions at Walls.....	39
3.5.2 Heat Transfer Calculations at Wall Boundaries.....	39
3.6 The Eulerian Multiphase Model.....	40
3.6.1 Volume Fractions.....	42
3.6.2 Conservation Equations.....	43
3.6.3 Summary of Multiphase Equations Solved.....	46
3.6.4 Description of Mass Transfer in the Multiphase.....	46
CHAPTER 4. MATERIALS AND METHODS.....	48
4.1 Overview of the Experimental Setup.....	48

4.2 Methods.....	52
4.2.1 Temperature Monitoring.....	52
4.2.2 Calibration of the Temperature Curve.....	52
4.2.3 Soil Sampling and Analysis.....	53
4.2.4 Nutrient Addition.....	56
4.2.5 Oven Heating Experiments.....	56
4.3 Materials.....	57
4.3.1 Scanning Thermometer and Thermocouples.....	57
4.3.2 Configuration of Power Supply and Electrodes.....	58
4.3.3 Soil Characteristics.....	58
CHAPTER 5. RESULTS AND DISCUSSION.....	60
5.1 Oven Experiments for Dover Soil.....	60
5.2 Box Experimental	
Studies.....	62
5.3 Temperature-Time Curve Analysis.....	65
5.4 PLFA Results.....	74
5.5 Comparison of PLFA and AODC Results.....	77
5.6 Theoretical Results.....	77
5.6.1 Grid and Time Step Sensitivity Analysis.....	79
5.6.2 Effect of Varying Heat Source Location in the Grid.....	83
5.6.3 Physical Parameter Sensitivity.....	86
5.6.4 Defining Density as a Function of Temperature.....	95

5.7 Comparison of Experimental and Theoretical Results.....	97
5.8 Multiphase Simulations.....	100
CHAPTER 6. CONCLUSIONS.....	113
CHAPTER 7. RECOMMENDATIONS.....	115
REFERENCES.....	117
APPENDIX: PLOTS OF PLFA ANALYSIS	122

LIST OF FIGURES

Figure	Page
3.1 Computational Grid Used in FLUENT.....	30
5.1 Lab Scale Lexan Box to Study Resistive Heating	49
4.2 (a) Arrangement of the Temperature Ports in the Experimental Setup.....	50
4.2 (b) Geometry of the Soil Sampling Ports Used in the Experimental Setup.....	50
5.1 (a) A Typical Resistive Heating Curve Indicating the Heating, Stationary and Cooling Phases.....	63
5.1 (b) Temperature Curve for Thermocouples 4 and 10.....	63
5.2 Temperature and Count Results for Organic Nutrient Treatment (Box 1)	66
5.3 Temperature and Count Results for Inorganic Nutrient Treatment (Box 2)	67
5.1 Temperature and Count Results for Water Nutrient Treatment (Box 3).....	68
5.5 Temperature and Count Results for Boxes 1, 2, 3 (Run 1).....	72
5.6 Temperature and Count Results for Boxes 1, 2, 3 (Run 2).....	73
5.1 Biomass PLFA After Resistive Heating and Nutrient Addition in Boxes 1, 2, 3 (Run 1).....	75
5.2 Community Structure of Microorganisms in Soil After Resistive Heating and Nutrient Addition.....	76
5.3 Grid Sensitivity in Fluent.....	80
5.4 Temperature Curve at Point 14 x 14 for Adiabatic Conditions and Low Values of Soil Properties.....	81
5.5 Time Step Sensitivity on a 30 x 30 Grid.....	82

5.12	Effect of Electrode Position on T_{\max} and T_{\min} During Heating (15 hours) and Cooling (19 hours) Under Adiabatic Conditions.....	84
5.1	Effect of Electrode Position on T_{\max} and T_{\min} During Heating (15 hours) and Cooling (19 hours) Under Non-Adiabatic Conditions.....	85
5.2	Effect of Varying Heat Transfer Coefficient at the Wall on the Temperature Distribution in Porous Medium at Grid Point 14 x 14.....	86
5.3	Temperature-Time Distribution for the Non-Adiabatic Case and Midpoint Values of Soil Properties.....	87
5.4	Temperature Contour in Grid After Heating regime Under Non-Adiabatic Conditions with Midpoint Values of Soil Properties and $h = 5 \text{ W/m}^2\text{-}^\circ\text{C}$	89
5.5	Temperature Contour in Grid After Cooling phase at 20.42 hours (top) and 38.88 hours (bottom) Under Non-Adiabatic Conditions with Midpoint Values of Soil Properties and $h = 5 \text{ W/m}^2\text{-}^\circ\text{C}$	90
5.6	Temperature -Time Distribution for Non-Adiabatic Case and Mid-Point Values of Soil Properties.....	91
5.7	Temperature -Time Distribution for Non-Adiabatic Case and Maximum Values of Soil Properties.....	92
5.8	Temperature -Time Distribution for Non-Adiabatic Case and Minimum Values of Soil Properties.....	92
5.9	Temperature -Time Distribution for Adiabatic Conditions and Low Values of Soil Properties.....	93
5.10	Comparison of Temperature Profiles for Low, Midpoint and Maximum Values of Soil Properties.....	94
5.1	Comparison Between Constant Density and Temperature Dependent Density Simulation for Non-Adiabatic Case and Midpoint Values of Soil Properties at Grid point 14 x 14.....	96
5.2	Comparison Between Constant Density and Temperature Dependent Density Simulation for Adiabatic Case and Minimum Values of Soil Properties at Grid point 14 x 14.....	97
5.25	Comparison of Experimental and Theoretical Data for Run 1.....	98

5.26	Comparison of Experimental and Theoretical Data for Run 2.....	99
5.1	Effect of Increasing Volumetric Heat Generation on Experimental- Theoretical Temperature Comparison.....	100
5.28	Temperature Contour Developing During the Heating Phase for Adiabatic Multiphase Simulation.....	103
5.29	Temperature Contour After Completion of Heating Phase in Multiphase Simulation Under Adiabatic Conditions.....	104
5.1	Liquid Volume Fraction at the Start of the Heating Phase.....	105
5.2	Liquid Volume Fraction at the End of the Cooling Phase.....	106
5.3	Velocity Profile During Heating For Multiphase Simulation.....	107
5.4	Liquid Velocity Profile at the End of the Heating Regime in Multiphase Simulation.....	108
5.5	Liquid Velocity Magnitude at the End of the Cooling Phase for the Multiphase Simulation.....	109
5.1	Single-Phase Temperature Contour Generated with the Symmetry Condition...	111
5.36	Comparison of Multiphase (top) and Single-Phase (bottom) Temperature Profiles Around Saturation Temperature	112
A.1	Relative Proportion of Actinomycete Bacteria After Resistive Heating and Nutrient Addition.....	123
A.2	Relative Proportion of Eukaryotic Organisms After Resistive Heating and Nutrient Addition.....	124
A.3	Relative Proportion of Gram Positive Bacteria After Resistive Heating and Nutrient Addition.....	125
A.4	Relative Proportion of Gram Negative Bacteria After Resistive Heating and Nutrient Addition.....	126
A.5	Cy 17:0/ 16:1 w7c Turnover in Gram Negative Bacteria After Resistive Heating and Nutrient Addition.....	127

A.6	Cy 19:0/ 18:1 w7c Turnover in Gram Negative Bacteria After Resistive Heating and Nutrient Addition.....	128
-----	---	-----

LIST OF TABLES

Table	Page
2.1 Characteristics of Different Soil Heating Methods.....	8
5.1 Properties of the Characterized Soil.....	59
5.2 Summary of AODC Results for Boxes 1, 2, 3 for Runs 1 and 2.....	69
5.3 Comparison of Initial and Final Counts (Plate Counts, AODC, PLFA) for Run 1.....	77
5.4 Physical Property Set Used for FLUENT Simulations.....	79
5.5 Physical Property Data for Liquid Water Used for the Dispersed Phase.....	79
5.5 Grid Sensitivity Analysis in FLUENT.....	80
5.6 Time Step Sensitivity on a 30 x 30 grid.....	82
5.7 Physical Property Data for Multiphase Simulations.....	101

LIST OF SYMBOLS

c_p	Specific Heat at Constant Pressure
F	External Body Force
g	Acceleration due to Gravity
h	Static Enthalpy
h	Heat Exchange Coefficient
J	Flux of Species
k	Thermal Conductivity
k_{eff}	Effective Thermal Conductivity
K	Exchange Coefficient
m	Mass Transfer Rate
Nu	Nusselt Number
p	Static Pressure
Pr	Prandtl Number
q	Heat Flux
r	Time Relaxation Parameter
R	Interaction Force
S	Source Term
T	Temperature
u	Velocity
V	Volume Fraction

Greek Symbols

α	Phasic Volume Fraction
μ	Molecular Viscosity
ρ	Density
τ	Viscous Stress Tensor
ϕ	Porosity

Subscripts

f	Fluid
i,j	Direction Vectors
i',j'	Species Nomenclature
l	Liquid
m	Mass Source
p,q	Phase Nomenclature
Ref	Reference
Sat	Saturation
s	Solid
v	Vapor
W	Wall

CHAPTER 1

INTRODUCTION

One of the challenging problems in hazardous waste site remediation is the removal of Dense Non Aqueous Phase Liquids (DNAPL's) from below the water table. These materials, mostly chlorinated hydrocarbon solvents, typically have low solubilities in water (of the order of 1,000 mg/l or less), and their diffusion constants in water are quite small, as are all diffusion constants in condensed phases. These characteristics make in situ remediation techniques difficult to implement on a field scale. Schwille's (1988) experimental work with chlorinated hydrocarbons demonstrated that these compounds quickly move down towards the water table leaving a substantial trail of DNAPL droplets/ganglia trapped interstitially in the porous medium. Wide ranges of remediation technologies have been proposed to alleviate the pollution effects of DNAPL's. The key to a successful remediation program is to limit the progress of the pollutant to beneath the water table by restricting the transport of the pollutant and removing the majority of the pollutant in the porous soil medium.

Soil heating technologies are increasingly being used for the in situ remediation of contaminated subsurface sites with difficult contaminant profiles and site characteristics

(Smith and Hinchey, 1993). These technologies show abundant promise for contaminated soils that have large fractions of DNAPL's. Resistive heating is a soil heating technology in which electrodes are placed in the contaminated site and the voltage increases the subsurface temperature to above 100 °C. The high temperatures in the subsurface solubilize and oxidize the target contaminants (Bergsmann, 1993). Resistive heating of soils has the advantage of heating the soil internally. Thus, low permeability zones or complex heterogeneous soils can be treated. Resistive heating provides in situ source of steam to remove contaminants (Bergsmann and Trowbridge, 1997). Higher molecular weight compounds that are not very volatile are removed either by direct venting or bioremediation by cultured microorganisms. Removal of soil moisture as a result of heating increases the gas permeability of soils and can reduce the mass transfer limitations associated with low permeability soils. A summary of the different in situ soil heating remediation technologies is presented in Chapter 2.

This research focuses on implementing the resistive heating process under laboratory conditions and studying the effect of heating technologies on the dynamics and activity of subsurface microorganisms. Performing meaningful studies of the effect of heating technologies on the dynamics and activity of soil microorganisms at either lab-scale or pilot-scale requires knowledge about the spatial and temporal temperature profiles in the system along with the transport profiles of water and the contaminants. Therefore, both experimental techniques and mathematical models were used to characterize the relationships between spatial and temporal temperature profiles and microbial dynamics.

Lab-scale box experiments were undertaken in a 2-dimensional, insulated Lexan[®] Box (0.5 m H x 0.5 m W x 0.1 m D) fitted with numerous thermocouples and soil sampling ports and filled with soil that was heated up to 100 ° C with resistive heating. Microbial analysis on the soil samples was conducted with the help of plate counts, AODC counts and PLFA tests. The repopulation of microorganisms after resistive heating was studied by amending the soil with different nutrients. A full discussion of the experimental setup and the materials and methods used are discussed in Chapter 4 of this study.

A mathematical heat transfer model was developed using FLUENT. It was used to simulate heating and cooling patterns in porous media under different heating rates and boundary conditions. The problem setup and the governing equations for the model are discussed at length in Chapter 3. Literature on heat transfer in porous media was studied to gain an understanding of the different phenomena involved. Some of the interesting aspects have been recorded in Chapter 2. The results of the model help us to compare the experimental and theoretical temperature curves. These comparisons along with the microbial repopulation curves under different treatment conditions are discussed in Chapter 5. The conclusions of this research and the recommendations have been detailed in Chapter 6.

CHAPTER 2

BACKGROUND

There are a number of soil remediation techniques that are presently being used for the remediation of contaminated subsurface sites. In recent times there has been great interest in the in situ soil remediation technologies. The first few sections of this chapter focus on the pros and cons of the different in situ methods with special emphasis on the thermal driven in situ technologies. To understand the dynamics of the microbial population under the thermal stress, a detailed discussion on the microbial response to heat is presented. The final sections of this chapter focus on the need for mathematical modeling and the available heat and mass transfer models in soils.

2.1 Soil Remediation Techniques

2.1.1 Soil Vapor Extraction

The Soil Vapor Extraction (SVE) system operates on the principle that organic hydrocarbons contained in contaminated sites can volatilize at temperatures typically found in the soil. The range of applicability of soil vapor stripping is bounded by the following constraints:

1. The chemicals to be removed must be volatile or at least semi-volatile; it is not possible to remove DNAPL's, metals, most pesticides, oil and greases, and PCB's by vacuum extraction because their vapor pressures are too low.

2. The chemicals to be removed must have relatively low water solubility, or the soil moisture content must be quite low; generally it is not feasible to vapor strip chemicals such as acetone or alcohol because their vapor pressures in moist soils are too low. However, many of these compounds biodegrade readily if an adequate oxygen supply is available.
3. The soil must be sufficiently permeable to permit vapor extraction wells to draw air through all of the contaminated domains at a reasonable rate; a basic principle in soil vapor stripping is that the air must be able to move through the contaminated domain if an effective clean up is to occur (Wilson, 1995).

The design of optimal, cost effective SVE installations tends to be highly site specific, and often at complex sites the technique is deployed in concert with other technologies such as pump and treat, in situ air sparging and fixation/stabilization.

2.1.2 Air Sparging

Air Sparging (AS) operates on the principle that volatile organic compounds (VOCs) can typically volatilize at temperatures that exist in the sub surface. Unlike SVE, AS introduces air into the subsurface through direct injection of compressed air as opposed to creating a vacuum and drawing in air from the perimeter. Air Sparging is basically the injection of air under pressure below the water table for the purpose of volatilizing the different phases of contaminants in the ground water into the vapor phase. The minimum pressure required to displace water in an AS system is that which is needed to overcome the resistance of the soil matrix to airflow. The resistance to flow is a function of the height of the water column that needs to be displaced and the flow

restriction of the soil matrix. In tight soils in which the permeability of the soil is very small, air sparging is difficult to implement as the sweep gas is unable to penetrate into the contaminated zones in the subsurface.

2.1.3 Bioventing

Soil Vapor Extraction may also be operated in such a manner as to optimize the extent to which biodegradation of contaminant occurs, a technique that is called bioventing or bio assisted SVE. Bioventing refers to the process of supplying air to the vadose zone to stimulate in situ biological activity. In DuPont's (1993) words, "Bioventing represents a hybrid physical/biological process utilizing venting systems for oxygen transfer, while focusing not on contaminant stripping but rather on in situ aerobic contaminant biodegradation." Engineered in situ remediation involves the design and installation of systems designed for supplying microbe-stimulating materials into the subsurface. Engineered systems can again be classified as biostimulated or bioaugmented systems. Biostimulation refers to the addition of oxygen alone or the addition of oxygen and nutrients to the subsurface. Bioaugmentation is the process of adding nonnative bacteria in the subsurface to work with the indigenous bacteria in breaking down the contaminants.

Essentially, the basic objective of all bioremediation systems is to create a favorable environment for contaminant-degrading microorganisms to flourish. As such, the fundamental aspect in the design of bioremediation systems pertains to the provision of adequate electron acceptors and nutrients to the microorganisms. Obviously, different mechanisms are deployed depending on the different site conditions. Since the

biodegradation process is crucial to the success of the bioventing technique, the next section discusses some of the important features of biodegradation.

2.2 Biodegradation

Biodegradation is a dominant mechanism of organic chemical transformation in soils and aquifers. One of the paradigms is that the biodegradation of small molecular weight ($MW < 600$) organic compounds occur intracellularly. Thus, the rate of biodegradation is limited by:

1. Any physical-chemical process (sorption, solubility, hydrodynamic dispersion) that lowers solute concentration in the solution phase.
2. Any soil or environmental factor (temperature, soil-water content and electron acceptor availability) that limits physiological activity of the appropriate microbial consortia.
3. Any microbial factor that limits substrate uptake by microorganisms (cell membrane permeation, hydrophobicity).
4. Any intracellular genetic or biochemical factor (enzyme systems and presence and expression of genes) that limits utilization of the compound.

Common soil microorganisms have the ability to degrade virtually all of the hydrocarbons found in common contaminants. Many researchers have confirmed fuel degradation under favorable aerobic conditions. Enhanced in situ bioremediation is an attempt to create these favorable aerobic conditions in an environment of heterogeneous soils and delicate geochemical balances.

2.3 Soil Heating Technologies

Some of the successful soil heating technologies are summarized in Table 2.1. Observations on the success and shortfall of in situ soil washing, enhanced biodegradation, soil venting and radio frequency soil heating are presented by Downey (1990). These field tests have shown that in situ decontamination techniques that use water as a contact medium to remove hydrocarbons from the vadose zone have consistently fallen short of their cleanup goals. These results indicate that the physical accessibility of fuel residuals to the treatment media is critical to the success or failure of soil decontamination techniques.

Table 2.1. Characteristics of Different Soil Heating Methods

Thermal Driven Technology	Salient Features
Heat Blankets	1. Poor Heat transfer characteristics 2. Long treatment times
Thermal Wells	1. Ineffective for low permeability soils 2. Water condensation causes mass transfer problems
Heating Elements in Soil	1. Poor Conductivity 2. Increased resistance near source
Applied Electric Fields	1. In situ source of steam 2. Adaptable to soil with mineral content
Radio Frequency Heating	1. Heating by rotation and vibration of molecules 2. Cost intensive

Thermally enhanced remediation has been studied for overcoming the mass transfer limitations that are often a part of the SVE concept. The limiting factors for efficient removal include desorption of contaminants, slow diffusion of contaminants from low permeable layers into areas with vapor exchange, vapor phase retardation due to adsorption and limited volatility of the contaminants at in-situ temperatures. The presence of low permeable soil layers leads to incomplete contaminant removal since such layers have high water saturations and potentially may retain significant amount of organics not directly affected by airflow in the surrounding permeable areas. Recently, temperature effects have been studied in the removal of Trichloroethylene (TCE) as a model compound (Hernon et al., 1998). It was shown that heating the soil from 20 to 100 degree Celsius would increase the volatility by a factor of 11-18, would increase diffusion coefficients in the air and water by a factor of 1.3-1.5 and would reduce the partition coefficients.

The methods of applying heat to contaminated sites include thermal conduction using heat blankets or thermal wells, injection of hot air or steam, hot water injection, low frequency electric heating and microwave heating. Injections of hot fluids suffer from the disadvantage that the heat only can be injected directly into a relatively permeable zone. However, low permeable silt/clay soils will typically be heated solely by thermal conduction, which is a slow process since soil is a good insulator and has a high specific heat capacity. Therefore, alternative methods such as resistive heating and radio frequency heating are desirable.

2.3.1 Radio-Frequency Thermal Decontamination

In 1985, the Air Force and the EPA began a joint research project to explore the use of radio frequency (RF) heating for in situ soil decontamination. Radio frequency heating uses electromagnetic energy directed through electrodes in the soil to create molecular vibration and rotation, which uniformly heats the soil. Field tests have proved the feasibility of heating rock formation from 200 °C to 400 °C (Downey, 1990). As most of the common soil contaminants have boiling points less than 150 °C, RF heating was seen as having great potential for soil decontamination. The RF process is not very widely used because of the costs involved in the operation.

In situ subsurface heating could also improve bioremediation by increasing the amount of the contaminant made available to microbes to utilize (Price et al., 1999). The fault with this theory is that little to no research has been done to show that indigenous microorganisms can survive at temperatures much higher than their ambient conditions. Radio Frequency Heating (RFH) is another subsurface heating technology that has been demonstrated to heat soils from ambient temperatures to temperatures of up to 300°C (Price et al., 1999).

2.3.2 Resistive Heating

Electric heating techniques are based on resistive (joule, ohmic) heating of the soil when an alternating current is applied. While silt and clay have low permeabilities to fluids, they are more conductive than quartz sand due to the higher charge density of the mineral surfaces and to higher water content caused by capillary forces. This fact may be exploited by preferentially heating fine-grained layers by low frequency ac heating.

Applied electric fields have the advantage of heating soils internally, where the soil itself acts as a heat source.

2.3.3 Six Phase Soil Heating (SPSH)

The six-phase approach gives uniform heating, requires fewer electrodes, and uses robust conventional power transformers. At the current state of development, an array can be as large as 12 meters in diameter, effectively heating a 17-meter diameter region of the soil. To treat large volumes of soil, several arrays can be operated simultaneously or the heated region can extend up to 60 meters below the surface. Currently available power supplies can treat up to 5000 cubic meters of soil at a time. SPSH has been demonstrated successfully at the Savannah River site where a clayey soil contaminated with TCE and perchloroethylene (PCE) were treated. More than 99% of the contaminants were removed in 25 days. Niagara Falls site and Dover AFB sites are other examples where SPSH were used (Bergsmann and Trowbridge, 1997). The system performance was gauged in terms of the energy usage and steam generation for the field site at Dover Air Force Base, Delaware, and the economics worked out as \$16 per cubic meter of contaminated soil for efficient removal standards.

The six-phase soil heating technique is based on the ability to split conventional three-phase electricity into six separate electrical phases. Each phase is delivered to a single electrode, requiring six electrodes placed in a circle. Because each electrode is at a separate phase, each one conducts to all the others. The phases are connected so that adjacent electrodes, which are spaced 60 degrees apart in the hexagonal pattern, are also electrically 60 degrees out of phase. A seventh, neutral electrode is inserted in the center

of the hexagon. The electrodes are constructed using standard metal well casing and can double as vapor extraction vents.

A primary concern of the six-phase soil heating described above is adverse mobilization of target compounds in the subsurface. Potential adverse mobilization pathways exist through the (1) water, (2) non-aqueous liquid (NAPL) and (3) gas phases:

1. Contaminants may dissolve into the aqueous phase and be transported by convection due to thermally induced buoyancy and diffusion.
2. If NAPL exists, it may move through the soil in response to gravity, moderated by the contaminant's viscosity and surface tension.
3. Once evaporated, a contaminant in the vapor phase might escape capture due to ineffective soil venting.

2.4 Microbial Response to Heat

Researchers have recognized that ecosystem functioning is governed largely by soil microbial dynamics. In their study, Kennedy and Smith (1995) found that microbial communities and their processes need to be examined by the effect of environmental stresses on their communities. Understanding the changes caused by perturbations can help in the rebuilding or maintenance of an ecosystem after a stress event. For microorganisms, stress can include changes in temperature, nutrients, presence of contaminants or any factor that alters the balance of their ecosystem. In response to stress, microorganisms may increase or decrease in number, form spores, change their sources of nutrition or change their genetic structure for survival.

Microorganisms have growth characteristics that are directly related to temperature (Russell and Fukunaga, 1990; Tu, 1982). Microorganisms can be classified into one of three thermal categories: psychrophiles (0-20°C), mesophiles (10-50°C), and thermophiles (40-110°C). Individual members of each group usually have temperature spans of 20-40°C. Although it may be convenient to classify bacteria into these groups, their overlapping growth temperatures are indicative that there are no real boundaries. Psychrotrophs, which can grow in Celsius temperatures at or close to zero, have an upper growth limit of up to 40°C. Environmental temperatures above the thermophile boundary are relatively rare, while habitats at the other end of the thermal scale are very common since more than 80% of the earth is permanently cold.

Other than growth characteristics, Russell and Fukunaga (1990) identify some genetic differences between psychrophiles and thermophiles. At temperatures above 60°C, only prokaryotes exist. Examples of these prokaryotes are eubacteria, archaeobacteria and cyanobacteria. Another genetic difference includes the lipid composition of membranes. Data indicates that when microbes are exposed to the outer extremes of their thermal ranges, the amount of lipids increase (phospholipids and glycolipids). The increased lipid content could reflect their increased cell size at lower temperatures, which is a mechanism to increase the cell membrane area and the efficiency of nutrient uptake. Likewise, data on thermophiles reflected an increase in content of phospholipids at high-end temperatures. When the growth temperature of one thermophile studied was increased from 50-75°C, there was a two-fold increase in content of phospholipids and glycolipids.

Lipid composition also changes in response to a change in growth temperature. Microbial response in this aspect varied, from the general pattern of thermosensitive conversion of phosphatidylserine to phosphatidylethanolamine or phosphatidylglycerol in psychrophiles, to thermosensitive conversion of phosphatidylglycerol to diphosphatidylglycerol in thermophiles. In thermophiles, the opposite effect is seen at higher temperatures. In relation to fatty acid composition, it has been found that there are few eubacteria or cyanobacteria, which do not alter their fatty acid composition with a change in growth temperature, while there is very little data on archaeobacteria. Eubacteria demonstrated the greatest diversity of response, a result of the multiplicity of fatty acid composition in this group. The common response to lowering growth temperature was a rise in unsaturation of lipids, which could be due to the energetic considerations involved in relation to the amount of alteration in membrane fluidity.

Zelles et. al. (1991) determined the effect of storage temperature and humidity conditions of soils has on microbial activity. They measured the differences between microbial activities in soils of various C-content, stored under different temperatures and humidity conditions. The researchers used measurements of ATP content, heat output, and fluorescein diacetate hydrolysis to show overall microbial activity. Glucosamine and ergosterol contents were related to fungal biomass muramic acid to bacterial biomass. The 5 different types of soils with their associated C-content levels were sandy (1.1%), loamy (1.4%), forest mineral layers (5.1%), peaty (11.9%) and forest organic layers (34.1%). The soils were stored moist at 4, -18, or -140 °C or air-dried at 21 °C for 1, 2, and 20 months. The researchers found that ATP-content decreased markedly, except in

peaty soils and forest organic layers stored for 20 months at all temperatures except at 4°C. Peaty soil showed a marked increase in heat output (except at 4 °C), while the forest organic layers stored at 21 or –140 °C for 20 months saw a slight increase in heat output. For the other soils, storage caused a significant decrease in heat output. In most cases, air-drying caused a significant decrease in the quantity of these indicators of microbial activity. The differences between the effects on samples stored at 4, -18 or –140 °C were slight and in most cases insignificant.

Laboratory scale oven heating experiments at temperatures over 100 °C have been shown to decrease bacterial activity (Tu, 1982; Diaz-Ravina et al., 1996). Bacterial activity can recover after heating, but not to the original activity (Diaz-Ravina et al., 1996). Re-inoculation of the heated soil with fresh soil or poultry manure improved the reestablishment of bacterial activity after a lag of about 13 weeks.

Chambers and Attiwill (1994) investigated the effects of a range of heating and partial sterilization treatments on the chemical, microbiological and physical properties in soil. All treatments produced more or less similar effects on microbial populations. Immediately following treatments, very few actinomycetes were isolated. Virtually no bacteria were isolated. Fungi were isolated following heating at 100 °C or air drying, but all of the other treatments reduced numbers to less than 100 per gram of soil. Numbers of bacteria in all of the treated soils equaled or exceeded that in the controlled soil within 33 days. At 133 days, bacterial numbers were extremely variable within four replicates of the same soil. Soil that had been heated to 100 °C contained bacterial populations four orders of magnitude greater than in untreated soil.

Joergensen et al. (1990) set out to examine the effects of prolonged incubation at different temperatures on the survival of microbial biomass in soil that had not received externally supplied substrate. They also wanted to see if this same treatment could throw light on the energy sources used by microorganisms. To do this, C and N mineralization were followed during incubations at 15, 25 or 35°C. Biomass was monitored during these incubations in 3 ways: fumigation-extraction method, ATP monitoring, and a fumigation-extraction method in which carbohydrate rather than total carbon was measured.

Unfumigated soil was incubated at 3 temperatures: 15, 25 and 35 °C. Fumigated soil was incubated at 25 °C. Treatments were removed at 0, 10, 25, 50, 76, 115, 150, 191 and 240 days for extraction with 0.5M K₂SO₄. ATP measurements were carried out at the same times. Results showed that increasing the temperature from 15 to 25 °C roughly doubled the amounts of organic carbon mineralized during incubation. A further increase of 10 °C to 35 °C tripled the amount of carbon mineralized. Of the organic carbon initially in the soil, 6.4% was mineralized to CO₂ after 240 days at 15 °C, 12.2% at 25 °C, and 35.4% at 35 °C. The soil that had been fumigated and then incubated at 25 °C mineralized a little less CO₂-C in 240 days (9.9% of the initial organic carbon), than the corresponding unfumigated soil incubated at 25 °C (12.2%). Cumulative mineralization of N closely followed the pattern for C for the 15, 25, and 35°C incubations on unfumigated soil. The soils incubated at 15 and 25 °C nitrified; soil incubated at 35 °C did not, nor did soil that had been fumigated and then incubated at 25 °C. Even at 15 and 25 °C, the nitrification rate varied greatly between replicate incubations. In contrast, total

mineralization of N varied much less between replicates. The sum of the organic carbon remaining in the soil at the end of the 240 day incubation and the CO₂-C evolved was between 99 and 103% of the original amount, which indicates that there were no serious losses of carbon other than that measured as CO₂. On the other hand, all treatments contained less N than they started with, with the most serious loss at 15°C. Total extractable organic carbon changed little when unfumigated soil was incubated at 15 or 25 °C. In contrast, incubation at 35 °C caused a huge increase in extractable carbon from 3% to 8% after the 240 days.

After some initial fluctuations, soil microbial biomass drifted slowly downward in unfumigated soils incubated at 15 or 25 °C. In sharp contrast, biomass carbon fell catastrophically during incubation at 35 °C. ATP contents increased rapidly when going from 15 °C to 25 °C. If ATP is taken as a measure of biomass, then an incubation of 240 days at 35 °C caused the biomass to fall to 16% of its initial value.

Kieft et al. (1994) studied the effects of stresses caused by starvation on two strains of bacteria isolated from deep subsurface environments by identifying changes in PLFA. *Pseudomonas aureofaciens* and *Arthrobacter protophormiae* were quantified in a starvation experiment in a silica sand porous medium under moist and dry conditions. Cells were washed and then added to sand microcosms and maintained under saturated conditions or desiccation by slow drying over a period of 16 days to final water contents of nearly 0% and water potentials of -7.5MPa for the *P. aureofaciens* and -15 MPa for the *A. protophormiae*

The numbers of culturable cells of both bacterial strains declined to below detection level within 16 days in both the moist and dried nutrient deprived conditions. The direct counts and total PLFAs remained relatively constant for both strains. Both strains maintained culturability in the nutrient amended microcosms. The dried *P. aureofaciens* cells showed changes in PLFA profiles that are typically associated with stressed gram negative cells, which include increased ratios of saturated to unsaturated fatty acids, increased ratios of trans- to cis-monoenoic fatty acids, and increased ratios of cyclopropyl fatty acids to their monoenoic precursors. *P. aureofaciens* starved under moist conditions showed few changes in PLFA profiles during the 16-day incubation. Cells incubated in the presence of nutrients showed decreases in the ratios of both saturated fatty acids to unsaturated fatty acids and cyclopropyl fatty acids to their monoenoic precursors.

The PLFA profiles of *A. protophormiae* changed very little in response to either nutrient deprivation or desiccation. Diglyceride fatty acids, which are believed to be the indicators of dead or lysed cells, remained constant throughout the experiment. Only the *A. protophormiae* desiccated for 16 days showed an increase in the ratio of diglyceride fatty acids to PLFAs. The two isolates in this study appeared to demonstrate poor survival characteristics under starvation and desiccation conditions of this experiment. This is surprising, since these isolates are truly subsurface microorganisms and must be able to survive long-term nutrient deprivation under in situ conditions. It could be that the conditions of the experiments were significantly different from those encountered in

situ by the bacteria, or that the microbes entered a viable but nonculturable state under starving conditions.

Atlas et al. (1991) demonstrated that the diversity of microbial communities decreases in response to environmental stress or ecological imbalance. Microbial samples were exposed to test disturbance factors that consisted of crude oil, lead gasoline, or the herbicide 2,4,5-trichlorophenoxyacetic acid (2,4,5-T). Response measurements included taxonomic, genetic, physiological, and nutritional diversity parameters. The results showed that disturbances led to the survival of relatively few populations compared with undisturbed communities. Lead gasoline, a substance that contains lead and low molecular weight hydrocarbons that are toxic to microorganisms, had the greatest impact on taxonomic diversity. Crude oil, which contains hydrocarbons that serve as substrates for hydrocarbon-degrading microorganisms, caused the second greatest impact on diversity. The herbicide caused only a slight decrease in diversity.

In addition to a decrease in diversity, it was also found that microorganisms exposed to disturbance factors also exhibited an increase in physiological tolerances and metabolic diversities. Populations that became dominant possessed nutritional characteristics that were directly related to the disturbance factor. For example, the communities exposed to petroleum demonstrated enhanced capabilities of utilizing hydrocarbons and carboxylic acids, which are directly related to the metabolism of petroleum hydrocarbons. Disturbed populations also became more tolerant of other extreme conditions not related to the disturbance factor as a result of the exposure. They became more capable of growing over a wider range of temperatures, pH values, and salt

concentrations than populations that had not been exposed to disturbance. These results suggest that although diversity of communities decreases as a result of stressing exposures, microbes have the capacity for generalized adaptations to ecological disturbances.

A similar result of adaptation of microorganisms to ecological disturbance was found by Zogg et al. (1997). This research involved the comparison of the changes in community function and composition due to soil warming. Soils were incubated for 16 weeks at 5, 15, or 25 °C. The molecular techniques of PLFA and LPS-OHFA analysis were used to examine the effects of temperature on the composition of microbial communities in conjunction with an examination of kinetics of microbial respiration to examine a change in the function of the communities. The results of this analysis indicate an increase in the pool size of carbon respired by soil microbes with an increase in temperature. The results also provided evidence that biomass numbers decrease with an increase in temperature. It was found that the largest pool of carbon respired in the experiment was metabolized by the smallest active microbial biomass. This is the evidence that shows that some significant changes in patterns of substrate utilization occur at higher temperatures (known as thermoadaptation). From this research, we see that with an increase in temperature, the communities' function changes and the size/diversity of communities decrease and become adapted to the disturbed environment.

2.5 Microbial Modeling

The modeling of bacterial transport is complicated by a number of factors that can substantively affect bacterial transport behavior. Several of these factors may be inter-

related through other processes. For example, the chemical conditions in the subsurface may influence several processes (survival, growth, attachment, and detachment) affecting abundance of bacteria traveling through the medium.

Models for describing subsurface transport of bacteria have employed both conceptual and data based approaches. Recent theoretical models have incorporated the effect of a number of governing processes (Corapcioglu and Haridas, 1985). However, extension to the field scale is problematic because of the complexity of the models and the number of parameters that are required to be determined a priori. Thus, the predictive ability of these models are restricted and in some cases they under predict the transport characteristics (Germann, 1987). More accurate models will be developed as knowledge is gained about the parameters that govern bacterial transport through the contaminated subsurface.

2.6 Multiphase Flow and Heat Transfer in Porous Media

Problems in multiphase flow, heat transfer and multicomponent mass transport in porous media arise in a number of scientific and engineering disciplines. Important technological applications include enhanced oil recovery, subsurface contamination and remediation, geothermal energy exploitation, multiphase trickle bed reactors and nuclear reactor safety analysis. In general, multiphase flows in porous media are driven by gravitational, capillary and viscous forces. Capillary forces play fundamental roles in controlling the phase distribution and hence multiphase flow and transport in heterogeneous media. Due to the complicated transport phenomena involved, the

multiphase flow and transport in porous media remains poorly understood and analytically intractable.

Owing to the complex, multiphase structure of soil, the resultant effect of heat transfer in the soil takes the following forms (Nerpin, 1975):

1. Direct transfer of heat from each soil grain to the neighboring grain through the point of contact between them,
2. Molecular transfer of heat through the intermediate medium (air and water) occupying the soil pores,
3. Convective heat transfer through the same medium,
4. Heat radiation from particle to particle.

A number of experiments carried out with soils of various structures and approximate calculations support the following conclusions with a high degree of reliability:

1. The major contribution of heat transfer in the soil is made by the first of the above four mechanisms,
2. With overmoistening of soil a convective heat transfer is observed in the soil. The presence of the liquid phase is associated with flow and mass transfer between the vapor and liquid phases at high temperatures. This phenomenon contributes to the convective heat transfer.

More accurate calculations establish the limits of moisture, temperature and degree of dispersion of soil particles for which, besides contact molecular transfer, other significant heat transfer mechanisms begin to play a role. As a rule, the most common

type of soils in natural conditions do not have temperatures above 50 °C or excessive wetness (above soil retention capacity), for which it would be necessary to attribute special significance to the processes of convection and radiation.

To a lesser or greater extent these factors have effects either individually or in specific combinations. Therefore, it is not possible to use the usual equation of heat conduction for the soil. One of the following three methods can be used to overcome this difficulty:

1. The equation of homogenous heat conduction in space is considered first to find the temperature as a function of depth and time. It is necessary to refine the solution so obtained by introducing corrections dependent on other mechanisms of heat transfer estimated on logical, physical and experimental considerations. However, this approach is cumbersome and requires elaborate laboratory setup, and the results have not been consistent with the experimental values.
2. The second approach is formulated by including equations for all types of heat transfer. However, it is not practically possible to realize this method for a medium like soil, because it is not possible to represent correctly the model of all these types of heat transfer and describe them mathematically. Also, very little is known about the various parameters that appear in these complex equations.
3. It is, therefore, suggested that a middle path be adopted in dealing with problems of such magnitude and complexity. This approach uses the equation of heat conduction for soil with modifications to account for the non-homogenous,

multiphase nature of the material and the presence of a solid framework, i.e. soil skeleton with gas and moisture in the pores.

2.6.1 Model Ignoring Moisture Movement in Soil

In using a model of heat transport in soil, one common prediction is whether microbes are killed by the thermal impact. Most plant tissue and microbial cells are killed when the temperature is raised to around 60 ° C. How far below the surface is this maximum temperature achieved? The simplest model for predicting that maximum depth during a spreading fire is one that ignores moisture movement within the soil and treats the moist medium as an inert solid with constant constitutive parameters. In forest fire literature, modeling the fire as a moving line heat source at the surface, Richon (1987) found that for the surrogate material properties explored, the problem could be simplified by idealizing the analysis to a one-dimensional transient situation. Steward et al. (1990) extended this idealization to include cooling of the heated surface using a constant Newtonian film heat transfer coefficient. They found analytical solutions in dimensionless form for four different profiles of heat transfer rate as a function of time, with Newtonian cooling occurring either at all times or only after heating had ceased.

2.6.2 Models for Thermally Driven Heat and Moisture Transport in Soils

To predict the temperature history profile in a soil we need to know the history of heat input to the soil surface or the surface temperature history and to model the response of the soil to this stimulus. The focus of this work is to address the challenge of modeling the response of the soil to the boundary heating or temperature history.

Modeling the soil's thermal response would be relatively simple if not for moisture and its movement because of spatially non-uniform heating. The very large heat of vaporization of water and the ease with which water vapor can move through a porous soil matrix cause the transport of heat to be dominated by water vapor movement for temperatures near the boiling point of water. The relative immobility of water as a liquid in soil, and the high value of liquid water's thermal conductivity relative to that of air in the soil pores, make the thermal conductivity of the bulk soil medium sensitive to its liquid water content when liquid water occupies a significant volume fraction within the medium.

All this complicates the accurate modeling of heat transport within soils by making it necessary to simultaneously model the movement and concentration of water in liquid and vapor phases as well as the transport of heat by thermal conduction. Furthermore, a complete model must include variations with moisture content and temperature of the parameters that control the transport of heat, liquid water and water vapor. The dependence of rate controlling parameters such as thermal conductivity, vapor diffusivity and hydraulic conductivity upon the dependent variables means that the equations are mathematically non-linear. This non-linearity makes it invalid to solve a series of simple problems and construct more complex cases by linear superposition of the simple solutions. Thus, we need to resort to numerical techniques to solve the partial differential equations.

Heat transport and moisture movement within soils has been studied in soil science and microclimatology. There is a wealth of theoretical and empirical knowledge

about this phenomenology and modeling of it. However, the models and relationships are frequently restricted to the temperature regimes, heating rates and spatial gradients of temperature and moisture that occur naturally in diurnal cycles of heating and cooling and as a result of precipitation, drought and irrigation. Only recently have investigations been extended to temperatures, heating rates, dryness states and gradient magnitudes that characterize the fire environment. We seek to follow a parallel approach to this methodology to represent the resistive heating scenario.

Hungerford (1990) offers a definitive statement of the motivation for modeling heat and moisture transport in soils for predicting the effects of wildlife fires. The pioneering works by Philip and De Vries (1958) explored and analyzed the movement of moisture and transfer of heat in soils by starting at the size scale of soil particles. This model had considerable success and is the current paradigm of the soil science community for modeling heat and moisture movement in response to the diurnal fluctuations of the forces driving them. Another early and important model is that of Aston and Gill (1976) who addressed the problem for conditions of heating by a surface fire. These authors address the modeling of heat and moisture transport in soils in the vertical direction only. Compared to the De Vries formulation, that of Aston and Gill embodies simplicity even though it rests upon three-coupled diffusion equations, each with a source term. Equations are posed as phenomenological descriptions of sensible heat transport, liquid water transport and water vapor transport. Numerical results generated from the computer code of Aston and Gill showed agreement with soil temperatures measured under spreading grass fire. Although these model predictions

agreed well with the data of Scotter (1970) the model has not performed well when applied under other conditions, and it appears to lack in generality.

Campbell's model embodies several significant extensions to the de Vries and Aston and Gill models. The thermal conductivity, hydraulic conductivity, and water potential functions used by Aston and Gill are empirical and are based only on low temperature data. The numerical techniques used by Aston and Gill (second order Runge Kutta) do not converge to an acceptable mass and energy balance for the non-linear differential equations needed to solve the soil heating problem (Campbell et al., 1995). Improvements of this model include an explicit description of the temperature dependence of soil thermal conductivity, simultaneous solution of the heat and water equations, and a Newton-Raphson solution technique for the non-linear differential equations. Schroder (1974) developed an optimized computer simulation model for heat and moisture transport in soils. Emphasis was on the efficiency of the computer code implementing the model and not the model itself. There was no extension, development, or experimental verification of the model. Jury (1973) discusses the physics underlying the processes modeled, and compares model predictions with experimental results. Jury's thesis remains valuable for the physical concepts behind the mathematical expressions in these complicated models. Peter (1992) studied the heat transfer in soil beneath a spreading fire. The basis of the model is the formulation of De Vries (1958), despite the reservations noted and the observations made by Jury (1973).

2.7 Objectives of this Study

The objective of this research is to determine the effect of soil heating technologies on the population dynamics, activity and community structure of microorganisms in subsurface soils under laboratory conditions. To accomplish the above, two studies have been undertaken: (1) Temperature profiles in the subsurface as a function of time and space has been measured by means of laboratory experiments. (2) Changes in the microbial community during resistive heating (heating and cooling regimes) have been measured by means of microbial analysis of soil samples.

To work towards accurate field-scale temperature profile predictions, heat transfer models have been solved and compared to experimental measurements. A Computational Fluid Dynamics (CFD) tool, FLUENT, was employed to predict the temperature profiles. The single-phase and multiphase models have been used to study the temperature profiles in porous media. The multiphase model addresses the effect of moisture content on the temperature response in porous media. Sensitivity Analysis was performed to study the effect of changing soil parameters in the single-phase model. A comparison between the single-phase and multiphase models and the capability of each model to accurately predict the temperature has been looked into.

CHAPTER 3

THEORY

FLUENT is a state-of-the-art computer program for modeling fluid flow and heat transfer in complex geometries. It was used in this work because it provides an interactive, menu driven interface with both tabular input and graphical user input of data for problem setup and simulation. FLUENT has been used in this work to solve transient mass, momentum, and energy conservation equations in two-dimensional Cartesian coordinates for a porous medium. This chapter describes the governing fluid flow equations and the boundary conditions used in FLUENT. The first part of the chapter discusses setting up a single-phase conduction problem in porous media and the second half focuses on solving heat and mass transfer (multi-phase) in unsaturated porous media.

3.1 Problem Solving Steps in FLUENT

The basic problem solving steps involved in setting up a problem in FLUENT are:

1. Creating the model geometry and grid.
2. Invoking appropriate solver for 2D or 3D modeling.
3. Choosing the basic equations to be solved, i.e., based on the complexity of the problem appropriate models have to be activated. For our problem, the heat transfer and porous media models were activated.
4. Specifying material properties of the porous medium and the fluid.

5. Specifying the boundary conditions such as the temperature and heat flux at the wall.
6. Adjusting the solution control parameters such as under-relaxation and time step.
7. Calculating a solution.
8. Examining the results.
9. If necessary, refining the grid or making revisions to the numerical or physical model.

3.2. Overview of Geometry and Grid Definition Options

FLUENT employs what could be termed a grid-based geometry, in which the geometry of the model is determined by control volumes defined by the grid. For our model, Cartesian coordinates in which the grid lines are aligned with the Cartesian (x, y, z) coordinates of the physical geometry is used. Figure 3.1 shows the computational grid that has been adopted for this particular study.

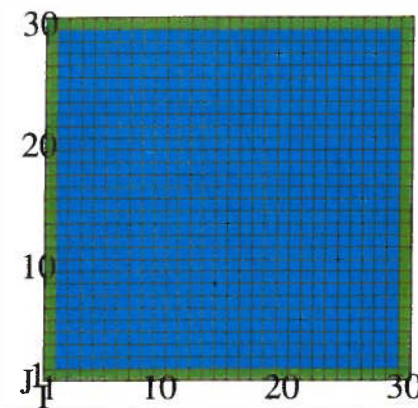


Figure 3.1. Computational Grid Used in FLUENT

The grid is a discrete representation of the continuous field phenomena that is being modeled, and the accuracy and numerical stability of the FLUENT simulations depend on the choice of the grid. In other words, the density and distribution of the grid lines determines the accuracy with which the FLUENT model represents the actual physical phenomena.

In FLUENT, the control volume method, sometimes referred to as the finite volume method, is used to discretize the transport equations. In the discrete form of the equations, values of the dependent variables appear at control volume boundary locations (cell faces). These values have to be expressed in terms of the values at the nodes of neighboring cells in order to obtain the algebraic equations. This task is accomplished via an interpolation practice, also called a 'Differencing Scheme'. The choice of the differencing scheme not only affects the accuracy of the solution but also the stability of the numerical method.

The use of an interpolation assumption introduces a discretization error that decreases as the grid spacing is reduced. In practice, it is necessary to obtain sufficiently accurate solutions by employing grids that are not excessively fine. One measure of the discretization error of a scheme is the so-called truncation error of a Taylor series approximation to the derivatives in the governing differential equations. Truncation error occurs due to the approximate nature of the finite difference representation and can be reduced by increasing the order of the interpolation method. The default differencing scheme used in FLUENT is the power-law scheme. The power-law scheme is very stable and gives physically meaningful (bounded) solutions but, in certain situations, is

susceptible to numerical diffusion (false diffusion) effects. The term false diffusion is used because its effect on a flow field is analogous to that of increasing the real diffusion coefficient. The phenomenon of false diffusion arises due to one-dimensional interpolation practices being employed in a multi-dimensional situation. Solutions in which truncation error and/or numerical diffusion are significant are termed grid-dependent. If the grid is refined until the solution no longer varies with additional grid refinement, a grid-independent solution is achieved. The ideal differencing scheme therefore has the following attributes: (1) low truncation error (2) low numerical diffusion (3) physically meaningful variation. Further discussion on the differencing scheme is presented later in this chapter.

3.3 The Equation Set for Single-Phase Model

The basic equations describing the laminar flow of continuous fluid for the single-phase model are:

1. Conservation of mass
2. Conservation of momentum
3. Conservation of energy

FLUENT normally solves the governing conservation equations using Cartesian spatial coordinates and velocity components. In the single-phase model, the porous medium is the only phase present and the temperature response of this medium on being heated and subsequently cooled was studied.

3.3.1 The Mass Conservation Equation

The conservation of mass or continuity equation used in FLUENT is

$$\frac{\partial \rho}{\partial t} + \frac{\partial}{\partial x_i}(\rho u_i) = S_m \quad (3.1)$$

The above equation is the general form of the mass conservation equation and is valid for incompressible as well as compressible flows. The source S_m is the mass added to the continuous phase from the dispersed second phase (e.g. due to vaporization of liquid droplets). For the single-phase model, mass transfer is absent and hence the value of S_m is zero. Density is assumed constant for most of the single-phase calculations.

3.3.2 Momentum Conservation Equation

Conservation of momentum in the i^{th} direction in an inertial (non accelerating) reference frame is described by (G.K. Batchelor, 1967)

$$\frac{\partial}{\partial t}(\rho u_i) + \frac{\partial}{\partial x_j}(\rho u_i u_j) = -\frac{\partial p}{\partial x_i} + \frac{\partial \tau_{ij}}{\partial x_j} + \rho g_i + F_i \quad (3.2)$$

in which p is the static pressure, τ_{ij} is the stress tensor and g_i and F_i are the gravitational acceleration and external body forces, respectively. The only flow encountered in this study was due to thermal gradients. In our model setup since no velocities are encountered u_i, u_j are zero. Pressure is held constant and the stress tensor and body forces models are not activated. Hence, all these terms do not contribute in the above equation. In essence, the momentum equation was not used for the single-phase calculations.

3.3.3 Energy Conservation equation

FLUENT solves the conservation of energy in terms of conservation of static enthalpy, h , defined as:

$$h = \sum_i m_i \cdot h_i \quad (3.3)$$

$$h_i = \int_{T_{ref}}^T C_{p,i} dT \quad (3.4)$$

in which m is the mass, T_{ref} is a reference temperature, and $C_{p,i}$ is the specific heat at constant pressure of species i .

The energy equation solved by FLUENT assumes that species diffusion due to pressure and external forces is negligible. Under this assumption, the energy equation cast in terms of h can be written as (Bird et al., 1960):

$$\frac{\partial}{\partial t}(\rho h) + \frac{\partial}{\partial x_i}(\rho u_i h) = \frac{\partial}{\partial x_i} \left(k \frac{\partial T}{\partial x_i} \right) - \frac{\partial}{\partial x_i} \sum_j h_j J_j + \frac{\partial p}{\partial t} + u_i \frac{\partial p}{\partial x_i} + \tau_{ij} \frac{\partial u_i}{\partial x_j} + S_h \quad (3.5)$$

in which T is the temperature, τ_{ij} is the viscous stress tensor, J_j is the flux of species j , k is the thermal conductivity of the mixture, and S_h is the source term that includes sources of enthalpy due to chemical reaction, radiation and exchange of heat with the dispersed second phase. None of these are present in the single-phase model.

For a porous medium, FLUENT solves the standard enthalpy equation in porous media regions with modifications to the conduction flux and the transient terms only. In the porous medium, the conduction flux uses an effective thermal conductivity and the transient term includes the thermal inertia of the solid region on the medium:

$$\begin{aligned} \frac{\partial}{\partial t}(\phi \rho_f h_f + (1-\phi) \rho_s h_s) + \frac{\partial}{\partial x_i}(\rho_f u_i h_f) = \frac{\partial}{\partial x_i}(k_{\text{eff}}) \frac{\partial T}{\partial x_i} - \frac{\partial}{\partial x_i} \sum_j h_j J_j + \frac{\partial p}{\partial t} + u_i \frac{\partial p}{\partial x_i} \\ + \tau_{ij} \frac{\partial u_i}{\partial x_j} + S_h \end{aligned} \quad (3.6)$$

in which

h_f = fluid enthalpy ($\int c_{p,f} dT$),

h_s = solid medium enthalpy ($\int c_s dT$),

ϕ = porosity of the medium,

k_{eff} = effective thermal conductivity of the medium.

The effective thermal conductivity in the porous medium, k_{eff} , is computed by

FLUENT as the volume average of the fluid conductivity and solid conductivity:

$$k_{\text{eff}} = \phi k_f + (1-\phi) k_s \quad (3.7)$$

in which,

ϕ = porosity of the medium,

k_f = fluid phase thermal conductivity,

k_s = solid medium thermal conductivity.

When this simple volume averaging is not desired, perhaps due to the effect of the medium geometry, the effective conductivity can be computed via a user-defined subroutine. In all cases, however, the effective conductivity is treated as an isotropic property of the medium. For the single-phase model, velocity terms are zero. In the absence of mass fluxes (as in the single-phase model) there is no contribution by the term J_j . S_h is the source term and represents the external heat that is added to the system. The terms subscripted with f stand for the properties of the fluid medium (liquid water).

3.3.4 Summary of Single-Phase Equations Solved

The terms contributing to the mass, momentum and energy equations presented in the previous section have been summarized here. In the absence of liquid velocities and source S_m , the mass conservation equation reduces to:

$$\frac{\partial \rho}{\partial t} = 0 \quad (3.8)$$

For the temperature dependent density calculations an outlet is added additionally to the grid to overcome problems of mass imbalance in the computational region. For the single-phase problem specification, the momentum conservation equation is not used in the calculations. Hence, the primary equation of interest for the single-phase model is the energy conservation equation, which in its reduced form is:

$$\frac{\partial}{\partial t} (\phi \rho_f h_f + (1 - \phi) \rho_s h_s) = \frac{\partial}{\partial x_i} (k_{eff}) \frac{\partial T}{\partial x_i} + S_h \quad (3.9)$$

The above equation is a transient second order partial differential equation that needs to be solved with appropriate initial and boundary conditions.

3.4 Fluid Properties and Equation of State

Closure of the conservation equations presented in the preceding sections requires a description of the fluid density and other fluid properties. FLUENT allows all fluid properties to be defined as constant or as temperature and/or composition dependent. In this section the equations employed by FLUENT for calculation of temperature and/or species dependent fluid properties are outlined.

3.4.1 Equation of State for Density

FLUENT allows the mixture density to be described as a function of temperature and composition and in ideal gases, as a function of temperature, pressure and composition. Density can be computed via the ideal gas law or by the expression

$$\rho = \frac{1}{\sum \frac{m_i}{\rho_i}} \quad (3.10)$$

in which ρ_i is the density of species i and can be defined via a polynomial or piecewise linear distribution. Constant density assumption has been made for most of the calculations.

3.4.2 Viscosity

FLUENT allows the fluid viscosity to be dependent on temperature and/or composition. In addition, several non-Newtonian viscosity models are available. In the case of ideal gases, the viscosity can be defined as a polynomial or piecewise-linear function of temperature. Kinetic theory can also be used for the computation of viscosity and involves the introduction of Lennard-Jones parameters.

In the case of non-ideal flows the viscosity can be defined as composition dependent and the mixture viscosity is calculated as

$$\mu = \sum_i m_i \mu_i \quad (3.11)$$

in which the individual viscosities may be piecewise linear or polynomial functions of temperature:

$$\mu_i = \mu_i(T) \quad (3.12)$$

A constant value of viscosity is used in the single-phase model as well as the multiphase models.

3.4.3 Thermal Conductivity and Specific Heat

In the single-component flows of ideal gases, the thermal conductivity, k is defined as a piecewise linear or polynomial function of temperature or in terms of the parameters involved in the kinetic energy theory. For our simulations, we consider thermal conductivity for the nonideal case, and represent it for a mixture as:

$$k = \sum_i m_i k_i \quad (3.13)$$

where the individual component thermal conductivity may be piecewise linear or polynomial functions of temperature:

$$k_i = k_i(T) \quad (3.14)$$

The same approach is adopted in the specification of specific heat in which the k 's (thermal conductivity) in the above equations are replaced by c_p . For both the single-phase as well as multiphase calculations, constant values of thermal conductivity and specific heat were used.

3.5. Heat Transfer

FLUENT allows including heat transfer within the fluid and/or within solid regions in the specified model. Problems ranging from thermal mixing within a fluid to conduction in composite solids can thus be handled by FLUENT using the physical

models and input commands available. Thermal boundary conditions at wall boundaries tell FLUENT the conditions at the wall that impact the rate of heat transfer between the wall and the adjacent live or conducting wall cells. These conditions are defined in terms of the heat flux at the wall/live interface.

3.5.1 Defining Thermal Boundary Conditions at Walls

When the energy equation is being solved (as in our model), thermal boundary conditions need to be defined at the wall boundaries. An external heat transfer boundary condition has been activated for our specific problem. Under this option values for heat transfer coefficient and ambient temperature are input. Another approach to study heat loss from the grid is by fixing the heat loss as a percentage of the heat supplied (also called the % heat removal boundary condition). In this approach the heat loss is fixed irrespective of the driving force of temperature. An adiabatic wall is set by inputting a heat transfer coefficient of zero. This is the default condition for all walls. All three of the models have been studied and are presented in Chapter 5.

3.5.2 Heat Transfer Calculations at Wall Boundaries

When a heat flux boundary condition is specified at the wall, it refers to the heat flux at the wall surface. Fluent uses the following equation and the user input value of the heat flux to determine the wall surface temperature adjacent to a fluid cell as

$$T_w = \frac{q'' - q_{rad}''}{h_f} + T_f \quad (3.15)$$

$$q'' = h_f (T_w - T_f) + q_{rad}'' \quad (3.16)$$

in which

h_f = fluid side local heat transfer coefficient,

T_w = Wall surface temperature,

T_f = local fluid temperature,

q' = convective heat flux from the wall,

q_{rad}' = radiative heat flux.

For all the model calculations q_{rad}' was assumed to be zero.

3.6 The Eulerian Multiphase Model

A large number of flows encountered in nature and technology are a mixture of phases. Temperature profile in porous media is influenced to a high degree by the presence of water in the matrix. Water in liquid as well as vapor forms affects the temperature distribution in porous media. The thermal conductivity of water in liquid and vapor form acts a resistance to the propagation of heat in the porous media. The multiphase model was employed in this study to analyze the behavior of the temperature curve at high temperatures where there is evaporation of liquid on heating and condensation on cooling.

In multiphase flow, a phase can be defined as an identifiable class of material that has a particular inertial response to and interaction with the flow and the potential field in which it is immersed. Currently there are two approaches for the numerical calculation of multiphase flows: the Euler-Lagrange approach and the Euler-Euler approach. The Lagrange dispersed phase model treats the fluid medium as a continuum and solves the time-averaged Navier stokes equation while the dispersed phase is solved by tracking a

large number of particles, bubbles, or droplets through the calculated flow field. A fundamental assumption made in this model is that the dispersed phase occupies a low volume fraction. This approach is suitable for modeling spray dryers, coal and liquid combustion but inappropriate for modeling of liquid-liquid mixtures, fluidized beds or any application where the volume fraction of the second phase is not negligible.

In the Euler-Euler approach, the different phases are treated mathematically as interpenetrating continua. Since the volume of a phase cannot be occupied by the other phases, the concept of phase volume fraction is introduced. These volume fractions are assumed to be continuous functions of space and time and their sum is equal to one. Conservation equations for each phase are derived to obtain a set of equations, which have similar structure for all phases. These equations are closed by providing constitutive relations, which are obtained from empirical information, or in the case of granular flows, by application of kinetic theory. For our problem, an Eulerian approach is suitable because the volume fraction of the second phase is not negligible.

The Eulerian multiphase model solves a set of continuity, momentum, and enthalpy equations for each phase. Coupling is achieved through the pressure and interphase exchange coefficients. The manner in which this coupling is handled depends upon the type of phases involved; granular (fluid-solid) flows are handled differently than non-granular (fluid-fluid) flows.

The number of secondary phases is limited only by the memory requirements and convergence behavior. Any number of secondary phases can be modeled, provided that

sufficient memory is available. Some of the characteristics of Fluid-Fluid flow modeling are:

1. A single pressure is shared by all phases,
2. Momentum, Enthalpy and Continuity equations are solved for each phase,
3. The ideal gas law can be used for the gas phase,
4. Temperature-dependent properties are available for all the phases,
5. m species can be solved for in each phase,
6. Homogenous reactions are allowed for each phase,
7. Mass transfer is allowed between the phases.

To change from the single-phase model, in which a single set of conservation equations for momentum and continuity is solved, to a multiphase model, additional sets of conservation equations must be introduced. In the process of introducing additional sets of conservation equations, the original set must also be modified. The modification involves among other things, the introduction of the volume fraction α_j for the multiple phases, as well as a mechanism for the exchange of momentum between the phases.

3.6.1 Volume Fractions

The description of multiphase flow as interpenetrating continua incorporates the concept of phasic volume fractions, denoted by α . Volume fractions represent the space occupied by each phase. The laws of conservation of mass, momentum and energy are satisfied by each phase individually. The derivation of the conservation equations can be done by ensemble averaging the local instantaneous balance for each of the phases or by using the mixture theory approach.

The volume of phase q, V_q , is defined by

$$V_q = \int_v \alpha_q dv \quad (3.17)$$

in which

$$\sum_{q=1}^n \alpha_q = 1 \quad (3.18)$$

The effective density of the phase q is

$$\rho = \alpha_q \rho_q \quad (3.19)$$

in which ρ_q is the physical density of phase q, which, in the case of a gas, can obey the ideal gas law.

3.6.2 Conservation Equations

The conservation equations for multiphase flows are presented in this section in general form.

Conservation of Mass

The continuity equation for phase q is

$$\frac{\partial}{\partial t}(\alpha_q \rho_q) + \nabla \cdot \alpha_q \rho_q \vec{u}_q = \sum_{p=1}^n \dot{m}_{pq} \quad (3.20)$$

in which \vec{u}_q is the velocity of phase q and \dot{m}_{pq} characterizes the mass transfer from the p^{th} to the q^{th} phase. From the mass conservation one can obtain $\dot{m}_{pq} = -\dot{m}_{qp}$ and $\dot{m}_{pp} = 0$. In the multiphase model the mass transfer between phases is used by the evaporation-condensation subroutine described later in this chapter.

Conservation of Momentum

The momentum balance for phase q yields

$$\frac{\partial}{\partial t}(\alpha_q \rho_q \vec{u}_q) + \nabla \cdot (\alpha_q \rho_q \vec{u}_q \otimes \vec{u}_q) = -\alpha_q \nabla p + \nabla \cdot \bar{\tau}_q + \alpha_q \rho_q \vec{F}_q + \sum_{p=1}^n (\vec{R}_{pq} + \dot{m}_{pq} \vec{u}_{pq}) \quad (3.21)$$

in which $\bar{\tau}_q$ is the q^{th} phase stress-strain tensor, \vec{F}_q is an external body force, \vec{R}_{pq} is an interaction force between phases, \otimes is a dyadic product, and p is the pressure shared by all the phases. In the multiphase model, the gravity term is included in the external body forces term and becomes important when density varies with temperature. The interaction forces between phases are absent and can be neglected.

Conservation of Energy

To describe the conservation of energy in multiphase applications, a separate enthalpy equation can be written for each phase:

$$\frac{\partial}{\partial t}(\alpha_q \rho_q h_q) + \nabla \cdot (\alpha_q \rho_q \vec{u}_q h_q) = \alpha_q \frac{dp_q}{dt} + \bar{\tau}_q : \nabla \vec{u}_q - \nabla \cdot \vec{q}_q + S_q + \sum_{p=1}^n (Q_{pq} + \dot{m}_{pq} h_{pq}) \quad (3.22)$$

in which h_q is the specific enthalpy of the q^{th} phase, \vec{q}_q is the heat flux, S_q is a source term that includes sources of enthalpy (e.g., due to chemical reaction or radiation), Q_{pq} is the intensity of heat exchange between the p^{th} and q^{th} phases, and h_{pq} is the interphase

enthalpy (e.g., the enthalpy of the vapor at the temperature of the droplets, in case of evaporation). The heat exchange between phases must comply with the local balance conditions $Q_{pq} = Q_{qp}$ and $Q_{qq}=0$. In the multiphase model the pressure is assumed constant and the stress tensors are absent.

The internal energy balance for phase q is written in terms of the phase enthalpy (equation for conservation of energy). In general phase q can be a mixture of species i' , ($i' = 1, m$), and its enthalpy is defined by

$$h_q = \sum_{i'=1}^m m_q^{i'} h_q^{i'} \quad (3.23)$$

in which

$$dh_q^{i'} = c_{p,q}^{i'} dT_q \quad (3.24)$$

and $c_{p,q}^{i'}$ is the specific heat at constant pressure of species i' in phase q . The thermal boundary conditions used with multiphase flows are the same as those for a single-phase flow.

The rate of energy transfer between phases is assumed to be a function of temperature difference

$$Q_{pq} = H_{pq} (T_p - T_q) \quad (3.25)$$

The heat transfer coefficient is related to the p^{th} phase Nusselt number Nu_p :

$$H_{pq} = \frac{6\kappa_q \alpha_p Nu_p}{d_p^2} \quad (3.26)$$

κ_q is the thermal conductivity of the q^{th} phase. The Nusselt number is typically determined from one of the many sources reported in literature. In case of fluid-fluid multiphase, FLUENT uses the correlation of Ranz and Marshall (1952):

$$\text{Nu}_p = 2.0 + 0.6 \text{Re}_p^{1/2} \text{Pr}^{1/3} \quad (3.27)$$

Since in our model no specific flow is encountered, details concerning the dimensionless numbers are not discussed.

3.6.3 Summary of Multiphase Equations Solved

The simplified form of the conservation equations for multiphase flow is presented in this section. The conservation of mass retains its original form as in equation 3.20. The term on the right hand side of this equation is adapted to incorporate the evaporation-condensation module. This is described in the next section. The conservation of momentum equation reduces to:

$$\frac{\partial}{\partial t}(\alpha_q \rho_q \vec{u}_q) + \nabla \cdot (\alpha_q \rho_q \vec{u}_q \otimes \vec{u}_q) = \sum_{p=1}^n \dot{m}_{pq} \vec{u}_{pq} \quad (3.28)$$

The pressure term, body force term, stress-strain tensor and the interaction force between the multiple phases have been neglected from the original equation. The energy conservation equation in its simplified form is represented as:

$$\frac{\partial}{\partial t}(\alpha_q \rho_q h_q) + \nabla \cdot (\alpha_q \rho_q \vec{u}_q h_q) = -\nabla \cdot \vec{q}_q + S_q + \sum_{p=1}^n (Q_{pq} + \dot{m}_{pq} h_{pq}) \quad (3.29)$$

The pressure term and the stress tensor term have been neglected from the original equation. The closure of the multiphase equations is obtained using the same set of fluid properties and equation of state.

3.6.4 Description of Mass transfer in Multiphase Model

The continuity equations for the p^{th} phase contain the source term

$$\sum_{p=1}^n \dot{m}_{pq} \quad (3.30)$$

which characterizes the amount of mass transfer from the p^{th} to the q^{th} phase per unit volume of mixture per unit time. A similar term appears in the momentum and enthalpy equations. There are numerous kinds of mass transfer processes, and these can be modeled with user-defined subroutines. FLUENT models are limited to two types: (1) unidirectional mass transfer, and (2) evaporation-condensation.

In our modeling, we have utilized the latter feature. The evaporation-condensation module (Lee Wen Ho, 1979) is a simple phenomenological model for a mixture of two phases (liquid and vapor).

The evaporation rate \dot{m}_v and the condensation rate \dot{m}_l are determined from

$$\begin{aligned} \dot{m}_v &= r_v \alpha_l \rho_l (T_l - T_{\text{sat}}) / T_{\text{sat}} & T_l &\geq T_{\text{sat}} \\ &= 0 & T_l &\leq T_{\text{sat}} \end{aligned} \quad (3.31)$$

$$\begin{aligned} \dot{m}_l &= r_l \alpha_v \rho_v (T_{\text{sat}} - T_v) / T_{\text{sat}} & T_v &\leq T_{\text{sat}} \\ &= 0 & T_v &> T_{\text{sat}} \end{aligned} \quad (3.32)$$

where r_v and r_l are time relaxation parameters with default values of 0.1.

CHAPTER 4

MATERIALS AND METHODS

4.1 Overview of the Experimental Setup

To study the microbial response to heat in the subsurface, a lab-scale experimental plan was designed. This chapter discusses the experimental setup, materials and methods applied to the experimental setup, calibration procedures and the operating conditions. The experimental setup used to study resistive heating of soils is shown in Figure 4.1. Three rectangular boxes (0.5 m H*0.5 m W*0.1 m D) made of Polycarbonate Lexan[®] were fabricated. The choice of material was based on the thermal behavior and insulation characteristics of the material. The box is filled with the soil (Piedmont, medium sand) to be heated. Stainless steel plates connected to a 240 V power source served as the electrodes for resistive heating. These plates were placed at the corners of each of the boxes. An additional layer of polystyrene foam was wrapped around the boxes to provide additional insulation. The depth of the boxes was kept intentionally small to minimize deviations in temperature along that direction. Under ideal conditions (assuming minimum heat loss), the problem could be studied in two dimensions. The front sides of the boxes were fabricated with numerous thermocouples (Cole Parmer, Type T) as seen in Figure 4.2 (a). The rear side of the box was equipped with soil sampling ports (3/8" pipe plugs) for microbial characterization (Figure 4.2 (b)). The soil sampling ports were arranged in a (3x3) matrix and named as port_{ij} where i and j represent the row and column

from top to bottom. A metal spatula was used for the sampling, and adequate care was taken to sterilize it to prevent external contamination.

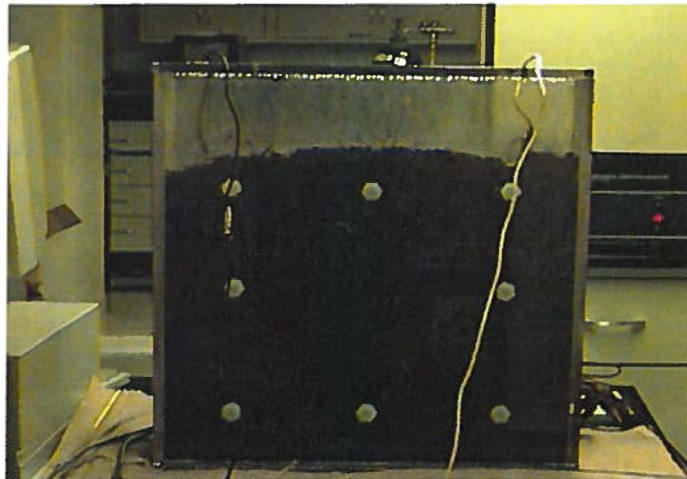


Figure 4.1. Lab Scale Lexan Box to Study Resistive Heating

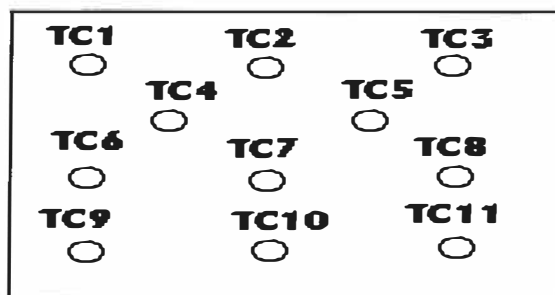


Figure 4.2 (a). Arrangement of the Temperature Ports in the Experimental Setup

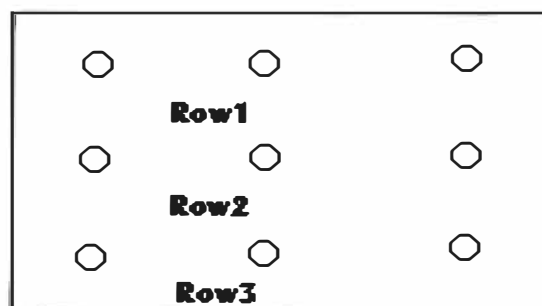


Figure 4.2 (b). Geometry of the Soil Sampling Ports Used in the Experimental Setup

There were three significant stages in the resistive heating implementation: heating, stagnation, cooling. The heating period in which the temperature increased from room temperature to around 100 °C was followed by a stagnation phase in which the temperature was maintained at 100 °C. The duration of this phase was dependent on the moisture distribution in the soil. The heating phase followed by the stagnation phase exposed the microbes to a harsh thermal environment for a prolonged period of time. The final step was the cooling phase in which the temperature was allowed to cool down to room temperature. The power sources were calibrated to control the rate of increase of temperature in the heat up period and maintaining the temperature in the stagnation period.

After the cool down period the three boxes were left undisturbed for a week to allow the soil microbes to repopulate. After this time, nutrients were added to each of the boxes to facilitate the repopulation of microbes. The nutrient addition was performed with a drip system and a peristaltic pump. A drainpipe at the bottom face of the boxes helped in removing excess nutrient solution. The repopulation was monitored over a period of one week. The microbial counts were quantitatively measured by means of plate counts and Acridine Orange Direct Counts (AODC). Phospholipid Fatty Acid Analysis (PLFA) tests were conducted at the University of Tennessee, Center for Biotechnology. These tests revealed the composition of the microbial community before and after resistive heating.

4.2. Methods

4.2.1. Temperature Monitoring

The temperature data with respect to time was recorded every 30 minutes throughout the experiment. A scanning thermometer, interfaced with a computer provided real time temperature readings. All thermocouples were placed at the midpoint along the depth of the box. Thermocouples 4 and 5 in the second row were the reference temperature ports for soil sampling. The temperature recorded by these ports served as an indicator as to when a soil sample was to be retrieved. The tips of the thermocouples were covered with a plastic cap. This helped to eliminate charge accumulation on the tips and eliminated bad readings.

4.2.2 Calibration of the Temperature Curve

The nature of the temperature curve depends on a number of operating conditions. One of them is the rate at which the power was supplied to the electrodes. This setting determined the duration of each of the phases involved in resistive heating (assuming that the other factors such as soil moisture, soil packing are approximately held the same). A number of preliminary runs were conducted to record the temperature increase with respect to time at various settings. It was observed that a setting of 80 % on the power source (240 V, 10 A) was ideal for the heating period providing a temperature increase of 5-10 ° C /hour. In the stationary phase more energy is required to hold the temperatures at around 100 ° C. Hence, the power setting was increased to maximum at 100 %. This

helped in maintaining the stationary phase for around 4-6 hours. For the cooling phase, the power source is shut down, and newtonian cooling is allowed to proceed.

4.2.3 Soil Sampling and Analysis

The soil was sampled at different temperatures (25 °C, 50 °C, 75 °C and 100 °C) during the heating phase. During the cooling phase samples were taken at 100 °C, 75 °C, 50 °C and at room temperature. Two 1-g samples were taken for microbial analysis at a particular port, and a 2-g sample was placed in an oven to study the moisture content of the soil during each observation. The sampling port (Port_{ij}) was rotated at every sampling iteration. This ensured that the soil samples were representative of the events occurring in the box.

The microbial population size was determined by CFU, AODC, MPN, and PLFA analysis. CFU was used to analyze the Dover soil as well as the box soil. CFU counts were done using a series of six dilutions with 9 mL of distilled, autoclaved water and 1 g of soil. Dilutions were plated in two sets in triplicate on R2A agar, (Becton Dickinson Microbiology Systems, Cockeysville, Maryland), and nutrient agar, (Difco Laboratories, Detroit, Michigan). One set of plates was incubated at 20 °C and the other set at the temperature to which the soil was heated for 2 to 4 days. Both were observed for bacterial growth.

Acridine orange direct counts were performed as specified by Ghiorse and Balkwill (1983) for the Dover soil and the box soil. A series of dilutions from 10^1 to 10^3 with 1 g of soil and 9 mL of distilled 3X filtered (using a vacuum pump and a 0.2 μm , 47

mm polycarbonate filter), autoclaved water were prepared. The 10^2 dilution was used to make the slides. Using a vacuum pump and a $0.2\mu\text{m}$, 47 mm polycarbonate filter, 0.55 mL of formaldehyde was filtered once and added to the dilution tube. One mL of dilution sample and 1 mL of acridine orange stain were added to a filter apparatus, sterilized by flaming with methanol, containing a $0.2\mu\text{m}$, 25 mm black polycarbonate membrane filter. Ten mL of the 3X filtered water was added to the apparatus. The mixture was allowed to stand for 2-4 minutes, then was filtered through by vacuum filtration. The filter was then removed and placed on a glass slide with one drop of immersion oil followed by a glass cover slip. Slides were read using a fluorescent light microscope (Olympus Optical Co., Ltd, Olympus, model BX40F4, Japan), containing a grid with an area of 10 mm^2 . Five fields of each slide were counted and then averaged to determine the value $\text{AODC}=\text{Y}$ for the formula used to determine the number of microbes for each temperature, $(\text{Average of the 5 fields} * \text{Area of the filter}) / (0.95 * \text{Area of the grid})$. All samples were corrected for moisture content. All filters were obtained from Poretics Corporation, Livermore, California.

MPN assays were used to analyze microbial population size for the Dover soil and were done according to the most probable number technique as defined by Lehmicke et al. (1979). One gram of soil with 9 mL of distilled water was added to each of nine 40 mL vials. A ten-fold dilution series was created from these vials. Two sets of dilutions were injected with 250 μL of sodium azide to create a control. The caps for each vial contained an accordian folded filter filled reaction cup. The reaction cup with filter was

injected with 250 μL of 1 N KOH to trap evolved CO_2 . Next, a radiolabelled substrate ($\text{NaH}_3^{14}\text{CO}_3$) solution was pipetted into each vial. The vials were capped and then allowed to incubate at the temperature to which the soil was heated for 1 week. Following incubation, vials were placed on a rotary shaker for 24 hours to help drive the CO_2 into the filters. The filters were then removed from reaction cups and placed in sterile scintillation vials with a scintillation cocktail. The samples were then counted by liquid scintillation counting. The dilutions were scored positive or negative for respiration compared to 3X the standard deviation of the controls.

PLFA analysis was used to determine the viable biomass of run 1 of the box experiments. Phospholipids are found in the membranes of all cells. Under the conditions expected in natural communities, the bacteria contain a relatively constant proportion of their biomass as phospholipids. Phospholipids are not found in storage lipids and have a relatively rapid turnover in some sediments, so the assay of these lipids gives a measure of the viable cellular biomass. Some specific groups of microbes contain characteristic fatty acid profiles. This information can be used to study the community structure of the microorganisms as well. Many subsets of the microbial community respond to specific conditions in their microenvironment with shifts in lipid composition. Insight into the nutritional and physiological status of the microbial community can be determined through application of signature of lipid biomarker analysis. The monoenic PLFA 16:1 ω 7c and 18:1 ω 7c are increasingly converted to cyclopropyl fatty acids Cy 17:0 and Cy 19:0, respectively, in gram negative bacteria as the microbes move to a stationary phase of growth. The proportion of poly- β hydroxyalkanoic acid (PHA) in

bacteria or triglyceride relative to PLFA provides a measure of the nutritional physiological status by indicating unbalanced growth. These changes were monitored during the heating and cooling phases of the experiment to determine the dynamics of the microbial community under a thermal stress.

4.2.4 Nutrient Addition

After the soil stabilized to room temperature, it was left undisturbed for a week to allow the microbes to repopulate. Organic (Nutrient Broth), Inorganic (0.1 N M9 Buffer) and Millipore water have been used as external amendments. This was done to analyze the response of the microbes to the different nutrients after a rigorous heating environment. A drip system was designed out of 1/2 " copper pipe (0.4 m long) to carry out nutrient addition. The perforations on the copper pipe were made using a 1/32" drill and spaced equally on the length of the copper pipe. The soil was flushed with the nutrient until a solution equivalent to one residence period was collected through the drainpipe at the bottom of the box. After the nutrient addition was completed, soil samples were retrieved on a daily basis from the three boxes, and the microbial analysis was continued for a week.

4.2 5 Oven Heating Experiments

A millipore drying oven was used to heat pans of the Dover soil to a range of temperatures. Tin pans containing 20 g of soil were placed in the oven beginning with a temperature of 30°C. The soil was allowed to heat for 1 week. CFU, AODC and MPN analysis were performed on the samples. This process was continued until oven

temperatures reached 60 °C. The results of microbial activity analysis on the heated soil were compared to the CFU and AODC analysis of the initial, unheated soil.

A drying oven set at 100°C was used to heat Dover soil samples for 1 day and 1 week. After each heating, CFU and AODC counts were done to determine the number of bacteria surviving, as compared to CFU and AODC counts on unheated soil.

A tin pan containing 250.0g of soil was autoclaved 3 times; once on each of 3 consecutive days. After each heating, CFU counts were done to determine the number of bacteria that survived the heating. This number was compared to original CFU counts on unheated soil.

A muffle furnace with a temperature of 340 °C was used to heat a 100-g soil for 1 hour. After the heating event, CFU counts were taken to determine the number of surviving microorganisms.

4.3 Materials

4.3.1 Scanning Thermometer and Thermocouples

A 12 port Cole Parmer Digisense temperature scanner read the temperature and interfaced with a computer to give real time data. The principle function of the scanner was to monitor up to 12 temperature sensor channels virtually simultaneously by first rapid scanning and then display/printout/ data logging each sensor channel at a slower rate. The thermocouples were connected through ANSI mini-connectors on the rear panel to provide quick hookup and changing of thermocouples. Each thermocouple was automatically read at the rate set by the thermocouple read time in the setup mode. The

auto alarm system provided instant audible and visual notification of an out-of-specification temperature condition or if an open thermocouple was present.

4.3.2 Configuration of Power Supply and Electrodes

A variable power supply capable of supplying 240 V at up to 10 A was used to inject electric current at 60 Hz between the two electrodes. The voltage was read by connecting the poles of the multimeter directly to the power source. Distilled water (2.5 l) was added to the soil before startup to provide adequate moisture for conduction of electricity. The tops of the boxes were sealed to prevent moisture loss from the box. The electrodes were fabricated out of stainless steel and placed at the ends of the box.

4.3.3 Soil Characteristics

For these experiments, two sets of soil were used. The first set was a sandy clay loam soil obtained from Dover Air Force Base in Dover, Delaware. It was received on April 28, 1998 and stored in an incubator at 4 °C until use. The soil was homogenized using a 16 U.S.A. standard testing sieve (A.S.T.M.E.-11 specification). The depth at which the soil was taken is 18 inches at a location 120 feet northwest of a resistive heating cell. This soil was heated by the millipore oven, drying oven, autoclave and muffle furnace methods.

For the box experiments, two sets of vadose zone sandy loam soil were collected from the piedmont region of North Carolina and were stored at 4 °C until use. Soil was homogenized using a 16 U.S.A. standard testing sieve (A.S.T.M.E.-11 specification). Table 4.1 presents the properties of both soil sets before heating.

Table 4.1 Properties of the Characterized Soil

Characteristic	Dover Soil	Box Soil
Organic Carbon	6.7%	4%
Particle Density	2.65 g/cm ³ *	2.65 g/cm ³
pH	6.11	7.49
Moisture Content	11%	4%
Particle Size	68% medium sand	81% medium sand
Distribution	8% fine sand	14% fine sand
	9% very fine sand	4.5% very fine sand
	15% silt and clay	0.6 % silt and clay

*Particle density values average 2.65 g/cm³, but may be lower in soils that contain heavy minerals such as iron oxides.

CHAPTER 5

RESULTS AND DISCUSSION

In this chapter, the results of this study will be presented and analyzed. There are three parts to this chapter. The first two parts present lab-scale oven and resistive heating experiment results. The third part concentrates on the results of the numerical modeling obtained using FLUENT for single-phase and multiphase simulations by solving the transient mass, momentum, and energy conservation equations in two-dimensional cartesian coordinates for a porous media.

5.1 Oven Experiments for Dover Soil

AODC analysis was performed for the Dover soil heated by the millipore oven from ~22 to 60 °C. The results show the overall trend of decreasing microbial counts with increasing temperature in nearly a linear pattern. From the initial, pre-heating sample count of 661.86 microorganisms/g 10^2 , the final count after heating was 261.67 microorganisms/g 10^2 . A drying oven was used to heat the samples at 100°C. Samples were first heated for 1 day and 1 week. Since the drying oven was used to heat the samples, there was a concern that lack of moisture may influence lower microbial counts. To test for this, water was added to additional samples to increase their moisture contents to between 33 and 64%. These samples were heated for one day and one week and were called the wet samples. The initial AODC count for the experiment was 661.86 microorganisms/g 10^2 . The 1-day dry sample yielded counts of 354.02 microorganisms/g

10². The 1-week dry sample yielded slightly lower counts at 315.54 microorganisms/g 10². All of the water amended samples produced microbial counts much lower than the dry samples of the previous trial. The average of the counts for the 1 day wet samples was 130.8 microorganisms/g 10². The average of the 1 week wet samples was 112.1 microorganisms/g 10².

To achieve heating to temperatures higher than 100°C, samples were heated by autoclave or by muffle furnace, which allowed for temperatures up to 340°C. AODC analysis for both experiments showed no detectable survival of microorganisms.

CFU analysis yielded similar results to the AODC analysis. For samples plated on nutrient agar and incubated at the temperature to which the soil was heated, there was a gradual, steady decline in counts from the initial sample count of 996.97 CFU/g 10⁴ until 0 CFU/g 10⁴ after the final sample was taken at 100°C. For soils incubated at 20 °C, an increase from the initial sample counts was seen up to 30 °C, after which a sharp decline occurs until negligible counts at 100 °C. On R2A agar for both incubation profiles, the higher initial count of 1968.18 CFU/g 10⁴ is maintained with only slight declines until the 40 °C sample, after which the sharp decline occurs until counts reach 0 CFU/g 10⁴ at 100 °C. For the samples heated by autoclave and muffle furnace, no detectable surviving CFU were found from the plate counts.

The results of the MPN analysis show an increase in counts from the initial, non-heated sample count of 188.5 microorganisms/g to 3,838 microorganisms/g for the sample heated at 30 °C. This increase is consistent with the results found by Jorergensen

et al. (1990). After the 30 °C sample, microbial counts decrease linearly down to the final 100 °C sample, with a count of 0.177 microorganisms/g.

In summary, with each method of analysis, the microbial response to heating at increasing temperatures up to 100 °C is to decrease in size. These results are consistent with those found in the literature (Diaz-Ravina et al., 1996; Joergensen et al., 1990; Tu, 1982).

According to Dunn (1985), microorganisms can become dormant in response to dry conditions. Originally, the nutrient broth and M9 Buffer were added in their full concentration. This resulted in CFU counts greater than could be analyzed (greater than 300 CFU/g at the 10^6 dilution). The recipe for nutrient broth was then diluted to 1/100 of its full concentration and the M9 Buffer diluted to 1/10 of its full concentration. This resulted in more manageable CFU counts. The rate at which the nutrients stimulated growth can not be determined by our results due to the variability of counts from day to day. This is a similar result to that found by Carmichael and Pfaender (1997), whose research showed that the effect of a particular supplement was often not uniform within or across soils. They also found that the addition of organic and inorganic supplements did not produce a statistically significant increase of (phenanthrene degrading) microorganisms over the same soils exposed only to distilled water.

5.2 Box Experimental Studies

As explained in the materials and methods section, temperature measurements were carried out in Lexan[®] boxes and thermocouples were arranged in a specific geometry to record the temperature profiles during the resistive heating process. The

resistive heating temperature curve is bell shaped and has three distinct phases, namely the heating, stagnation and the cooling stages (Refer Figure 5.1(a)). The heating phase is

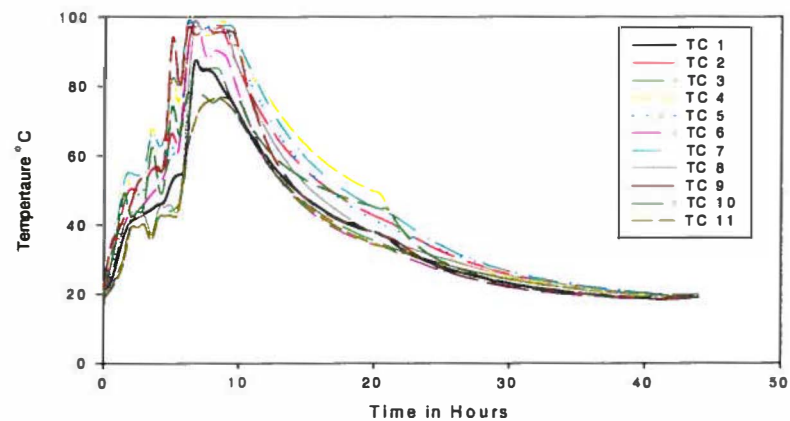


Figure 5.1(a). A typical Resistive Heating Curve Indicating the Heating, Stationary and Cooling Phases

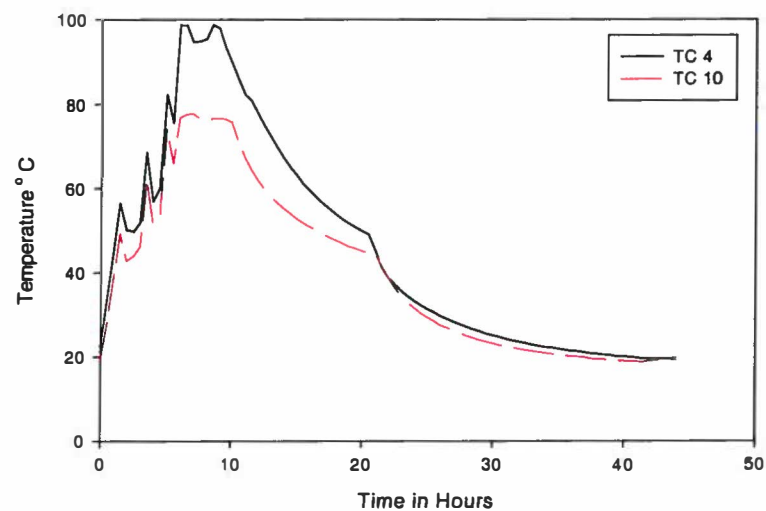


Figure 5.1 (b). Temperature Curve for Thermocouples 4 and 10

the region in which the temperature increased from room temperature to around 100 °C. The duration of this phase is typically 12-14 hours. To expose the microbes to a harsh thermal stress, the temperatures were held at around 90- 100 °C for a period of 6-8 hours.

The final step in a resistive heating experiment was the cooling phase in which the temperature decreased from about 100 °C to room temperature over a period of 18-20 hours. Overall, a resistive heating experiment lasted 40-60 hours. Figure 5.1 (b) shows the individual temperature curves for Thermocouples 4 and 10. It can be observed that the temperature curves are not smooth. As the temperature increases, the soil water begins to circulate and this movement is associated with a drop in the local temperature. The thermal conductivity of the liquid water is large and acts as a sink for the heat that is input into the system. Thus, temperature gradients develop in the experimental setup. The temperatures at the bottom of the box are relatively less compared to the top of the box. The concentration of liquid water is larger at the bottom of the box during commencement of resistive heating. Hence, a larger sink is available for heat loss at the bottom of the box. So the slope of the heating curve is small for thermocouples 9, 10, and 11.

To estimate the effect of temperature on repopulation rates of microbes, three boxes were used in each experiment. The three boxes were classified according to the nutrient fed after the cooling phase. After the cooling phase, the three boxes were left undisturbed for a period of 1 week. After this time, nutrient addition was carried out in the following manner: an organic nutrient (Nutrient Broth) was added to Box 1, an

inorganic nutrient (0.1 N M9 buffer) was added to Box 2, and deionized Millipore water was added to Box 3. To establish reproducibility of results, two experiments were conducted and were designated as Runs 1 and 2. To analyze the temperature results obtained from these two runs, two approaches can be adopted as discussed next.

5.3 Temperature-Time Curve Analysis

As explained earlier the temperature measurements were recorded at 11 different points in the Lexan Box (Figure 4.2 (a)) during the resistive heating process. It would be a cumbersome task to compare all of these curves for the individual runs. The temperatures at the 11 different locations in the box were averaged to give a mean temperature at each time interval. One data analysis approach involves comparing the different runs for each of the boxes, i.e. replicates of the same nutrient treatment were compared (see Figures 5.2, 5.3, and 5.4). In all these figures the temperature distribution with respect to time is compared with the microbial counts on the same scale. The figure at the bottom indicates the microbial counts obtained from AODC during the heating, cooling, and nutrient addition phases. The drawback of this approach is that the runs were carried out at different times. Even though care was taken to control soil initial properties (physical, chemical and biological), inspection of Figure 5.2 shows that some significant soil property differences did exist. Table 5.1 compares the AODC counts obtained from Boxes 1, 2 and 3 for Runs 1 and 2 at different stages of the resistive heating process. It can be inferred that after the heating and the stagnation phase the microbial numbers decrease. On post-heating nutrient addition, the microbes begin to rebound in all the three treatments. Although there is a scatter in the microbial data, the

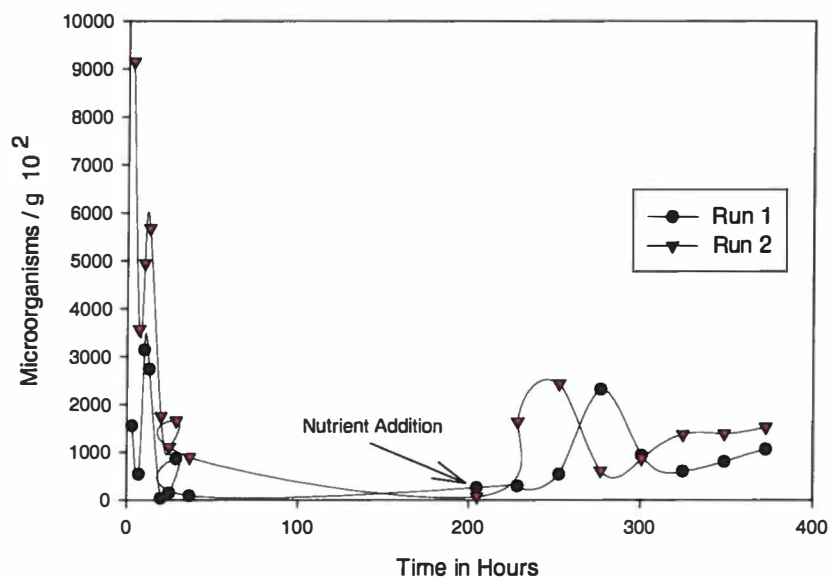
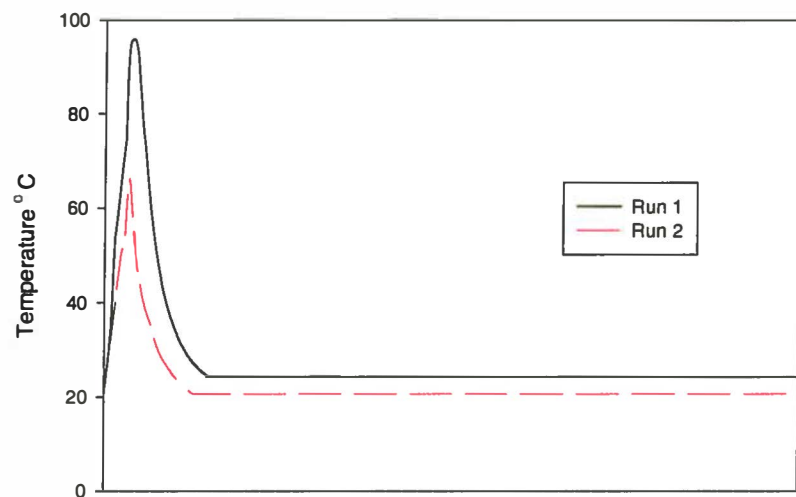


Figure 5.2. Temperature and Count results for Organic Nutrient Treatment (Box 1)

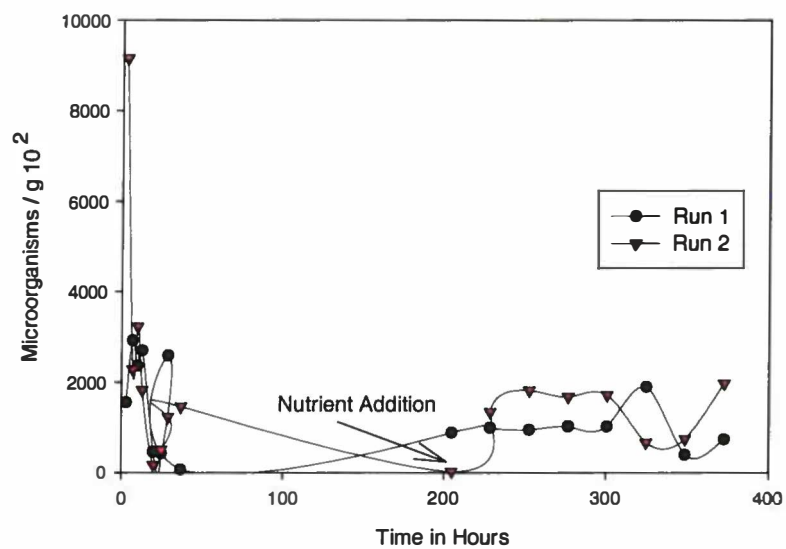
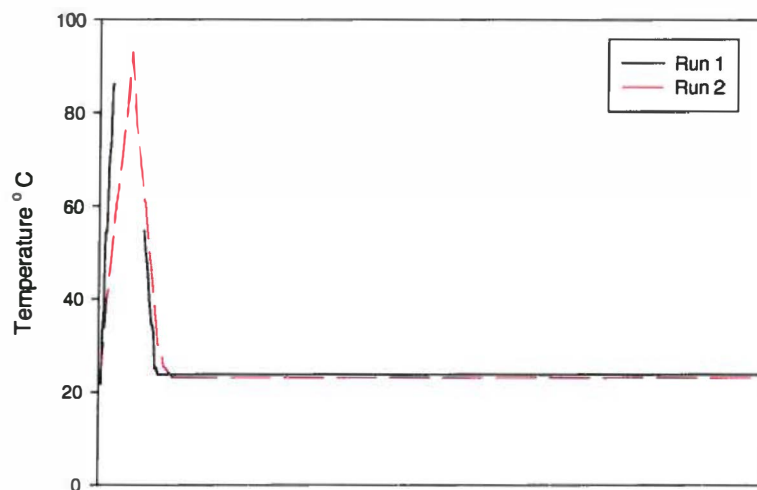


Figure 5.3. Temperature and Count Results for Inorganic Nutrient Treatment (Box 2)

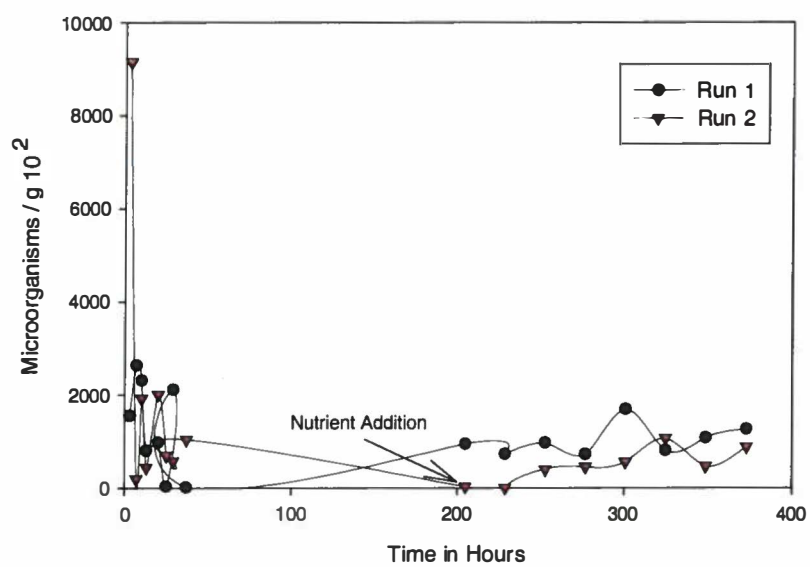
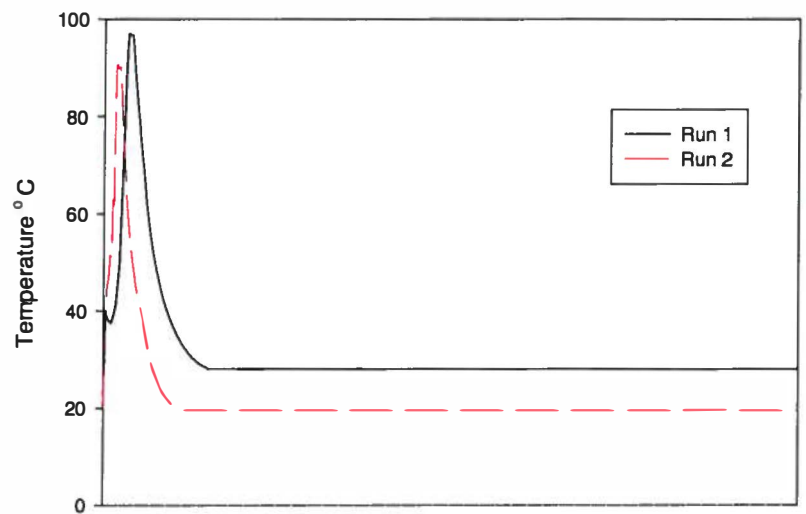


Figure 5.4. Temperature and Count Results for Water Nutrient Treatment (Box 3)

Table 5.1. Summary of AODC Results for Boxes 1, 2, 3 for Runs 1 and 2

Treatment	Initial Count	Count After Stagnation	Count After Cooling	Count At Nutrient Addition	Final Count
Box 1:Run 1	1556.7	33.9	83.8	259	1061.2
Run 2	9151	1753.8	893.6	68.6	1521.6
Box 2:Run 1	1556.7	465.6	70.6	887.5	741.8
Run 2	9151	171.4	1462.4	21.6	1970.6
Box 3:Run 1	1556.7	984.1	17.4	951	1263.8
Run 2	9151	2005.5	1040.4	26.6	882.2

overall trends for Run 1 and 2 for all the nutrient treatments are the same. A more quantitative conclusion regarding the nutrient treatments can be made after studying the PLFA data.

For Box 1, Run 1 reached temperatures near 100 °C whereas for Run 2 the temperature peak is around 70 °C. A possible explanation for this behavior can be attributed to the non-uniform distribution of moisture in the box. Presence of spots where no electrical conduction occurs could have decreased the temperature in the box during Run 2. Stationary phase is well pronounced in Run 1 compared to Run 2. Run 1 can be expected to have lower counts of microbes as to Run 2 because of the longer exposure to the higher temperatures. Results of Box 2 (Figure 5.3) indicate that for Runs 1 and 2 the resistive heating process was completed at a faster rate. A higher heat loss was observed in Run 1 as the cooling gradient is very steep. Run 2 had a very small stationary regime.

Box 3 (Figure 5.4) exhibits similar resistive heating curves for Runs 1 and 2. The only distinguishing feature is the peaks are spaced out in time. In other words the heating phases were of different duration. The stationary regions for all the runs are similar and the cooling rates are also comparable. The microbial counts for all the runs were determined with Acridine Orange Direct Counts (AODC). The microbial counts are measured in the units of microorganisms/g of soil sample. As the temperature increases from room temperature to about 50 °C the AODC counts for all the boxes show a corresponding increase in value. However, as the temperatures increase beyond 75 °C the microbial count starts to drop. The minimum counts are found in the vicinity of 100 °C. The cooling phase is also associated with small microbial counts and can be attributed to death and spore formation. On nutrient addition there is a recurrence of microorganisms in all the three boxes. The AODC counts do not indicate the nature of the microbial community and its structure. To establish this, Phospholipid Fatty Analysis (PLFA) was conducted at the University of Tennessee, Center for Biotechnology. The results of this study are documented in the next section.

In the second data analysis approach the run number is held constant and the temperature curves with respect to time are plotted for Boxes 1, 2 and 3 (refer to Figures 5.5-5.6). Since the soil for a particular run was processed at one time, the variation in soil composition was minimized. This approach also helps to compare the response to microbes to different nutrients on the same scale by comparing the microbial data for each of the boxes (i.e., compare the microbial response to the different nutrient treatments). Figure 5.5 shows the curves for Run 1. Boxes 1 and 3 have identical

temperature response with respect to time. Box 2 had faster heating and cooling rates and the stationary phase is also minimal. Box 1 is amended with organic nutrient (nutrient broth solution). On nutrient addition, repopulation of microorganisms is observed. The highest microbial count was observed for Box 1 on day 3 (2500 microorganisms/g). On day 7, Box 3 showed the highest count (1300) followed by Box 1 (1000) and Box 2 (700). Normally, one would expect the organic or inorganic nutrient treatment to have higher counts than distilled water treatment. However, in this case insufficient availability of nutrients and consequent predation could have caused significant changes in the microbial counts.

Figure 5.6 shows the temperature distribution for Run 2 and the profiles indicate that Box 1 peaks at 60 °C and Boxes 2 and 3 have temperature as high as 100 °C. However, the heating rate is different for Boxes 2 and 3 and the peaks are spaced out in time. Box 2 was amended with 0.1 N M9 buffer solution. After nutrient addition, Boxes 1 and 2 show identical response after day 7. The count for Box 3 remains lower at around 1000 microorganisms/g. The repopulation numbers are higher for Run 2 than Run 1. This is because of the higher initial microbial count in the soil prior to resistive heating.

The spatial orientation of the temperature curves highlights the dependence of the curves on a variety of factors that are very difficult to control under lab conditions. Some of these factors include initial temperature and moisture distribution in soil, thermal conductivity of the soil, liquid and vapor and the influence of the changing temperature on these parameters. To improve on some of these aspects further research is needed into the soil packing and moisture distribution in porous media.

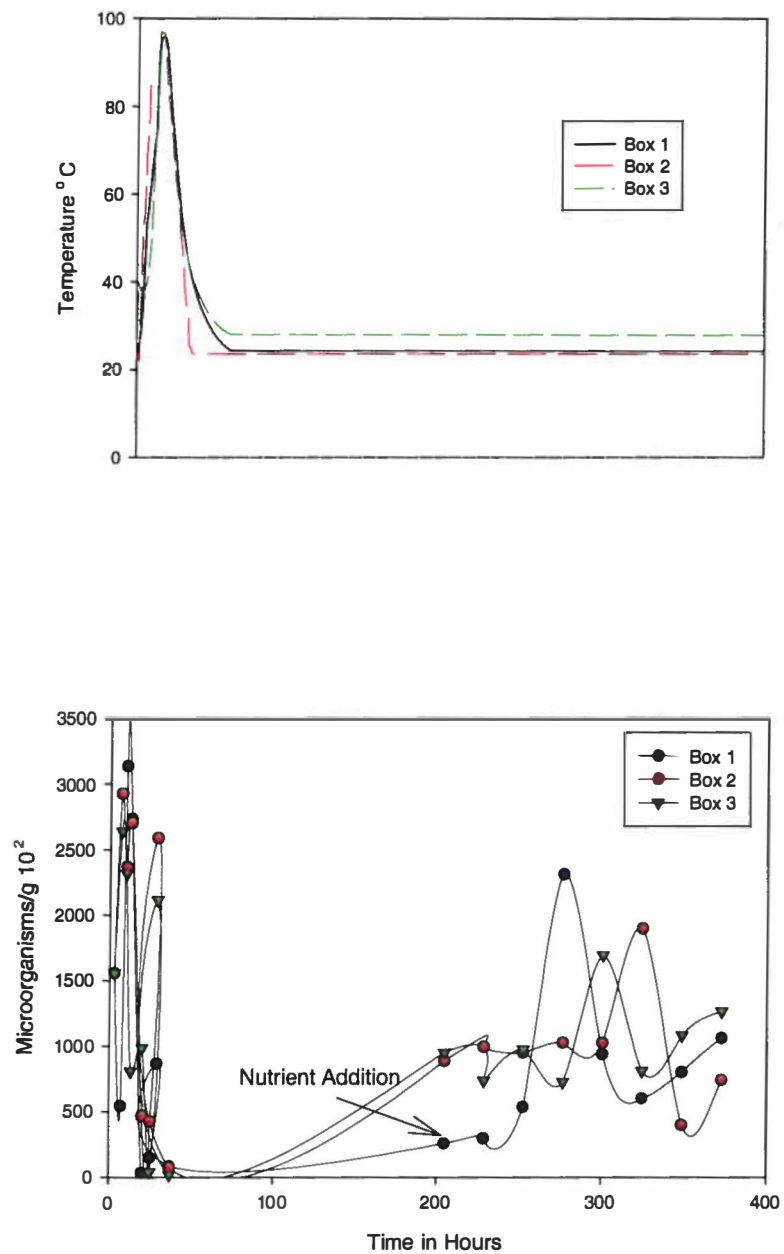


Figure 5.5. Temperature and Count Results for Boxes 1, 2, 3 (Run 1)

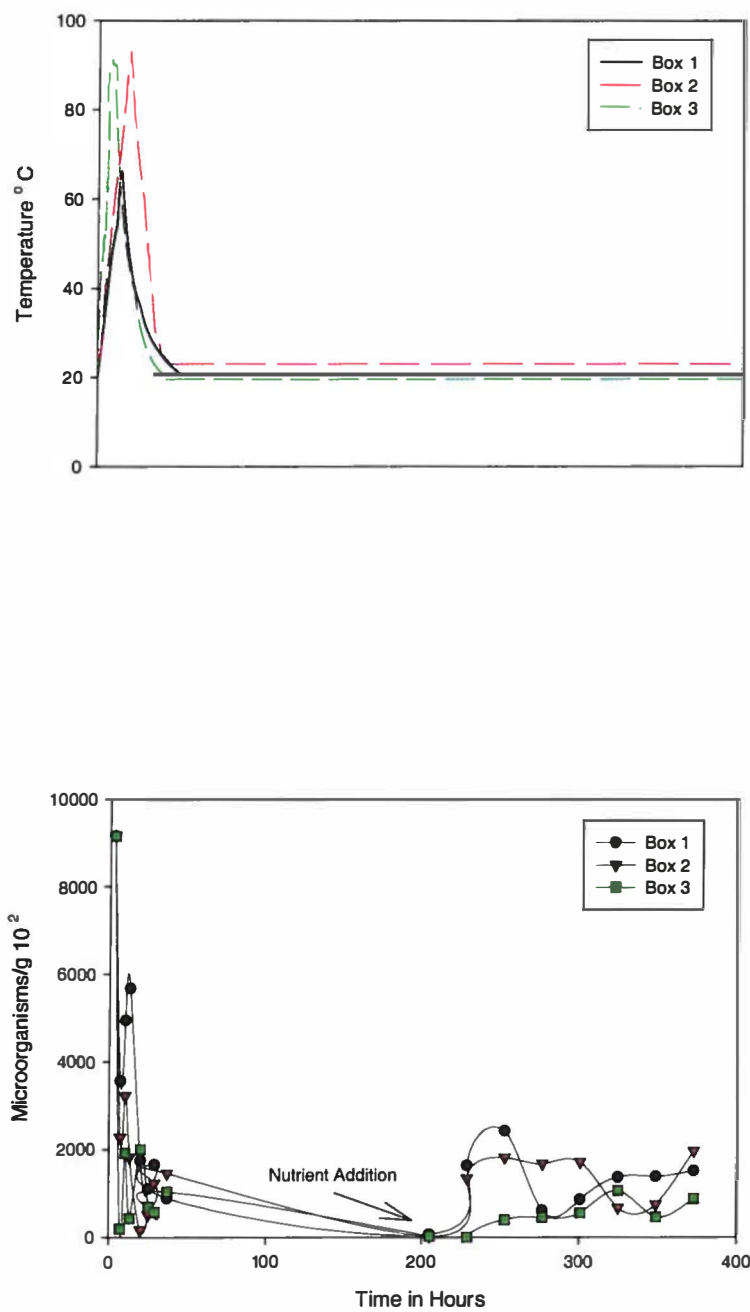


Figure 5.6. Temperature and Count Results for Boxes 1, 2, 3 (Run 2)

5.4 PLFA Results

Phospholipid ester-linked fatty acid analysis (PLFA) gives a quantitative measure of the viable biomass after resistive heating. Figure 5.7 compares the biomass PLFA versus the nutrient treatments for all the three boxes for Run 1. These counts were taken a week after nutrient addition was completed. This was done to give microorganisms adequate time to repopulate. It can be inferred from this figure that the biomass was highest in the initial soil sample and lowest in Boxes 2 and 3. The community structure of microorganisms in soil after resistive heating and nutrient addition is presented in Figure 5.8. Each of the boxes had a unique community structure. The midbranched saturated PLFA indicative of Actinomycete type bacteria showed a similar level in Box 1 to the initial sample and lower counts in Boxes 2 and 3.

Terminally branched fatty acids indicative of gram positive bacteria showed an increase from initial sample to Box 3. Gram positive bacteria are more resistant to environmental factors over gram negative organisms. Monosaturated PLFA indicative of gram negative bacteria showed an opposite trend with Box 1 having a higher count and Box 3 the least. Gram negative organisms are generally faster growing than the rest of the community and take advantage of the added nutrients first. Polyunsaturated PLFA are indicative of eukaryotic organisms. Box 2 had a higher relative proportion than Boxes 1 and 3. This part of the community was able to use the substrate added in Box 2 (0.1 N M9) more efficiently than the rest of the community.

Two measures of nutritional status for the gram-negative community were used. The first (Cy 17:0/16:1 ω 7c) showed lowest turnover from Box 1 to the highest turnover

in Box 3 for that portion of the gram-negative community. The second measure of Cy 19:0/18:1 ω 7c showed Boxes 1 and 3 with higher turnovers than Box 2 for that portion of the gram-negative community. Appendix A (Figures A.1-6) has a compilation of graphs obtained from the PLFA tests.

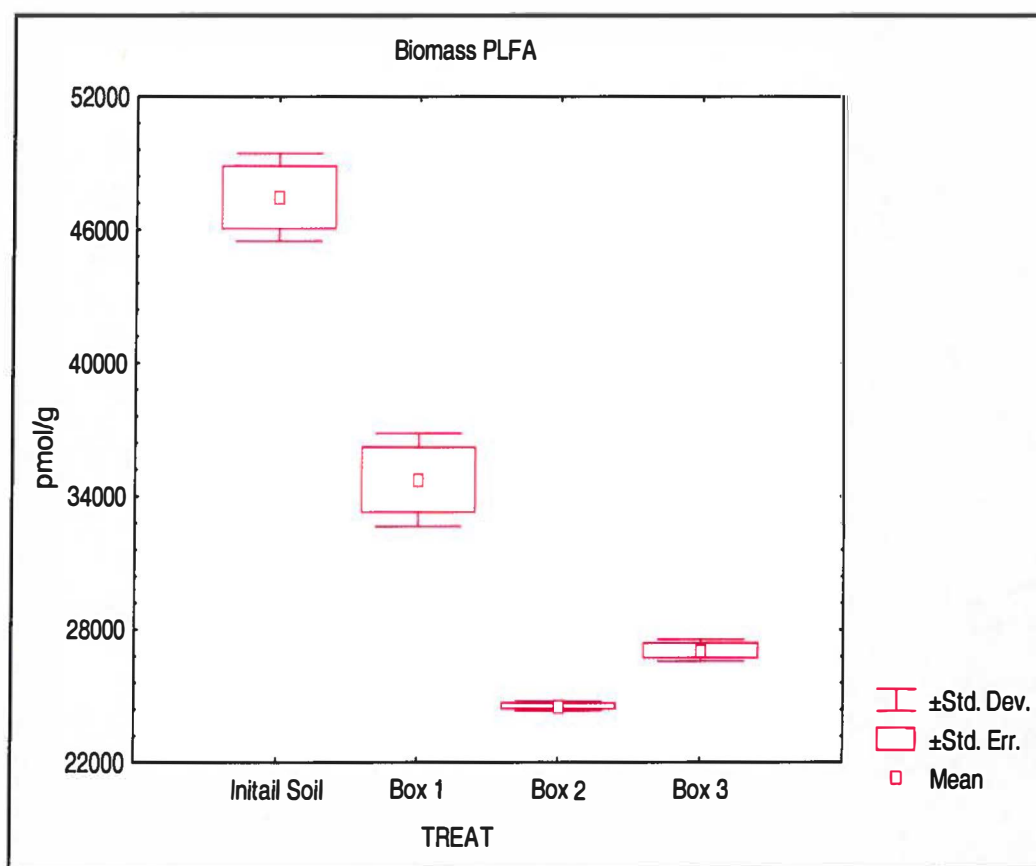


Figure 5.7. Biomass PFLA After Resistive Heating and Nutrient Addition in Boxes 1, 2, 3 (Run 1)

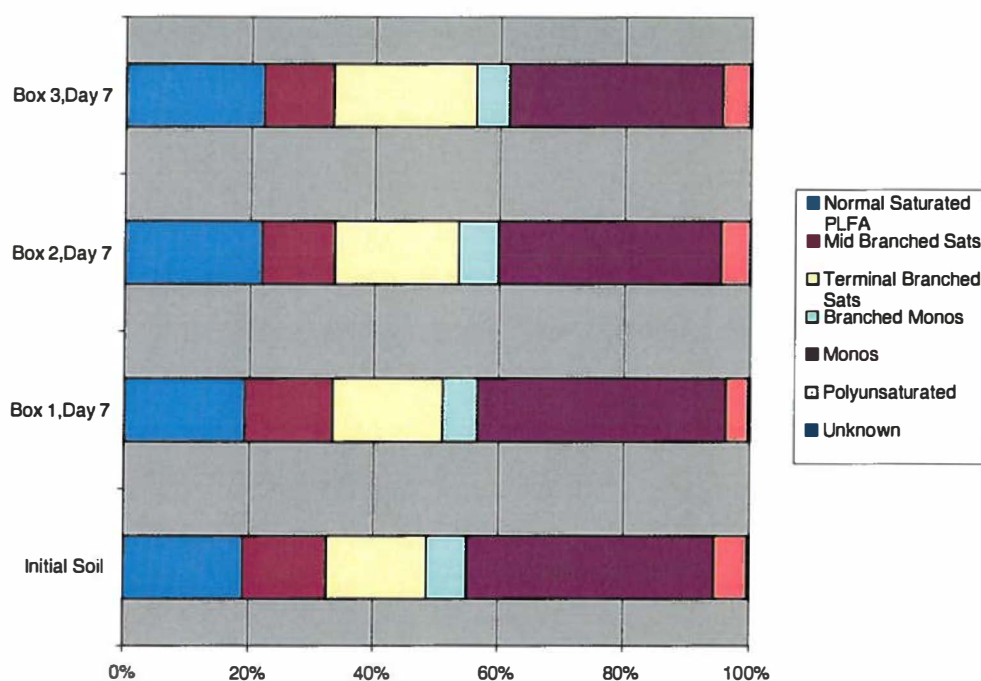


Figure 5.8. Community Structure of Microorganisms in Soil After Resistive Heating and Nutrient Addition

PLFA results indicate the complexity in studying the microbial dynamics during resistive heating. There is a competition for survival when the microbes are exposed to high temperatures. Only the microbes that form spores overcome temperatures as high as 100 °C. When the nutrient addition is started, the microbes sense the favorable conditions and begin to compete for the available nutrients. There is also a high chance of predatory relationships, which explains the high counts at one stage of the process and low counts at another time. In the next section, we try to compare the numbers obtained for the plate counts, AODC tests and PLFA analysis.

Table 5.2. Comparison of Initial and Final Counts (Plate Counts, AODC, PLFA)
for Run 1

	Initial Counts (Microorganisms/g)			Final Counts(Microorganisms/g)		
	Plate Counts	AODC	PLFA	Plate Counts	AODC	PLFA
Box 1 10 ⁴	2.6 x 10 ⁷	10 x 10 ⁴	9.2 x 10 ⁴	1.4 x 10 ⁸	1.1 x 10 ⁵	6.8 x
Box 2 10 ⁴	2.6 x 10 ⁷	7.5 x 10 ⁴	9.2 x 10 ⁴	2.6 x 10 ⁸	8 x 10 ⁴	4.8 x
Box 3	2.6 x 10 ⁷	6 x 10 ⁴	9.2 x 10 ⁴	1.5 x 10 ⁸	1.2 x 10 ⁵	5.4 x 10 ⁴

5.5 Comparison of PLFA and AODC Results

Table 5.2 compares the microbial counts obtained by the plate counts, AODC counts and PLFA analysis. The initial and final counts have been compared in the units of microorganisms/g. A conversion unit of 2×10^{12} was used to convert the PLFA counts from picomol/g to microorganisms/g (Balkwill, 1988). It can be seen that both the AODC and PLFA methods yielded comparable counts. The plate counts yielded a very rough estimate of the microbial population. Hence, these numbers vary from the AODC and PLFA numbers by a few orders of magnitude. It can be inferred that for both the AODC and PLFA methods the initial counts are higher than the final counts. This is consistent with the trends expected in resistive heating.

5.6 Theoretical Results

In this section, the results obtained through the FLUENT simulations will be presented, and comparison between the experimental and theoretical results will be made.

Two Models were used for generating the temperature distribution in porous media using FLUENT. The first model is a single-phase approach in which soil is considered as a porous medium with constant physical properties. For the numerical solution, heat transfer was the only driving force that was included. In the second model, driving forces of heat and mass transfer were incorporated and a multiphase Eulerian approach was used for the simulation. Adiabatic and non-adiabatic calculations have been performed to determine the effect of heat loss from the box on the temperature distribution in the box. The electrodes were patched as a volumetric heat source (6000 W/m^3) inside the grid. The value of the heat source was derived using a simple calculation. The product of the voltage and current gives the power output in the units of watts. This value was divided by the volume of soil to give the result in terms of W/m^3 . For the calculations, a voltage of 240 V and resistance of 500 ohm was used with dimensions of the electrodes being 0.5 m X 0.5 m X 0.1 m. The effect of the position of the electrodes on the temperature distribution in the grid is discussed in section 5.5.2. Transient solution was obtained with the time step of 700 seconds for the single-phase calculations. Space and time step sensitivity is discussed in the next section. The following table (Table 5.3) is the set of physical property data that were used for the simulations. These values are applicable to clay soils and have been adopted from Jumikis (1966) and Mitchell (1976). For the dispersed second phase, the properties of water were used. The values are documented in Table 5.4

Table 5.3. Physical Property Set Used for FLUENT Simulations

Property	Units	Max. Value	Midpoint	Min. Value
Porosity	m ³ /m ³	0.6	0.5	0.4
Density	kg/m ³	2600	2200	1800
Permeability	m ²	1x10 ⁻⁷	1x10 ⁻⁸	1x10 ⁻⁹
Thermal conductivity	W/m-K	3	1.625	0.25
Specific heat of soil	J/kg-K	1000	800	600

Table 5.4. Physical Property Data for Liquid Water Used for the Dispersed Phase

Density	1000 kg/m ³
Thermal Conductivity	0.6 W/m-K
Viscosity	9 X 10 ⁻⁴ kg/m-s
Specific Heat	4180 J/kg-K

5.6.1 Grid and Time Step Sensitivity Analysis

One of the important problem solving steps in FLUENT is the determination of the grid size to be used in the numerical calculations. The grid and time step sensitivity tests were performed in FLUENT for the adiabatic settings on Model I (heat transfer only) with standard parameter values for clay soils (midpoint values of Table 5.3). For a fixed value of the time step of iteration (t=700 seconds), the space step was varied and the maximum and minimum temperatures recorded in the calculation were recorded. A heat source of

6000 W/ m³ was used for the heat source. The results of the grid sensitivity study are summarized in Table 5.5 and Figure 5.9.

Table 5.5. Grid Sensitivity Analysis in FLUENT

Run No	Grid Size	T Max. (K)	T Min. (K)
1	10 x 10	373.10	354.71
2	16 x 16	373.53	354.95
3	20 x 20	373.99	355.01
4	26 x 26	373.93	354.98
5	30 x 30	373.82	354.93
6	34 x 34	373.92	354.95

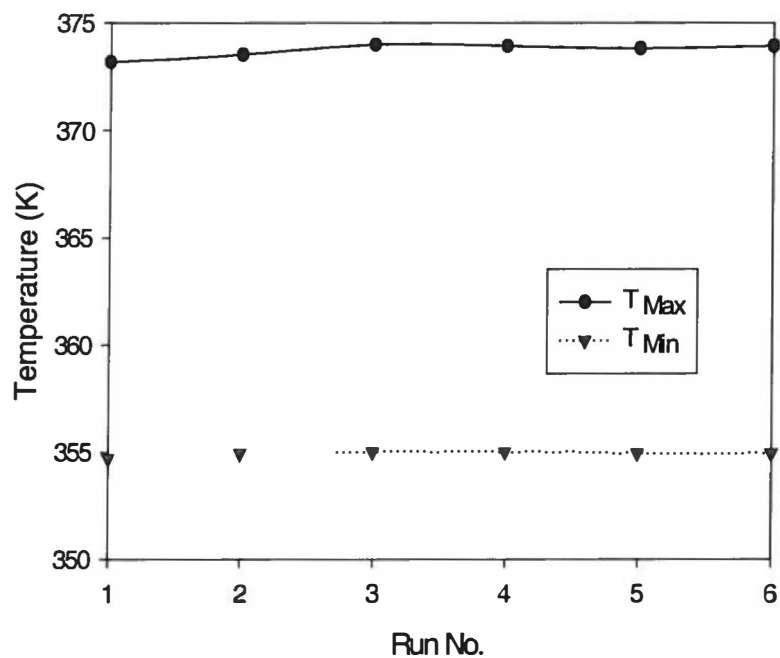


Figure 5.9. Grid Sensitivity in FLUENT

It can be observed that for the different grid sizes the temperatures (maximum and minimum) converge around the same value. This is an indication of convergence. However, it should be noted that further refining of the grid would not be a healthy practice as problems might arise in the convergence of the solution. For this reason a grid size of 30 x 30 cells was adopted for this particular study with the dimensions of the grid made to match that of the experimental box. This helps in correlating the heating and cooling events in both the numerical grid and the actual experimental setup. A typical temperature-time plot recorded at grid point 14 x 14 for low value of soil properties and adiabatic conditions is presented in Figure 5.10. No oscillations are observed in the temperature curve. This was an indicator of a good solution.

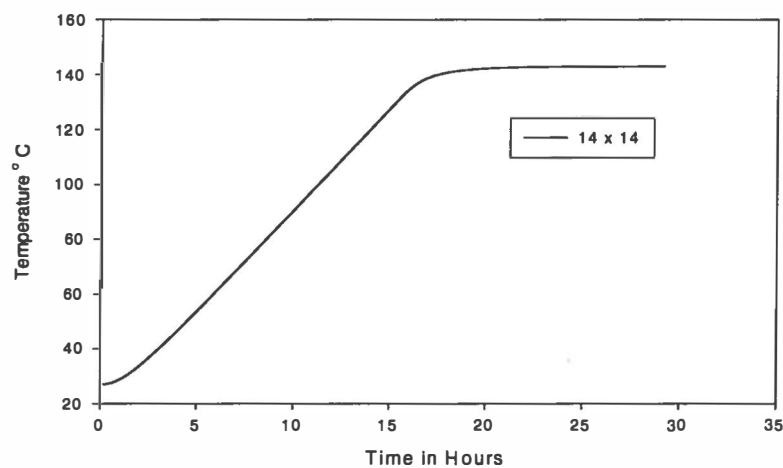


Figure 5.10. Temperature Curve at Point 14 x 14 for Adiabatic Conditions and Low Values of Soil Properties

On completion of the grid sensitivity test, the time step was varied holding the space step constant at 30 x 30 cells. The time step was varied in the vicinity of 700 seconds (Figure 5.11 and Table 5.6). The maximum and minimum temperatures observed under these settings showed convergence. Based on the results, a time step of 700 seconds was used for the single-phase simulations.

Table 5.6. Time Step Sensitivity on a 30 x 30 Grid

Run Number	Time Step (s)	T Max. (K)	T Min. (K)
1	680	369.14	346.95
2	690	369.27	347.07
3	700	369.38	347.18
4	710	369.47	347.28
5	720	369.58	347.41

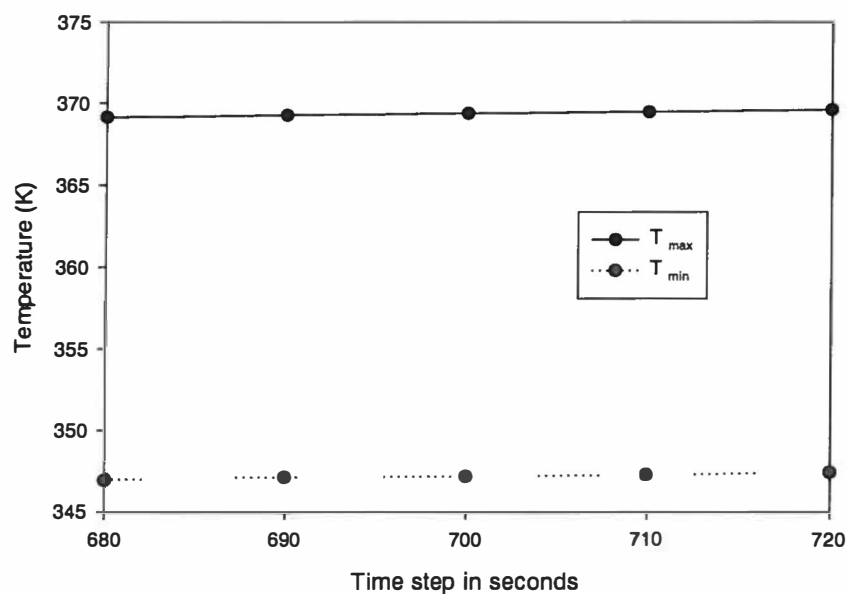


Figure 5.11. Time Step Sensitivity on a 30 x 30 Grid

5.6.2 Effect of Varying Heat Source Location in the Grid

In the model for resistive heating, two heat sources (electrodes) are placed in the grid at a specified distance from the wall cell. A volumetric heat source is patched in these cells. The position of the electrodes affected the temperature distribution during the heating and cooling stages. One method of estimating the effect of changing the electrode position in the grid was to monitor the maximum and minimum temperatures at the end of the heating and cooling stages. Figures 5.12 and 5.13 depict the sensitivity of temperature to the electrode position for the adiabatic and non-adiabatic cases, respectively. These simulations were carried out for model I (single phase) at the midpoint values of soil properties. A volumetric heat source of 6000 W/ m³ was used. In the non-adiabatic case, an external heat transfer coefficient determined the rate of heat loss from the box. In both adiabatic and non-adiabatic cases, with increase in distance of the heat source from the wall there is a corresponding increase in the maximum temperature. This suggests that for the same set of parameters, altering the electrode position can achieve higher temperatures in the grid. As the electrodes were further moved from the wall, there was a point of inflection around 0.1 m from the wall. The temperature starts to drop from this point. In the adiabatic case, as there is no external heat loss, the cooling curve equilibrates between the maximum and minimum temperatures and reaches a steady value. For the non-adiabatic case, there exists a temperature gradient between the grid and the surroundings and hence, separate curves are present for the maximum and minimum temperatures. In the remainder of the

calculations, the electrodes were placed at a distance of 0.05 m from the wall. This is approximately the location of the electrodes in the lab-scale experimental setup.

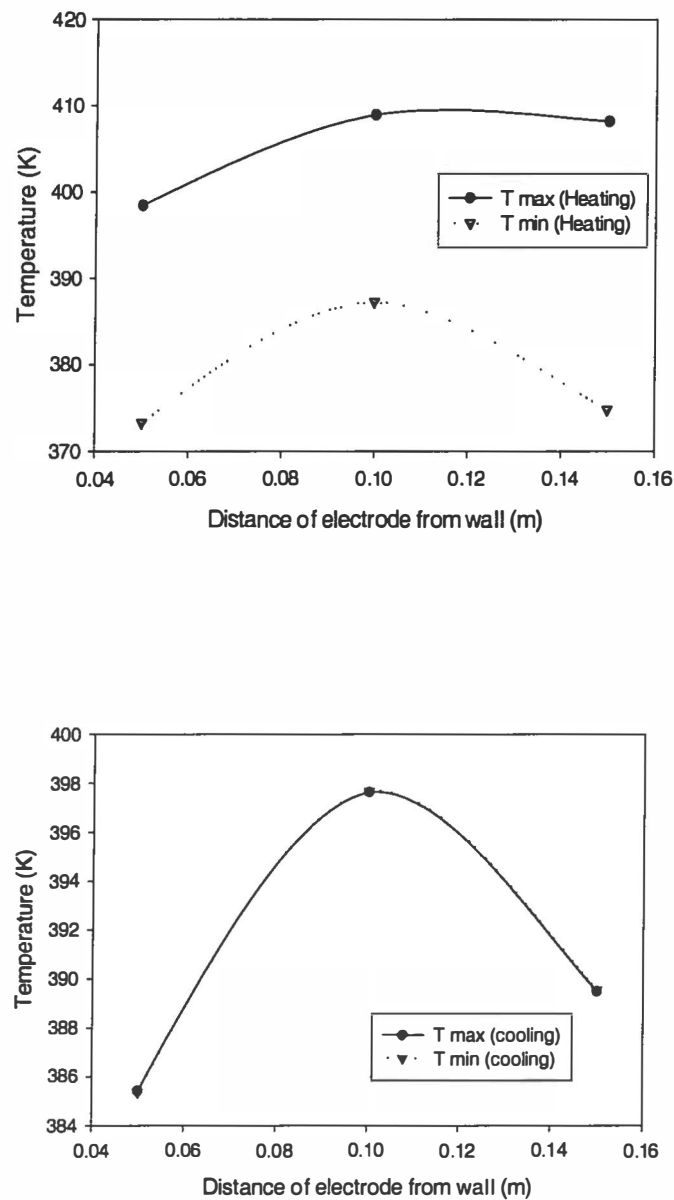


Figure 5.12. Effect of Electrode Position on T_{\max} and T_{\min} During Heating (15 hours) and Cooling (19 hours) Under Adiabatic Conditions

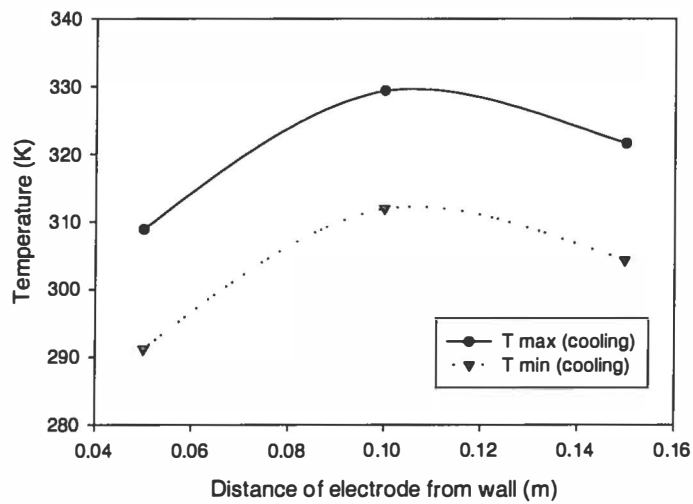
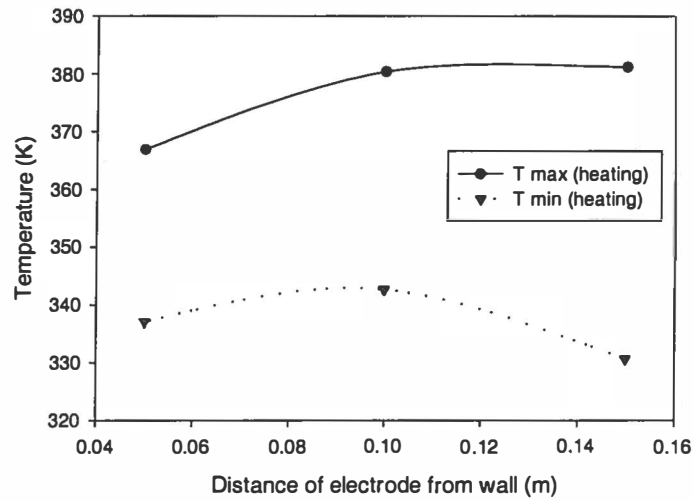


Figure 5.13. Effect of Electrode Position on T_{\max} and T_{\min} During Heating (15 hours) and Cooling (19 hours) Under Non-Adiabatic Conditions ($h = 5 \text{ W/m}^2\text{-}^\circ\text{C}$)

5.6.3 Physical Parameter Sensitivity

FLUENT simulations were carried out at the maximum, midpoint and minimum values of the soil properties (Table 5.3). For the heating phase, a volumetric heat source of 6000 W/m^3 was used. Before these simulations were executed, the effect of varying the heat transfer coefficient for non-adiabatic cases was studied for the midpoint values of soil properties. Figure 5.14 shows that as the heat transfer coefficient from the wall is increased (i.e., as heat loss increases) the maximum temperatures in the box drop to lower values. Based on this information a heat transfer coefficient of $5 \text{ W/(m}^2 \cdot ^\circ\text{C)}$ was used for the simulations. Under these conditions, the theoretical curves matched the experimental temperature curves.

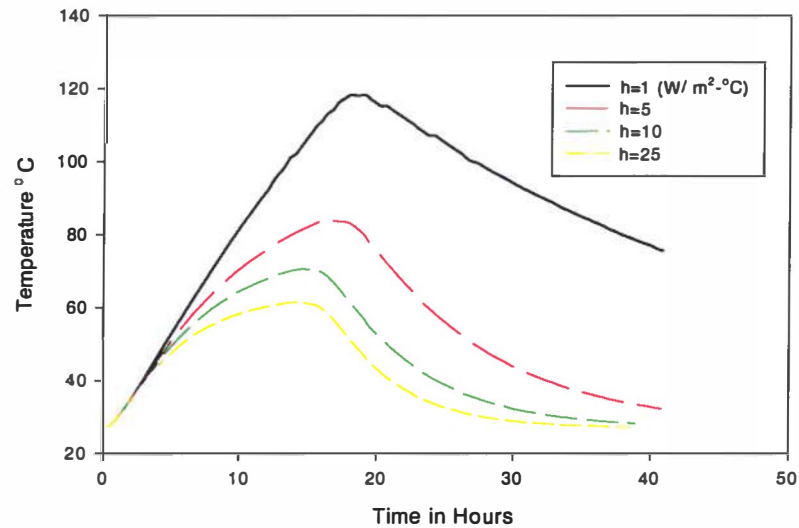


Figure 5.14. Effect of Varying Heat Transfer Coefficient at the Walls on the Temperature Distribution in Porous Medium at Grid Point 14 x14

Instead of the convective heat wall boundary condition an alternate method can be used. In this method, the heat flux at the wall is specified as a percentage of the volumetric heat supplied. A case of 2 % heat loss is presented in the Figure 5.15 for non-adiabatic case and midpoint values of soil properties. The two-dimensional plots for the temperature were recorded at various locations in the grid. In such a model, the heat loss is fixed irrespective of the temperature gradient existing between the wall and the surroundings. An important aspect worth mentioning is the slope of the cooling curve. Since a Newtonian cooling is not activated for this model, there is a steep fall in the temperature rather than an exponential fall.

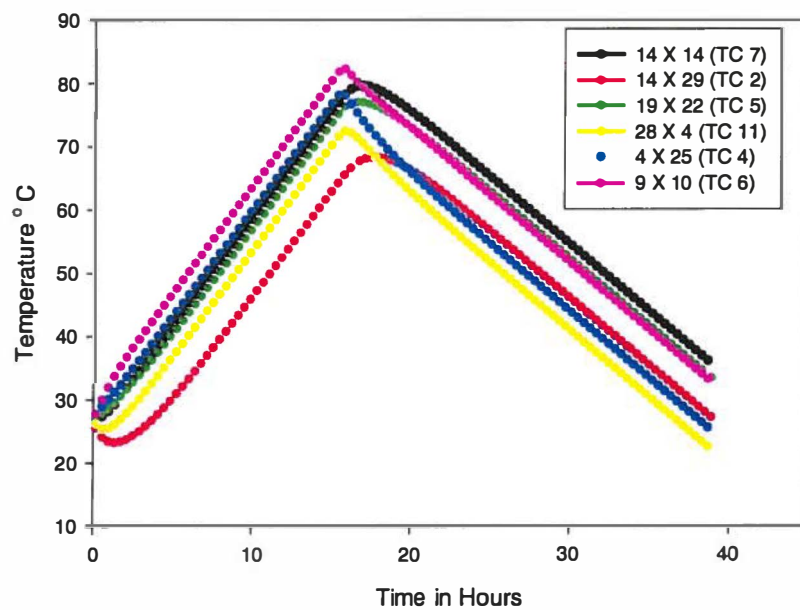


Figure 5.15. Temperature-Time Distribution for the Non-Adiabatic Case and Midpoint Values of Soil Properties

The total number of iterations for the single-phase simulations was chosen in such a way that the duration of the simulations was comparable to the experimental heating and cooling duration. This amounted to 80 iterations for the heating regime and 100 iterations for the cooling regime. The only difference between the different runs is the values for the porous medium that were used for the simulations. A typical temperature contour obtained after the heating regime under non-adiabatic conditions for the midpoint values of soil properties is illustrated in Figure 5.16. It can be observed that the hottest regions are near the electrodes. As we progress towards the center of the box, relatively cooler regions appear. The maximum temperature obtained in the non-adiabatic run is 367 K near the electrodes (indicated by red) and the minimum is 337 K at the center of the box (indicated by blue). The stationary phase is modeled by reducing the value of the heat flux that was patched in the grid cells. A value of 4500 W/m^3 was used to generate the flat portion of the resistive heating curve. With the use of this volumetric heat generation we can approximately match the rate of heat generation and heat loss. Thus, a phase of constant temperature appears. Once the heating is complete, the patched values of the volumetric heat source are set to zero. The cooling phase starts from the established heating profile. This is an important design aspect because we would like the cooling to progress from an already established heating profile rather than assuming a constant temperature throughout the box. The cooling profiles are shown in Figure 5.17.

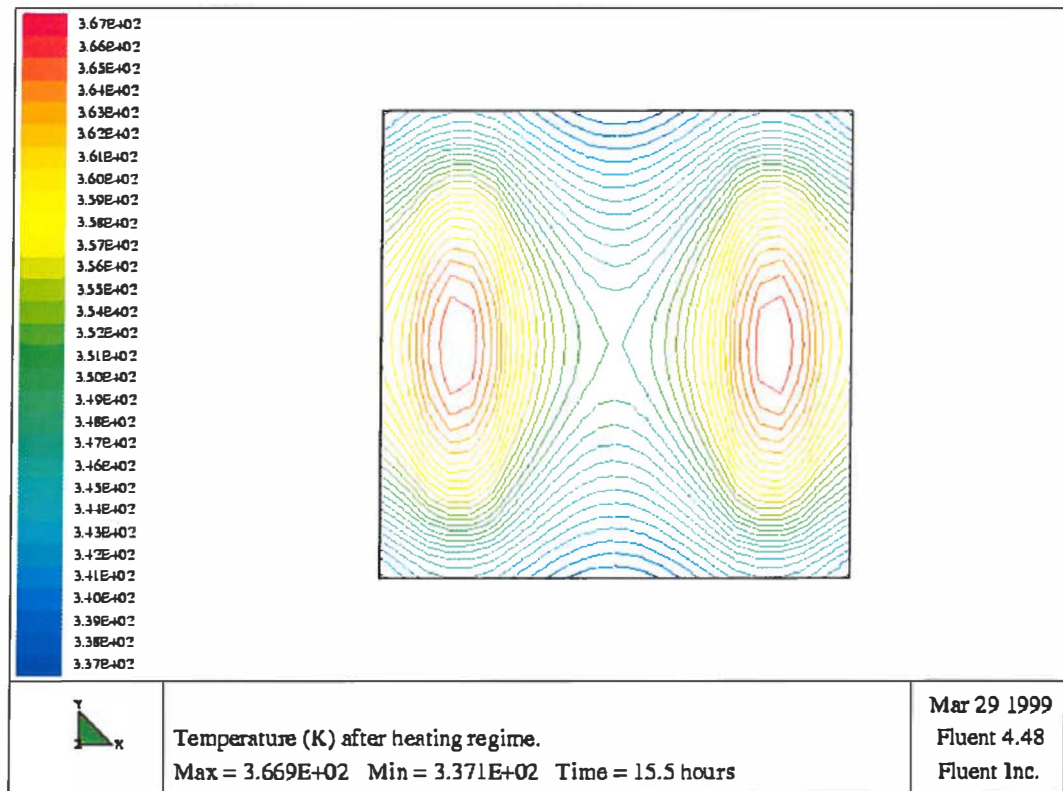


Figure 5.16. Temperature Contour in Grid After Heating Regime Under Non-Adiabatic Conditions with Midpoint Values of Soil Properties and $h = 5 \text{ W/m}^2\text{-}^\circ\text{C}$

Cooling brings down the box temperatures from a high value of 367 K to a maximum value of 347.78 K at the center of the box after 20.42 hours. As cooling proceeds to 38.88 hours the temperature profile has a maximum value of 309 K. The minimum temperature of 291 K is observed along the corners of the grid. At 20.42 hours, the cooling contour is elliptical and the final cooling contour is in the form of a circle. For the adiabatic simulations, similar profiles are obtained, but since there is no heat loss, the observed maximum and minimum temperatures are much higher than the

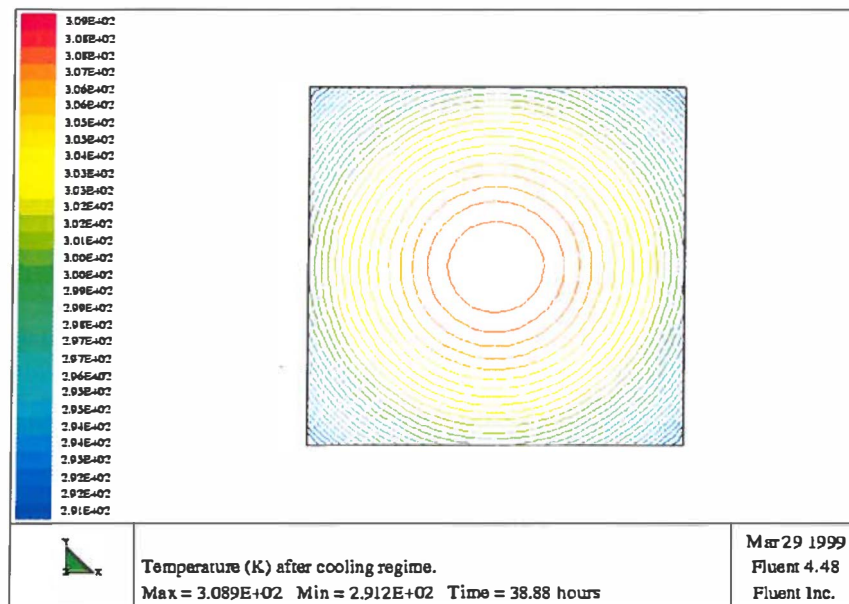
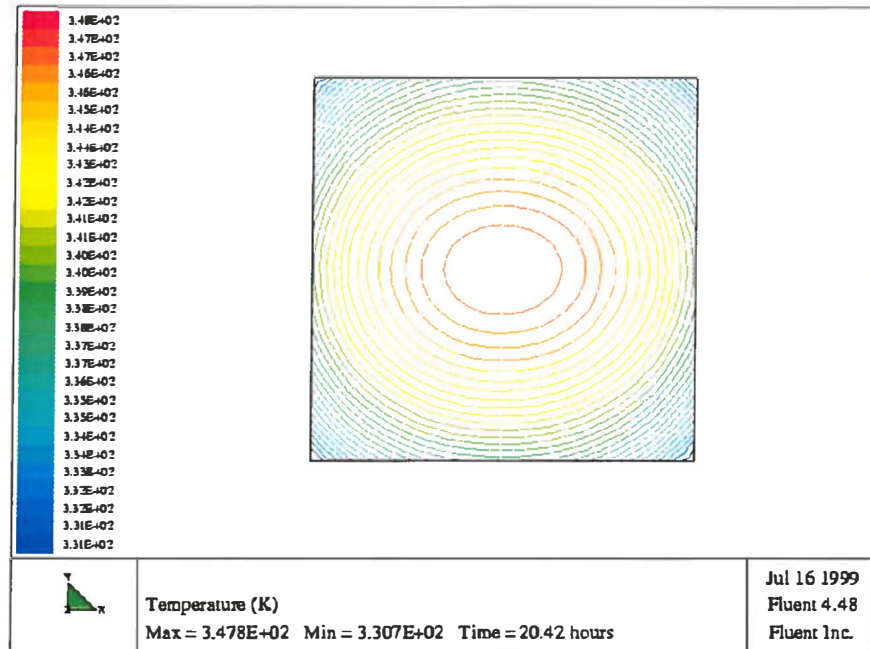


Figure 5.17. Temperature Contour in Grid After Cooling Phase at 20.42 hours (top) and 38.88 hours (bottom) Under Non-Adiabatic Conditions with Midpoint Values of Soil Properties and $h= 5 \text{ W/m}^2\text{-}^\circ\text{C}$

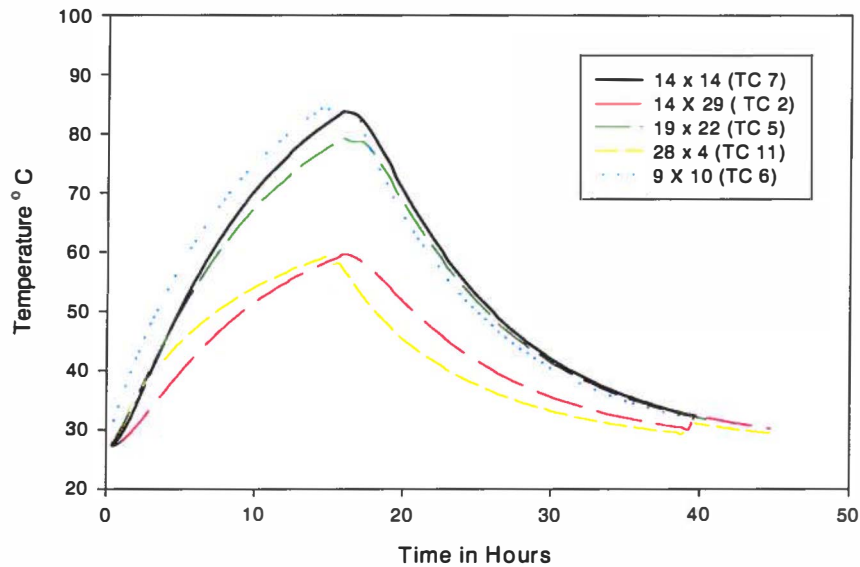


Figure 5.18. Temperature-Time Distribution for the Non-Adiabatic Case and Midpoint Values of Soil Properties

non-adiabatic case. FLUENT has the capability of storing the temperature-time data in the form of a XY plot. This feature can be used to store temperature readings with respect to time at various points in the grid similar to the thermocouple measurements at various locations in the box. Figures 5.18, 5.19, and 5.20 are XY-plots made for the non-adiabatic case and midpoint, maximum and minimum values of soil properties, respectively. The temperature gradients existing inside the grid are established by such a depiction. The temperature curves were monitored at 5 different grid points. The corresponding thermocouple positions in the experiment are indicated by the side.

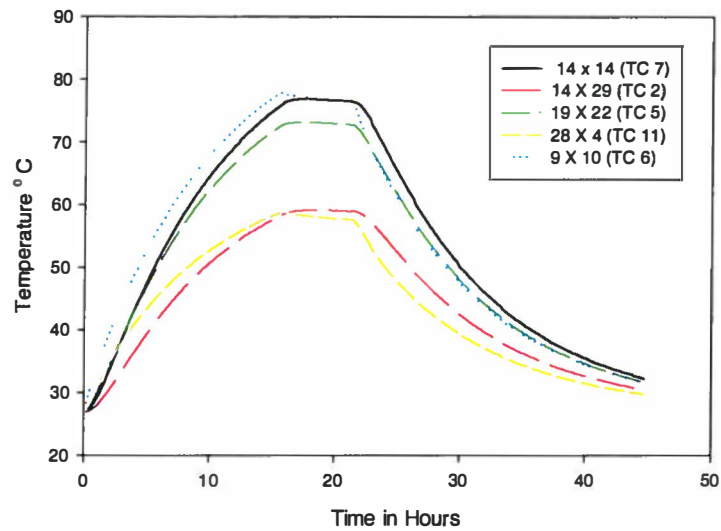


Figure 5.19. Temperature-Time Distribution for the Non-Adiabatic Case and Maximum Values of Soil Properties

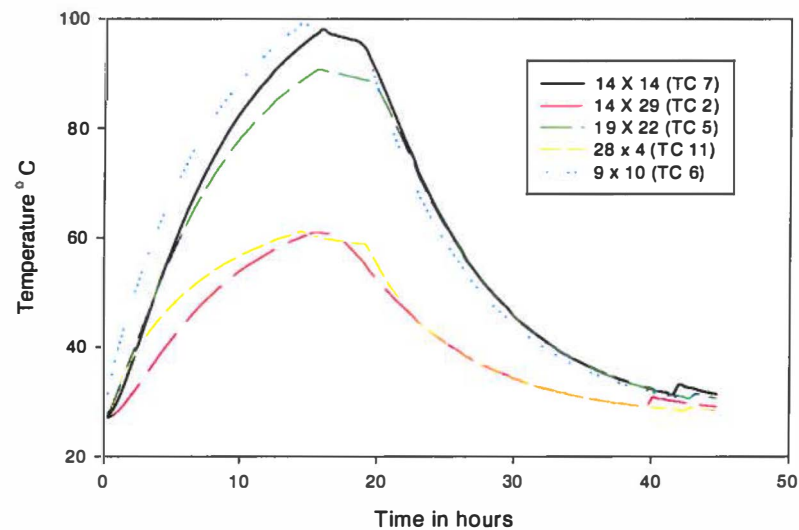


Figure 5.20. Temperature-Time Distribution for the Non-Adiabatic Case and Minimum Values of Soil Properties

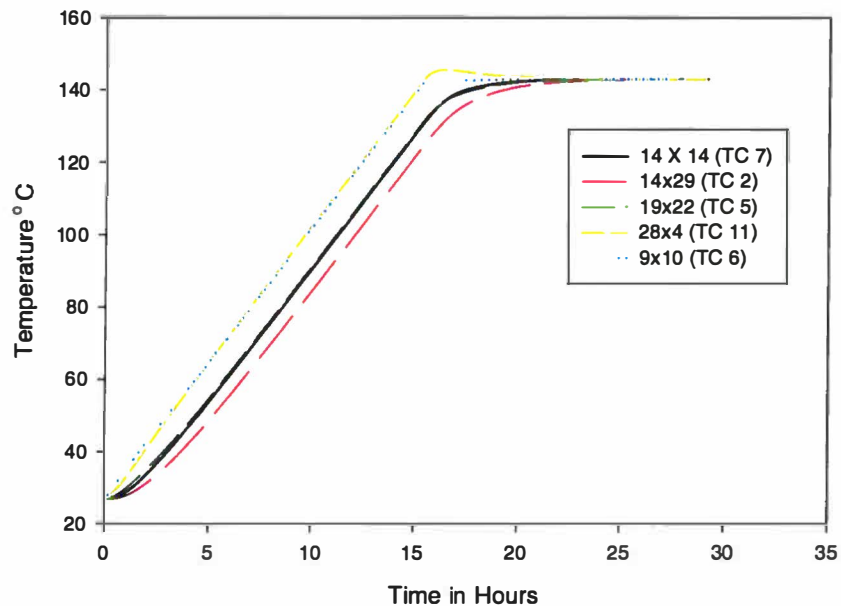


Figure 5.21. Temperature-Time Distribution for Adiabatic Conditions and Low Values for Soil Properties

The XY plot for the adiabatic case is made in Figure 5.21. Since there is no external heat loss a cooling phase does not exist. The temperature stabilizes between the maximum and minimum values and a uniform temperature distribution is achieved.

We now proceed to compare the temperature response with respect to time for the different settings of the soil properties. The temperature readings taken at various points in the grid (14 X 14, 14 X 29, 19 X 22, 28 X 4, 9 X 10) are averaged to give an average temperature distribution for each of the physical property settings. The grid points

correspond to the TC 7, TC 2, TC 5, TC 11, and TC 6 locations in Figure 4.2 (a). These points were chosen to obtain the temperature behavior at various locations in the box. Figure 5.22 shows this comparison. The maximum temperature is observed for the minimum setting of the soil properties. The lowest temperatures are observed for the maximum setting of the soil properties.

The gradient between the maximum and minimum temperatures increases as we move from maximum value of soil property to the minimum value of soil property. Thermal diffusivity is the driving force in our model, and its magnitude affects the outcome of the final temperature. For the adiabatic runs, the final temperature settles to a value between the maximum and minimum temperatures for all the three settings. It was

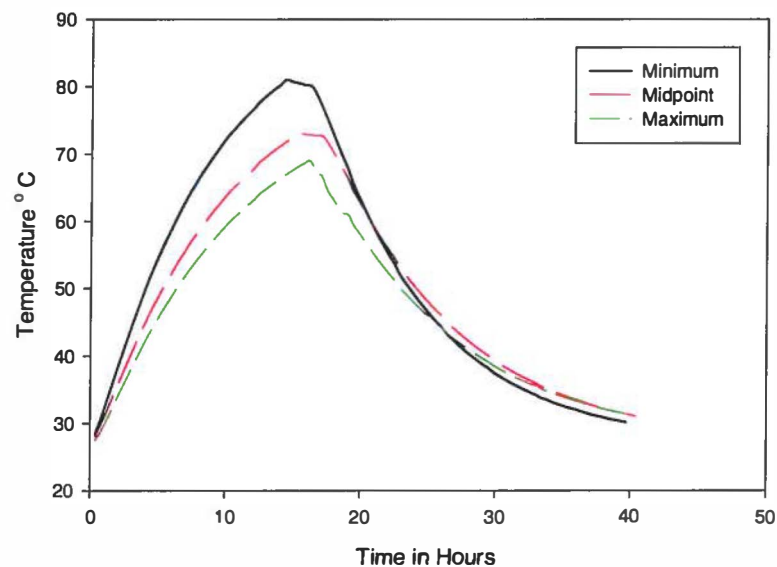


Figure 5.22. Comparison of Temperature Profiles for Low, Midpoint and Maximum Values of Soil Properties

inferred from the adiabatic and non-adiabatic runs that the numerical model was able to sufficiently reproduce natural phenomena.

5.6.4 Defining Density as a Function of Temperature

In all the above calculations for the single-phase, density of the dispersed medium (water) was assumed constant. It would be an interesting exercise to solve for the temperature profile with a temperature dependent density function. A linear equation for the temperature dependence was input using FLUENT. This equation was obtained by linear curve fitting the density values of liquid water in the temperature range 0 °C to 120 °C (McCabe and Smith, 1993). The temperature dependence equation used was of the form $\rho(T) = 1.009 \times 10^3 - 0.5921 T$. Both adiabatic and non-adiabatic simulations were carried out for the minimum and midpoint values of soil properties, respectively. The non-adiabatic simulations were compared for constant density and temperature dependent density at grid point 14 x 14 (Figure 5.23). It can be observed that the constant density curve shows a higher temperature response compared to the temperature dependent density curve. Thus, the constant density assumption overpredicts the temperature values as seen in Figure 5.23. The complexity of the calculations increases with the addition of the temperature dependent density function. To avoid problems with the convergence of the solution, constant density assumption has been made in the rest of the single-phase calculations.

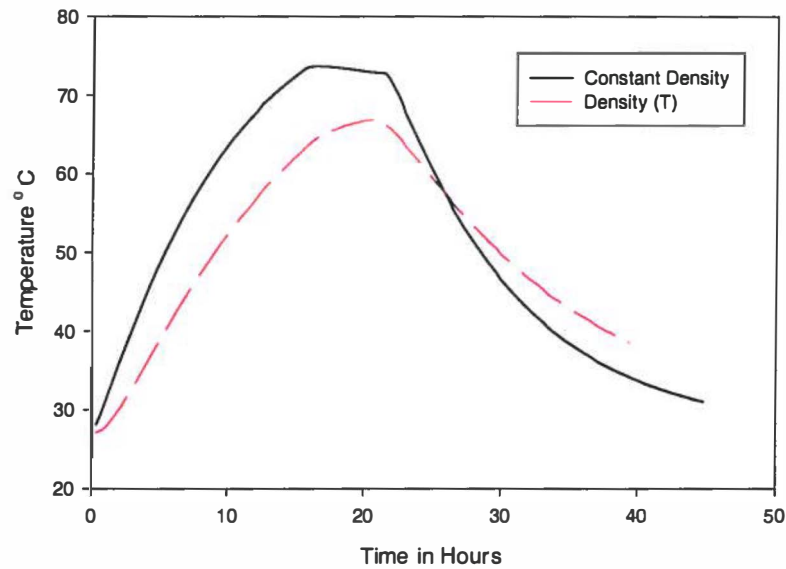


Figure 5.23. Comparison Between Constant Density and Temperature Dependent Density Simulation for Non-Adiabatic Case and Midpoint Values of Soil Properties at Grid Point 14 x 14

The adiabatic single-phase simulations were conducted for constant density and temperature dependent density at the grid point 14 x 14 for the minimum value of soil properties. The results of this simulation are presented in Figure 5.24. For the temperature dependent density curve, the maximum temperature saturates around 100 °C. For the constant density curve the temperature rises even after the volumetric heat source was reduced to zero. This was because of the presence of very large temperature gradients in the grid.

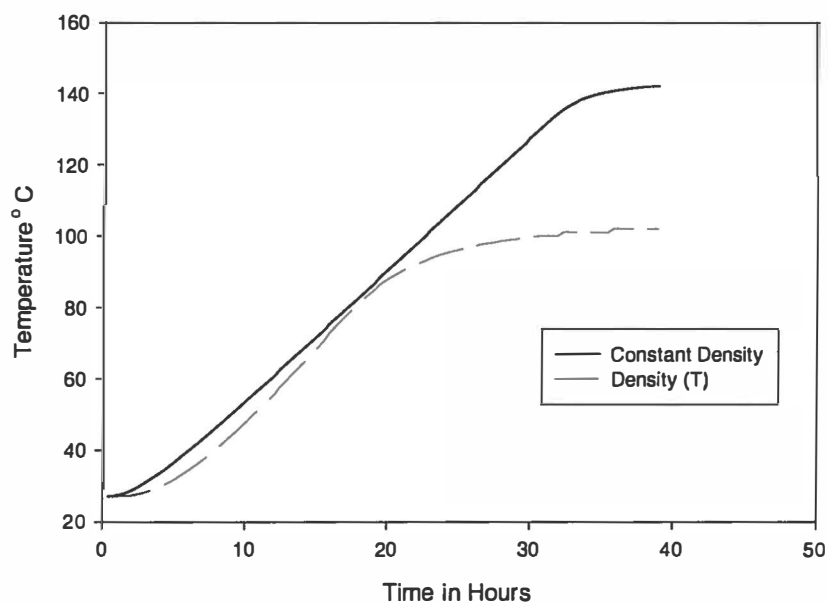


Figure 5.24. Comparison Between Constant Density and Temperature Dependent Density Simulation for an Adiabatic Case and Minimum Values of Soil Properties at Grid Point 14 x 14

5.7 Comparison of Experimental and Theoretical Results

Figures 5.25 and 5.26 compare the theoretical and experimental results for Runs 1 and 2, respectively. The theoretical curves for the maximum, midpoint, minimum values of soil properties are compared with the average temperature curves for boxes 1, 2 and 3. Under the given set of values for the simulation the theoretical curves take more time to reach temperatures around 100 °C compared to the experimental runs.

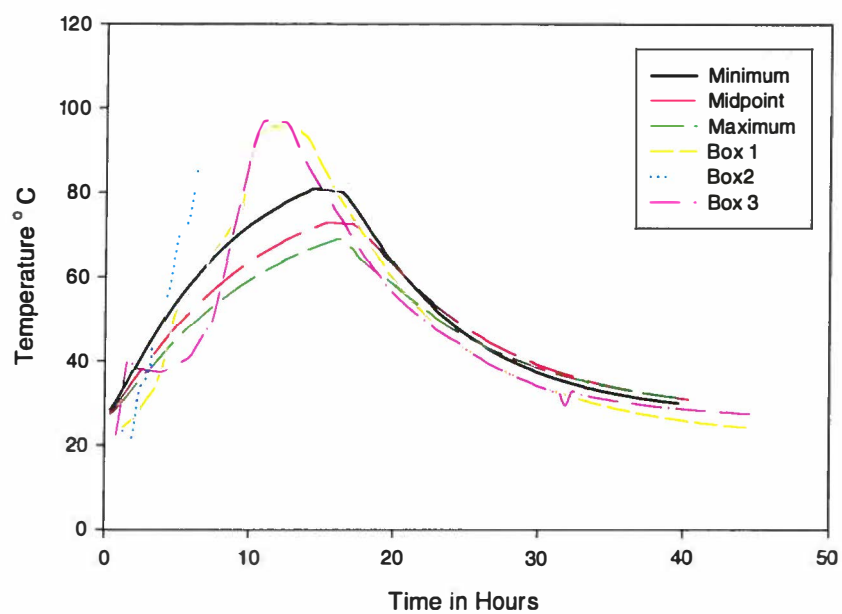


Figure 5.25. Comparison of Experimental and Theoretical Data for Run 1

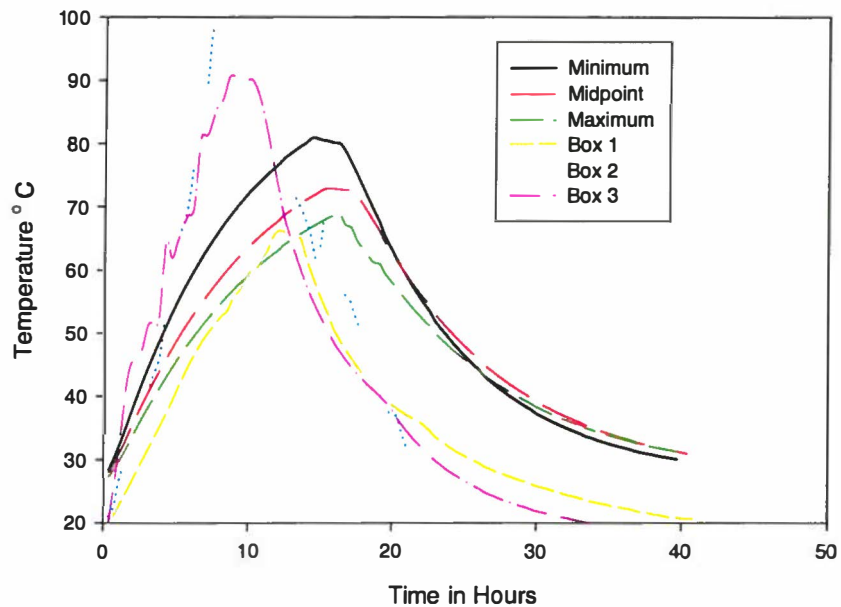


Figure 5.26. Comparison of Experimental and Theoretical Data for Run 2

The slope of the temperature curve obtained by simulations is a function of the volumetric heat generation. To match the theoretical and experimental curves the heat source was increased to a larger value (8000 W/m^3) in Figure 5.27. By such a modification the temperature curves obtained from FLUENT simulations can be made to match with that of the experimental curves.

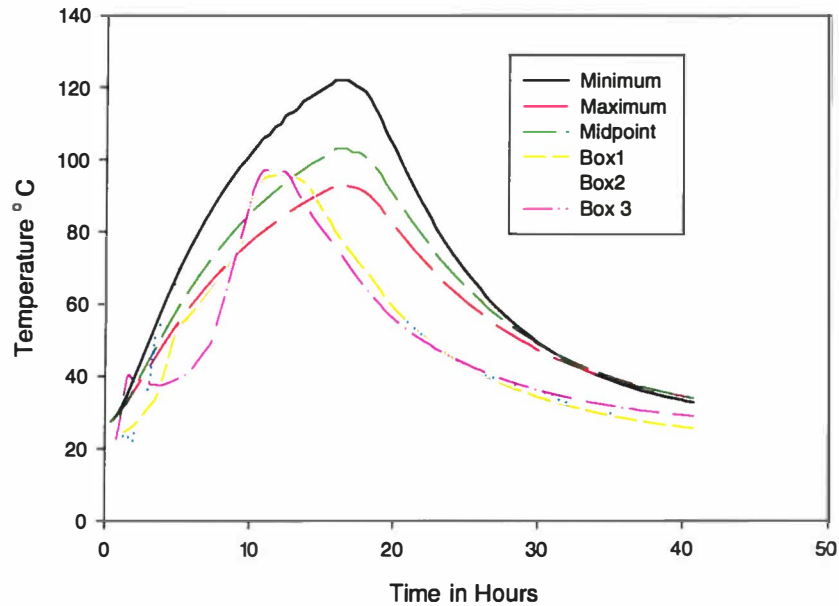


Figure 5.27. Effect of Increasing Volumetric Heat Generation on Experimental-Theoretical Temperature Comparison

5.8 Multiphase Simulations

In the single-phase model, the effect of water on the temperature distribution in porous media was neglected. However, as the temperature reaches around 100 °C, there will be significant phase transformation of water from the liquid phase to the vapor phase on heating and vice versa on cooling. To accommodate this phenomenon, multiphase simulations were studied. In the multiphase simulations, the Eulerian Multiphase model was activated. The grid for the multiphase problem was retained as 30 x 30 grid size as

in the single-phase model. Two phases, namely liquid (water) and vapor (water) were defined as the multiple phases. The porous medium properties were activated and the midpoint values of the soil properties were input. The porous medium does not participate in the phase change calculations. The Evaporation-Condensation module was activated with a saturation temperature of 373 K. Whenever the temperature of a cell reaches 373 K, this module would be activated in that cell to perform mass transfer calculations. The property values used for liquid and vapor have been summarized in Table 5.7. A volumetric heat source (6000 W/m^3) was patched in the live cells ($i=13-17$, $j=2-20$) similar to the approach in the single-phase calculations. The multigrid solver and the Line Gauss siedel methods were used to solve for the discretized equations. The under-relaxation of enthalpy and temperature was kept high to facilitate convergence of the solution.

Table 5.7. Physical Property Data for Multiphase Simulations

Property	Liquid	Vapor
Density (ρ)	1000 kg/m^3	0.5542 kg/m^3
Viscosity (μ)	$9 \times 10^{-4} \text{ kg/m-s}$	$1.34 \times 10^{-5} \text{ kg/m-s}$
Specific Heat (C_p)	4180 J/Kg-K	2014 J/kg-K
Thermal Conductivity (λ)	0.6 W/m-K	$2.61 \times 10^{-2} \text{ W/m-K}$

The multiphase problem with the data input for the multiple phases and the porous media becomes very difficult to solve, often leading to divergence of the solution. The calculations were time intensive often running into days before a sample solution was reached. Therefore, detailed grid size and time step sensitivity study could not be done

for the multiphase simulation. Based on a few trial runs, a grid size of 30 x 30 and a time step of 1 second were used. The focus of this section is to look at the multiphase behavior around 373 K. To simplify the problem, the symmetry of the grid was utilized. If the computational grid was divided into four rectangular quadrants, it was observed that all the four zones were symmetric. Hence, only one quadrant was used for the multiphase calculations. The grid dimensions were changed to 0.25 X 0.25 X 0.1 from the previous values of 0.5 x 0.5 x 0.1. Adiabatic boundary conditions were enforced on the wall cells (blue) and symmetry boundary condition on the remaining two sides (yellow). In the single-phase simulations the initial temperature of 300 K was used for all the calculations. To concentrate on the evaporation-condensation phenomenon and its effect on the temperature distribution in porous media, an initial temperature of 372 K was used in the multiphase calculations. A total of 3600 simulations were conducted for generating heating curves and 1000 iterations were used to generate the cooling patterns.

Temperature contours obtained for the multiphase model are shown in Figures 5.28 and 5.29. Figure 5.28 presents the progress of the solution and this contour shows a developing temperature profile. Figure 5.29 depicts the temperature contour after the heating phase is completed. It can be inferred that the temperature profile matches the contour generated for the single-phase model when the figure is extended over the entire grid.

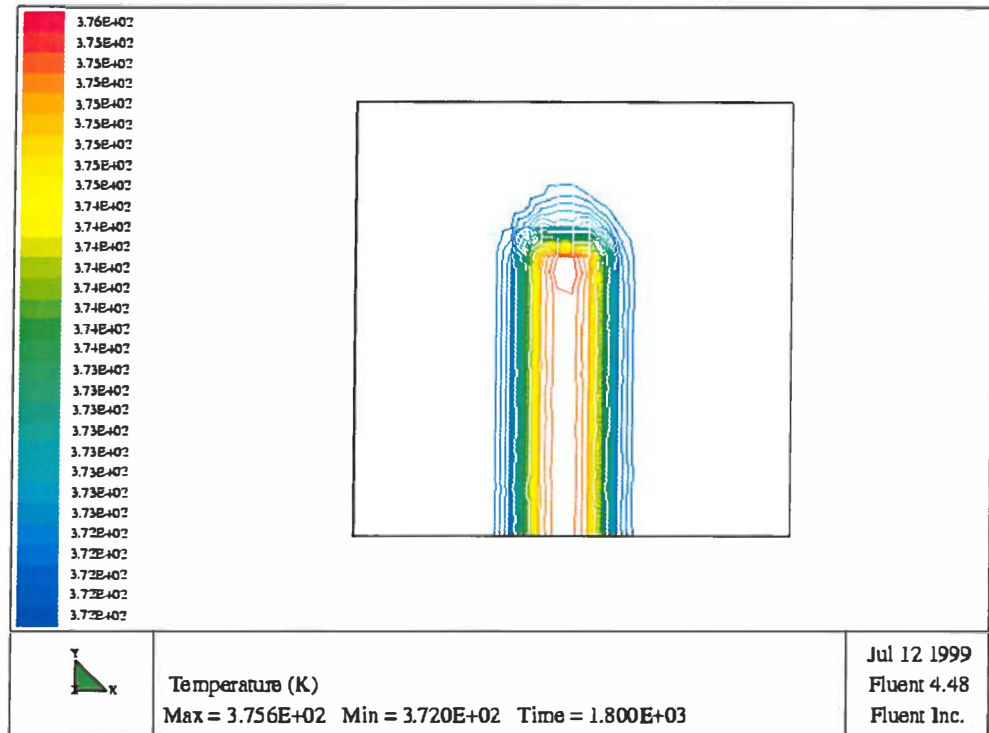


Figure 5.28. Temperature Contour Developing During the Heating Phase for an Adiabatic Multiphase Simulation

The temperature contour shows a maximum value of 400.25 K near the heat source and a minimum value of 372.13 K near the top of the grid. Between these regions there exists layers of constant temperature. Since we reached temperatures above 100 °C at 3600 iterations, the heat source was turned off and cooling phase was allowed to commence. This was done by deactivating the patched value of the volumetric heat generation in the grid. On cooling the temperature equilibrated at 372 K, which was the starting point of the simulation.

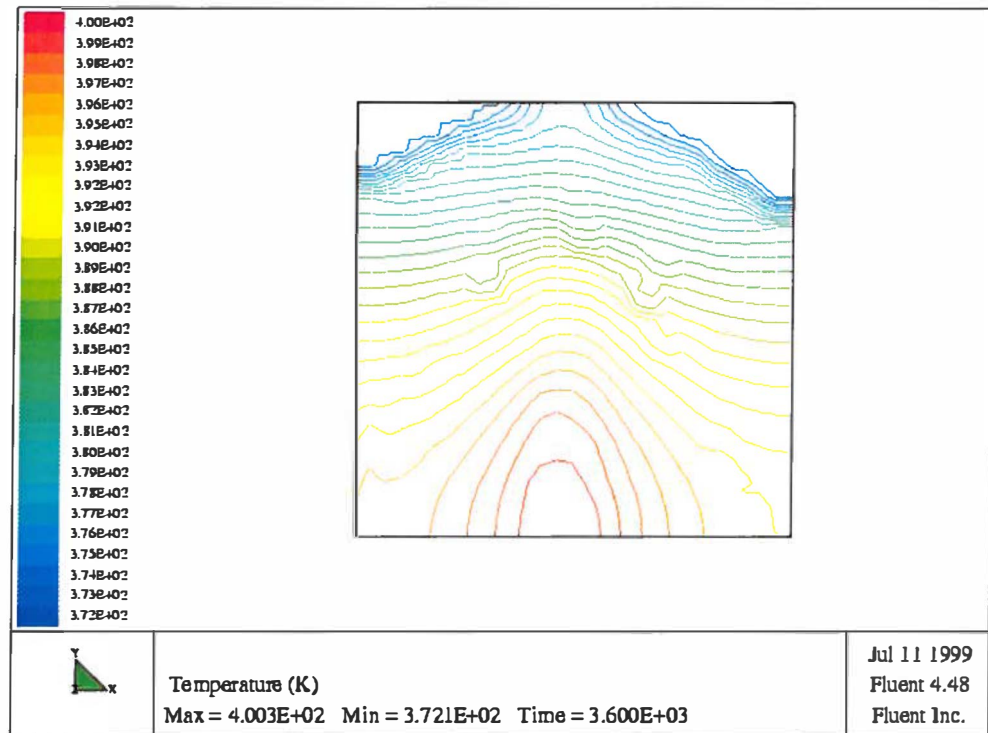


Figure 5.29. Temperature Contour After Completion of Heating Phase in Multiphase Simulation Under Adiabatic Conditions

The liquid volume fraction was also monitored during the heating and cooling stages of the multiphase simulation. Figure 5.30 shows a plot of the liquid volume fraction as soon as heating is started. It can be seen that vapor formation is observed near the heat source. The liquid volume fraction near the electrode is at a minimum value of 1.1×10^{-7} . In vapor volume fraction contour the maximum volume fraction will be located near the heat source consistent with the volume fraction theory.

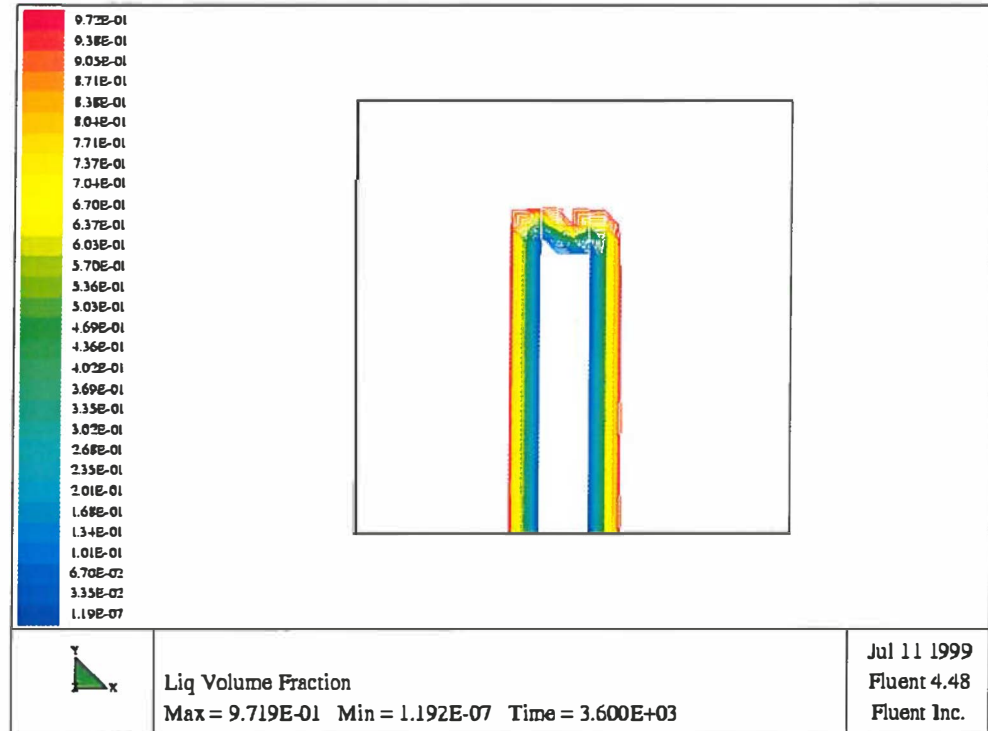


Figure 5.30. Liquid Volume Fraction at the Start of the Heating Phase

Figure 5.31 shows the liquid volume fraction after cooling. As the heating is completed, most of the liquid is driven into the vapor phase. On cooling, the temperature of the grid starts to decrease and the condensation of vapor begins. This is demonstrated in Figure 5.32 where on condensation the droplets contribute to the liquid volume fraction at the top of the grid (red). The rest of the grid is vapor (blue) with volume fractions as high as 0.9.

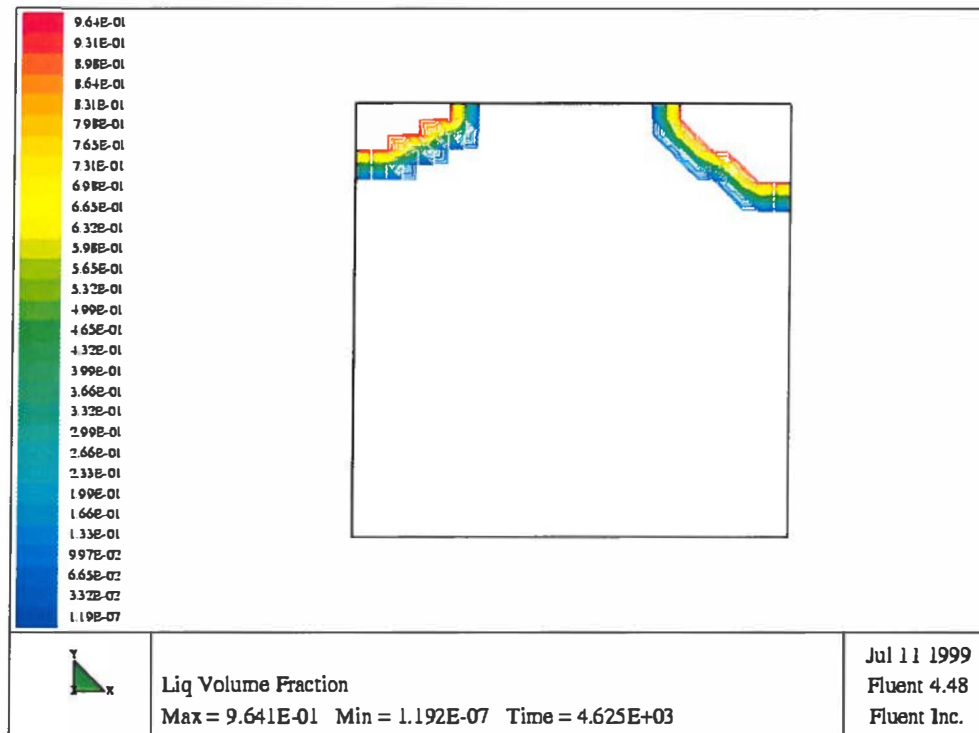


Figure 5.31. Liquid Volume Fraction at the End of the Cooling Phase

One of the important aspects of the multiphase model was to track the velocities of the liquid and vapor during the period when evaporation/condensation phenomena were active. Figures 5.32-34 present the velocity profiles of the liquid during different stages of the heating and cooling. Figure 5.32 shows an intermediate velocity profile during the heating phase. Due to the heat source, the region where the electrode was patched (cells $i=13-17$, $j=2-20$) was devoid of liquid water and the liquid velocities in this region were zero. As the heating progressed, this region expanded (Figure 5.33), and the liquid was limited to the top of the grid. If the vapor velocities were presented, it would

have appeared as an exact opposite of the liquid velocity contours. Most of the vapor movement activity would have been concentrated near the heat source and smaller velocities would have been shown at the top of the grid.

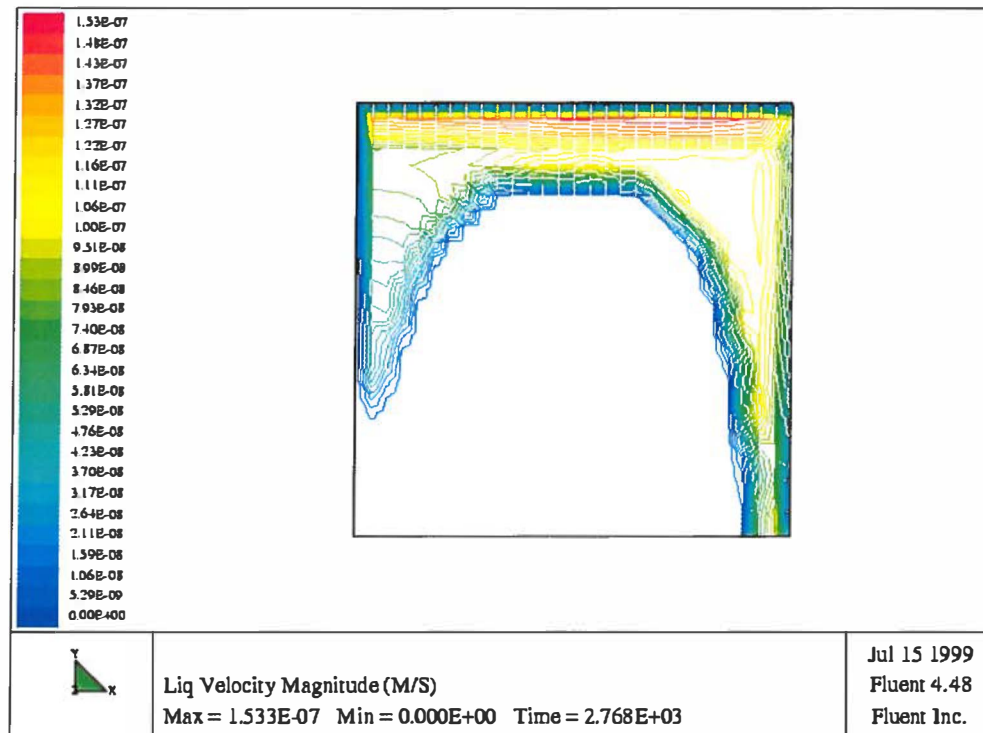


Figure 5.32. Velocity Profile During Heating for Multiphase Simulation

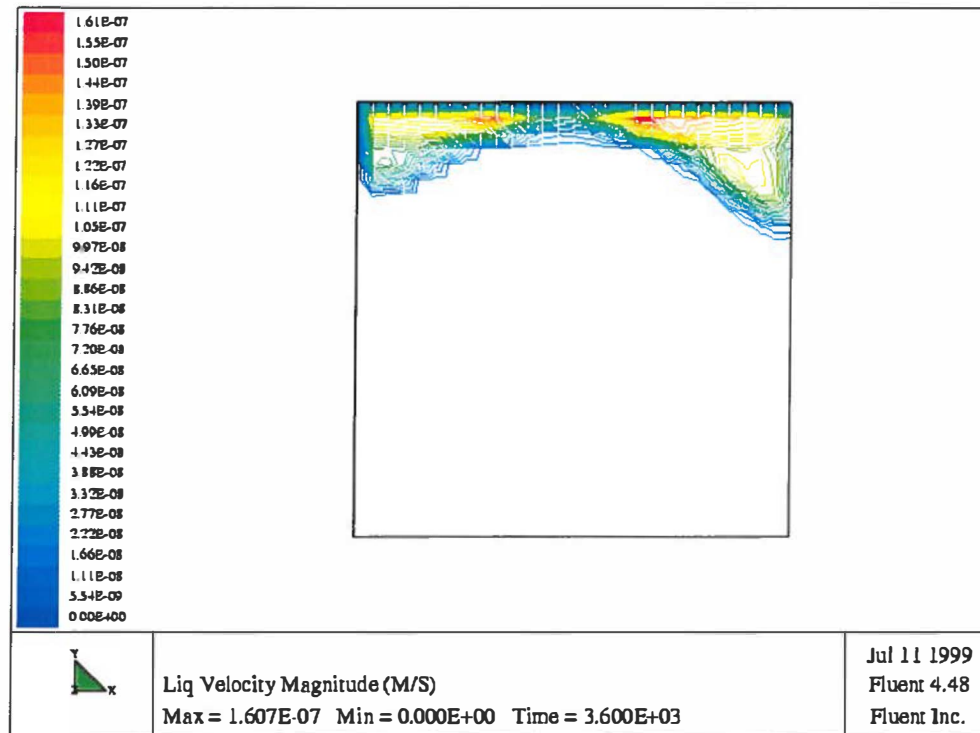


Figure 5.33. Liquid Velocity Profile at the End of the Heating Regime in Multiphase Simulation

Figure 5.34 shows the liquid velocities at the end of the cooling phase. This contour shows that the liquid velocities are now restricted to the corners at the top of the grid. However, the grid has not sufficiently cooled to produce the condensation of the vapor. The simulation would have to be run for an extended period of time to catch the reemergence of the liquid velocities. One of the important drawbacks of the multiphase model is the absence of an explicit expression of force balance. The vapor tends to move from high temperature to low temperature as well as move from high toward low moisture concentration. Thus, the phenomenon that non-uniform pressure accelerates a

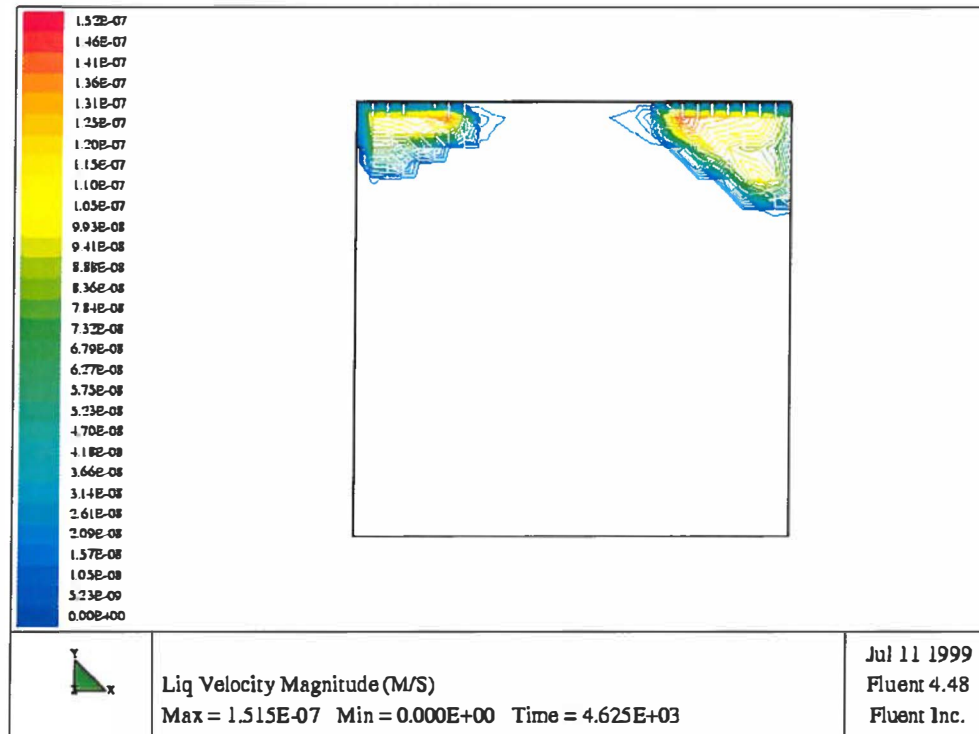


Figure 5.34. Liquid Velocity Magnitude at the End of the Cooling Phase for the Multiphase Simulation

fluid toward lower pressure is omitted, so water vapor has no buoyancy or tendency to rise. Conditions under which the neglect of buoyancy is valid need to be established.

One of the objectives of this study was to compare the temperature profiles generated by the single-phase and multiphase models and compare them alongside the experimental temperature-time data. However, the multiphase model available in FLUENT could not be adapted in such a way to generate temperature curves for the heating, stagnation and cooling phases. The temperature profiles were generated only for

the region where the evaporation-condensation aspects could be studied. To compare the single-phase and multiphase results it is important that both these models be run under the same set of parameters and conditions. Therefore, the single-phase calculations were redone with the symmetry boundary condition, a reduced time step of 1 second, and adiabatic conditions. The temperature contour obtained is presented in Figure 5.35. It can be seen that the temperature contour obtained for both the models resemble one another. To study the temperature variation with respect to time at a specific location in the grid, two-dimensional plots were generated for both the models. Figure 5.36 compares the time history at the grid location 15 x 21 (the cell directly above the region where volumetric heat is generated).

It is interesting to observe that the temperature curve predicted by the multiphase model is not smooth as the curves predicted by the single-phase models. In fact, the purpose of the multiphase calculations was to identify such behavior around the saturation temperature of water (373 K). The temperature presented in Figure 5.36 is a composite of the porous media, liquid and vapor temperatures taken at grid point 15 x 21. Therefore, the variation in this temperature curve is dependent on the concentration of liquid and vapor at a particular time assuming that there is no change in the volume of the porous media. As the temperatures reach 373 K, the evaporation-condensation module is activated and there is a transformation of the liquid to vapor. The heat capacity of vapor is smaller than the liquid and hence it takes less energy to heat the vapor to higher temperatures. This explains the peaks in the figure. Accompanied by this phenomenon is the flow of liquid to other parts in the grid and the large heat of vaporization requires

extra heat energy. Hence, more energy is expended at heating the liquid and consequently the temperature drops. The experimental results presented earlier in the chapter also showed these peaks and that proves that our model is able to identify with the physics of the problem.

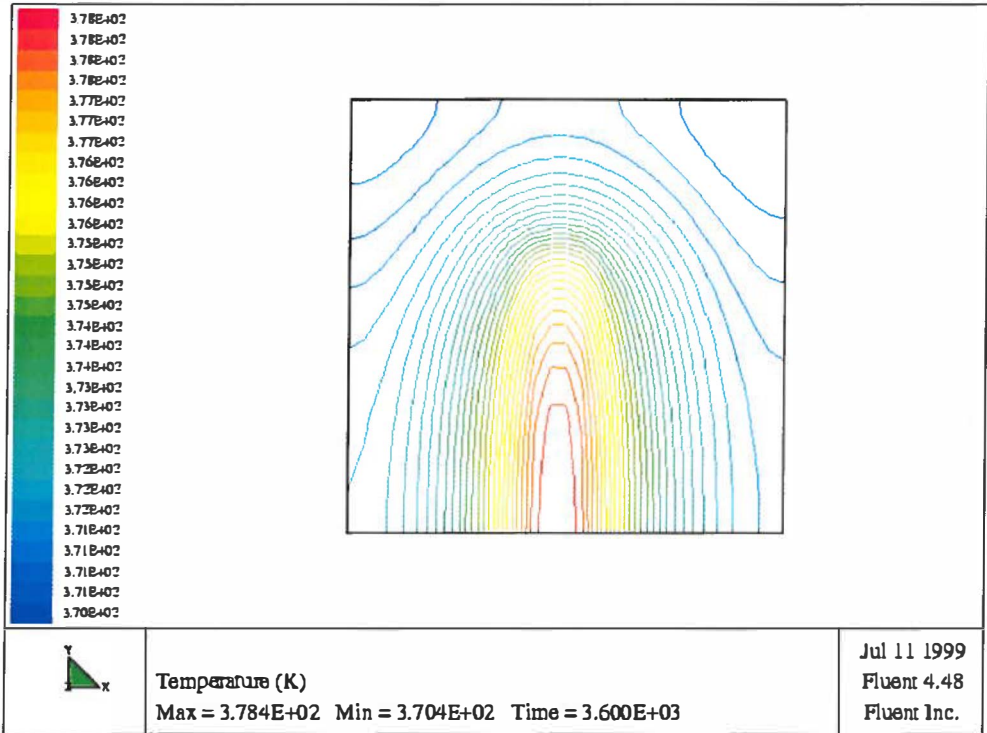


Figure 5.35. Single-Phase Temperature Contour Generated with the Symmetry Condition

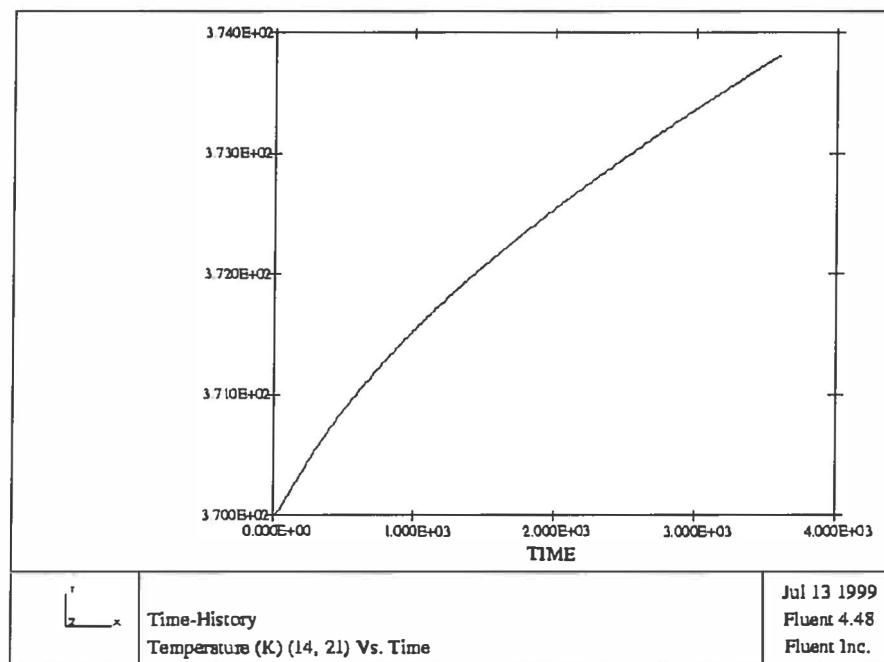
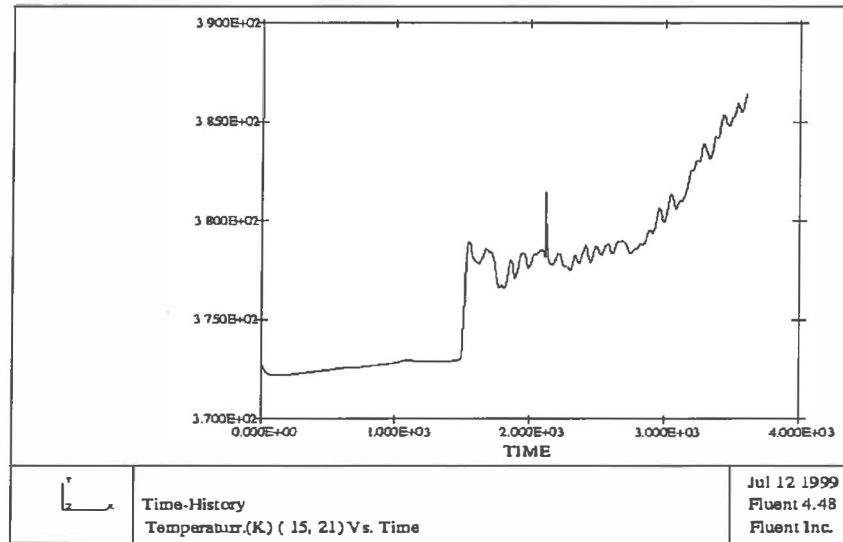


Figure 5.36. Comparison of Multiphase (top) and Single-Phase (bottom) Temperature Profiles Around Saturation Temperature

CHAPTER 6

CONCLUSIONS

The following conclusions were reached from the lab-scale heating experiments and the FLUENT modeling of temperature behavior in porous media:

1. Resistive heating at temperatures between 60 °C and 100 °C affects the microbial community by causing a decrease in population or microbial activity. This was exhibited in both the oven heating experiments and the resistive heating experiments. Microbial counts as high as 9,152 microorganisms/g (AODC) pre-heating were reduced to no detectable counts after the heating event.
2. When ambient temperatures return to normal after a heating event, and given some time, small-scale population recovery can occur. In the resistive heating experiments, after a period of 1 week, population recovery began, but counts did not reach those of the pre-heating samples.
3. Amending heated soils with nutrients will aid in microbial population recovery. The nutrients that were added affected the community structure of the soil. Actinomycete type bacteria and Gram-negative bacteria utilized the organic nutrients. Eukaryotic organisms preferred the inorganic nutrients. Gram-positive bacteria were able to withstand the environmental stress and were able to recover in number with the addition of water.

4. The temperature profile modeling results indicated that by using typical soil properties and values of the convective heat transfer coefficient, good agreement could be reached between the experimental and theoretical temperature profiles.
5. Better agreement between the experimental and theoretical temperature profiles is obtained by allowing the density to vary with temperature.
6. Multiphase effects need to also be incorporated into the model as the temperature approaches 100 °C.

CHAPTER 7

RECOMMENDATIONS

Based on the experiments and modeling studies conducted, it is recommended that this work be continued as suggested in this section:

1. An assumption made in all model runs was that the soil and fluid properties other than density were constant in the temperature range of interest. The extension to the study would be a case in which the soil and fluid properties of thermal conductivity, specific heat, and porosity are made temperature dependent.
2. A multiphase model involves allocating memory for each additional phase and this leads to instances of stack overflow, which was traced back to a computer memory problem. Hence, to accommodate multiphase simulations it is desirable to have a computer with greater memory.
3. The species transport model of FLUENT can be used to model the movement of a contaminant during resistive heating. An overall mass balance can be studied under these circumstances to calculate the concentration of the species in different phases.
4. The entire mathematical modeling results presented in this thesis looked at two-dimensional models only. In the field, three-dimensional models will be useful. To understand this aspect, the models should be extended to include all three dimensions.

5. Soil moisture determines the flow of electricity during resistive heating. Therefore, to get consistent heating trends in all the boxes it is important that the soil moisture be uniformly distributed throughout the soil. More samples should be analyzed to get more accurate estimates of the moisture distribution in the boxes.
6. Observing the results of the laboratory scale resistive heating experiments over a longer period of time may provide results more meaningful for in-situ applications.
7. Microbial enumeration assays used for these experiments include CFU analysis, AODC, MPN assays, and PLFA analysis. For future experiments, it is not necessary to use all of these techniques. MPN assays are very time consuming, expensive, and require licensing to use the radiolabeled substrate. They also provide results comparable to AODC. With AODC analysis, it is critical that all dilution blanks, stain solutions, and equipment be particle free since the technique does not differentiate between particles present in samples and those present in contaminants. Low levels of contamination can result in large errors in counts. CFU analysis is also sensitive to contamination, but this can be overcome by following the normal laboratory techniques for maintaining sterility. PLFA analysis tells us the most about our samples. It goes beyond enumeration to identify the types of microorganisms present, as well as damage done to these cells due to environmental stress. For future microbial analysis, more meaningful results can be obtained using PLFA and either CFU or AODC analysis.

REFERENCES

- Alef, K. Methods in Applied Soil Microbiology and Biochemistry, Boston, 124-126, 1995.
- Aston, A.R., and A.M. Gill. 1976. Coupled soil moisture, heat and water vapor transfers under simulated fire conditions. *Australian Journal of Soil Research*. 14:55-66.
- Atlas, R. M., Horowitz, A., M. Krichevsky, and A. K. Bej. Response of Microbial Populations to Environmental Disturbance. *Microbial Ecology*, vol. 22:249-256, 1991.
- Balkwill, D.L, F.R. Leach, J.T. Wilson, J.F. McNabb, and D.C. White. 1988. Equivalence of Microbial Biomass Measures based on Membrane Lipid and Cell Wall Components, Adenosine Triphosphate, and Direct Counts in Subsurface Aquifer Sediments. *Microbial Ecology*: 16: 73-84.
- Batchelor, G.K. 1967. An Introduction to Fluid Dynamics, Cambridge Univ. Press, Cambridge, England.
- Bergsmann T.M., L.M. Peurrung. 1997. Six phase soil heating of the saturated zone. Application Analysis Report. Dover Airforce Base, Delaware.
- Bergsmann T.M., and B. Trowbridge. 1997. Soil Vapor Extraction to the sixth degree: Six phase Soil Heating takes SVE to the next level. Soil and Ground water cleanup. July: 6-11.
- Bergsmann T.M., J.S. Roberts, and M.H. Shlender. 1993. Soil Heating Technology shown to accelerate the removal of volatile organic compounds from clay soils. *Federal Facilities Environ. Journal*. Winter: 69-79.
- Bird, R.B, W.E. Stewart and E.N. Lightfoot. 1960. Transport Phenomena, Chapter 6, John Wiley and Sons, New York, pp. 180-207.
- Campbell, G.S.; J.D. Jungbauer, K.L. Bristow and R.D. Hungerford. 1995. Soil temperature and water content beneath a surface fire. *Soil Science*. 159(6): 363-374.
- Carmichael, L.M. and F.K. Pfander. The Effect of Inorganic and Organic supplements on the Microbial Degradation of Phenanthrene and Pyrene in Soils. *Biodegradation*, vol. 8: 1-13, 1997.

Carmichael, L., Powell, R., Jayaraman, V., Schimmel, K., "Lab-Scale Resistive Heating Effect on Soil Microbial Communities," In *In Situ Bioremediation of Petroleum Hydrocarbon and Other Organic Compounds* (B.C. Alleman and A. Leeson, eds.), Battelle Press, 1999.

Chambers, D.P., and P.M. Attiwill. 1994, The ash-bed effect in eucalyptus regnans forest: chemical, physical and microbiological changes in soil after heating or partial sterilization. *Australian Journal of Botany*. 42: 739-749.

Chapelle F.H. 1993. Ground Water microbiology and Geochemistry. John Wiley and Sons, New York.

Corapcioglu, M.Y., and A. Haridas. 1984. Transport and fate of microorganisms in porous media: a theoretical investigation. *J. Hydrology*. 72:149-169.

De Vries, D.A. 1958. Simultaneous transfer of heat and moisture in porous media. *Transactions of the American Geophysical Union*. 39:909-916.

Diaz-Ravina, P., Angeles, and E. Baath. Bacterial Activity in a Forest Soil After Soil Heating and Organic Amendments Measured By the Thymidine and Leucine Incorporation Techniques. *Soil Biology and Biochemistry*, vol. 28, No. 3: 419-426, , 1996.

Downey, D., and M.G. Elliot. 1990. Performance of selected in situ Soil Decontamination Technologies: An Airforce Perspective. *Environ. Progress*. Vol. 9, No: 3, 169-173.

Dunn, P.H., S.C. Barro and M. Poth. 1985. Soil moisture affects survival of microorganisms in heated chaparral soil. *Soil Biology and Biochemistry*. 17:143-148.

Dupont, R. R. 1993, Fundamentals of Bioventing applied to fuel contaminated sites. *Environmental Progress*. 12(1): 45-53.

Fernandez, I, A. Cabaneiro,. and T. Carballas. Organic Matter Changes Immediately After A Wildfire in an Atlantic Forest Soil And Comparison with Laboratory Soil Heating. *Soil Biology and Biochemistry*, vol 29: No. 1, 1-11, 1997.

Gauglitz, P.A., J.S.Roberts, T.M. Bergsman, , S.M. Caley, W.O. Heath, M.C. Miller, R.W. Moss, R. Schalla, M.H. Schlender, T.R. Jarosch, , C.A. Eddy-Dilek and B.B. Looney, *Field Test of Six-Phase Soil Heating at the Savannah River Site*. 1994, Pacific Northwest Laboratory, Richland, Washington.

Germann, P.F., M.S. Smith, and G.W. Thomas. 1987. Kinematic Wave approximation to the transport of E.coli in the vadose zone. *Water Resour. Res.* 23:1281-1287.

Hernon, G., M. Van Zutphen, T.H. Christensen, and C.G. Enfield. 1998. Soil Heating for Enhanced Remediation of Chlorinated Solvents: A laboratory study on Resistive Heating and vapor Extraction in a silty, Low-permeable soil contaminated with Trichloroethylene. *Environ. Sci. Technol.* 32,1474-1481.

Hungerford, R. D. 1990. Describing downward heat flow for predicting fire effects, Problem analysis, problem no: 1, addendum, 7/9/90. Fire effects: prescribed and wildfire. Missoula, MT. U.S.Department of Agriculture, Forest service, Intermountain research station, Intermountain Fire sciences laboratory.

Hurst, C. 1991. Modeling the Environmental Fate of Microorganisms. American Society of Microbiology, Washington D.C.

Joergensen R.G., P.C. Brookes, and D.S. Jenkinson. 1990, Survival of the soil microbial biomass at elevated temperatures. *Soil Biology and Biochemistry.* 22: 1129-1136.

Jumikis, A.R. 1966. Thermal Soil Mechanics. Rutgers University Press, New Brunswick, NJ.

Jury, W.A. 1973. Simultaneous transport of heat and moisture through a medium sand. Physics department: The university of Wisconsin. 191 p. Dissertation.

Kennedy, A.C. and K.L Smith. Soil Microbial Diversity and the Sustainability of Agricultural Soils. *Plant and Soil*, vol. 170: 75-86, 1995.

Khanna, P.K. and R.J. Raison. *Effect of Fire Intensity on Solution Chemistry of Surface Soil Under a Eucalyptus pauciflora Forest.* Division of Forest Research, SCIRO, P.O. Box 4008, Queen Victoria Tererace, A.C.T. 2600, 1983.

Kieft, T.L. , D.B. Ringelberg, and D.C. White. Changes in Ester-Linked Phospholipid Fatty Acid Profiles of Subsurface Bacteria During Starvation and Desiccation in a Porous Medium. *Applied and Environmental Microbiology:* 3292-3299, 1994.

Lee, W. H., " A pressure Iteration scheme for Two-Phase Modeling," LA-UR-79-975, Los Alamos Scientific Laboratory, Dept. of Energy, Contract W-7405-ENG-36, 1979.

Lehmicke, L.G., R.T. Williams and R.L Crawford. ¹⁴C Most Probable Number Methods for Enumeration of Active Heterotrophic Microorganisms in Natural Waters. *Applied Environmental Microbiology*, vol 38: 644-649, 1979.

McCabe, W., J.C. Smith, and P. Harriot. 1993. Unit Operations of Chemical Engineering, McGraw-Hill, Inc.

Mitchell, J.K. 1976. Fundamentals of Soil Behavior. Wiley, New York.

Narayanan, J.V., M.S.Ch.E., July 1999, Lab-Scale Modeling of the Effect of Resistive Heating Remediation Technologies on the Dynamics and Activity of Subsurface Microorganisms, North Carolina A&T State University, Greensboro, NC.

Narayanan, J.V., Schimmel, K., Powell, R., Carmichael, L., "Modeling of the Effect of Thermal In Situ Technologies on the Dynamics of Subsurface Microorganisms," In *Proceedings of the 1998 National Conference on Environmental Remediation Science and Technology* (G.A. Uzochukwu and G.B. Reddy, eds.), Battelle Press, 1998.

Nerpin, S.V., and A.F. Chudnovskii. 1975. Heat and Mass transfer in the Plant-soil-Air System. Gidrometeoizdat Publishers, Leningrad. Translated from Russian. Published for U.S Dept. of Agriculture by Amerind Publishing, New Delhi, 1984.

Patankar, S.V. 1980. Numerical Heat Transfer and Fluid Flow, Hemisphere Publishing Corp., Washington, DC.

Peric, M., R. Kessler, and G. Scheuerer. 1988. Comparison of Finite Volume Numerical methods with staggered and collocated grids. *Comput. Fluids*. V. 16(4), pp. 389-403.

Peter, S. J. 1992. Heat transfer in soils beneath a spreading fire. Department of chemical engineering, University of New Brunswick. 479 p. Dissertation.

Price, S.L., R.S. Kasevich, M.A. Johnson, D. Wiberg and M.C. Marley. Radio Frequency Heating for Soil Remediation. *Journal of Air and Waste Management Association*, vol 49: 136-145, 1999.

Powell-Jones, R., M.S.C.E., October 1999, Laboratory Scale Experiments to Determine the Effect of Resistive Heating on Soil Microbial Communities, North Carolina A&T State University, Greensboro, NC.

Ranz, W.E., and W.R. Marshal Jr. 1952. Evaporation from Drops, Part II, *Chem. Eng. Prog.* V: 48(4), pp. 173-180.

Richon, J.B. 1987. Heat Transfer in soils beneath a spreading fire. Department of Chemical Engineering. University of New Brunswick, Fredericton. (Citation after Steward, Peter and Richon 1990). Thesis.

Russell, N. J. and N. Fukunaga. A Comparison of Thermal Adaptation of Membrane Lipids in Psychrophilic and Thermophilic Bacteria. *FEMS Microbiology Reviews* 75:171-182, 1990.

Schroder, C. N. 1974. The development of an optimized computer simulation model for heat and moisture transfer in soil. Texas A&M university. 318 p. Dissertation.

Schwille, F. 1988, Dense chlorinated solvents in porous and fractured media: Model experiments. Lewis publishers. Chelsea, MI

Scotter, D.R. 1970, Soil temperatures under grass fires. *Australian journal of soil research*. 8: 273-279.

Smith, L.A., and R.E. Hinchee. 1993. In situ Thermal Technologies for site remediation. Lewis Publishers, Boca Raton.

Spalding, D.B. 1980 Numerical Computation of Multi-Phase Fluid flow and Heat transfer. Taylor, C., et al., eds., Recent Advances in Numerical Methods in Fluids, Pineridge Press, pp. 139-167.

Steward, F.R., S. Peter, J.B. Richon. 1990. A Method for predicting the depth of lethal heat penetration into mineral soils exposed to fires of various intensities. *Canadian Journal of Forest Research*. 20: 919-926.

Tu, C.M. 1982, Physical treatment and reinoculation of soil: effects on microorganisms and enzyme activities. *Soil biology and Biochemistry*. 14: 57-61.

White, D.C, H.C. Pinkart, and D.B. Ringelberg. 1997. Biomass measurements: Biochemical approaches. pp 91-101. In C.J. Hurst (ed.), Manual of Environmental Microbiology. ASM Press, Washington D.C.

Wilson, D. 1995. Modeling of in situ techniques for Treatment of Contaminated Soils, Soil vapor Extraction, Sparging and Bioventing. Technomic Publishing Company, Basel, Switzerland.

Zelles, L., P. Adrian, Q.Y. Bai, K. Stepper, M.V. Adrian, A.M. Fischer and A. Ziegler, Microbial Activity Measured In Soils Stored Under Different Temperature and Humidity Conditions. *Soil Biology and Biochemistry*, vol. 23, No. 10: 955-962, 1991.

Zogg, G. P., , D.R. Zak, D.B. Ringelberg, N.W. MacDonald, K. S. Pregitzer, and D.C. White. Compositional and Functional Shifts in Microbial Communities Due to Soil Warming. *Soil Science Society of America*, vol 61: 475-481, 1997.

APPENDIX

PLOTS OF PLFA ANALYSIS

This section summarizes the different plots obtained from the PLFA Analysis. Figures A.1-A.6 represent the dynamics of the microbial community after resistive heating and nutrient addition. Mid-chain branched PLFA, indicative of Actinomycete bacteria, showed (Box 1) a similar level to the initial sample and lower levels in Boxes 2 and 3 (see Figure A.1). Polyunsaturated PLFA are indicative of eukaryotic organisms. This part of the microbial community was able to use substrate added in Box 2 (inorganic nutrient) more efficiently than the rest of the community.

Terminally Branched Fatty acids, indicative of Gram positive bacteria, showed an increase from initial soil sample to Box 3 (Figure A.3). Since Gram positive bacteria are resistant to environmental factors, we can conclude that microbes in Box 3 had high resistance to heat and were able to repopulate faster on nutrient addition. Gram negative bacteria are generally faster growing bacteria and take advantage of the added nutrients first. Box 1 shows higher counts of Gram negative bacteria, indicating that Gram negative bacteria prefer organic nutrient medium for their repopulation.

Two measures for nutritional status for the gram-negative community were used. The first (Cy 17:0/16:1 ω 7C) as seen in Figure A.5 showed lowest turnover from Box 1 to highest turnover for Box 3 for that portion of the gram negative community. The other measure of gram negative turnover was Cy 19:0/18:1 ω 7C (Figure A.6). Boxes 1 and 2 showed higher turnover than Box 3 for that portion of the gram negative community.

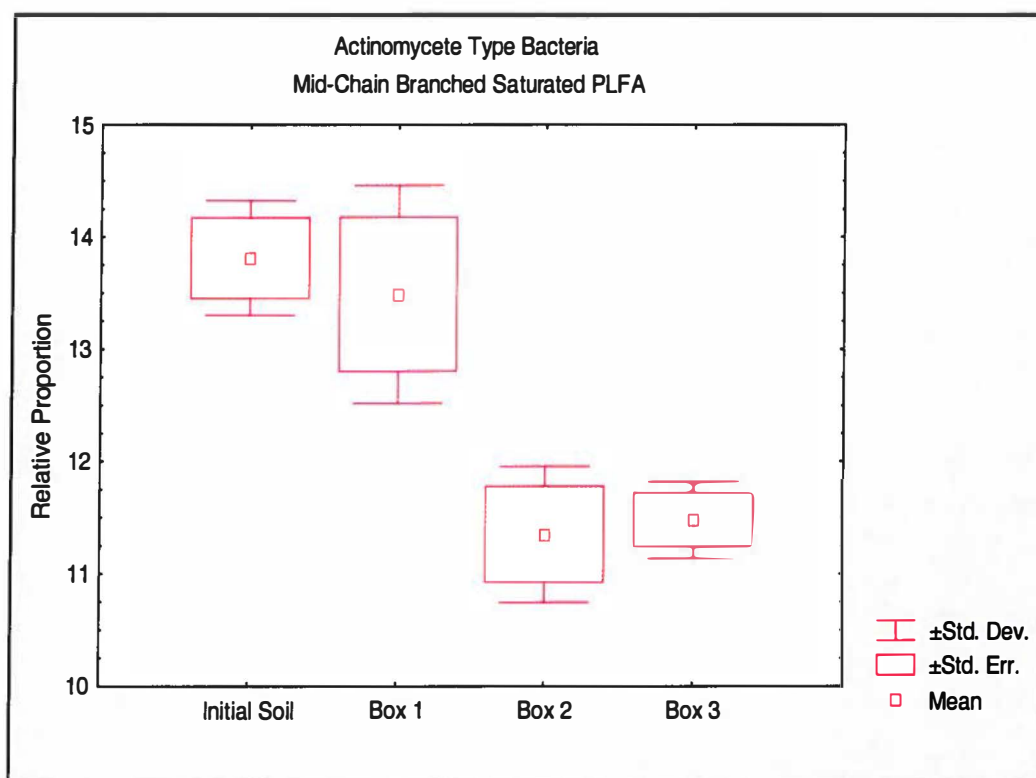


Figure A.1. Relative Proportion of Actinomycete Bacteria After Resistive Heating and Nutrient Addition

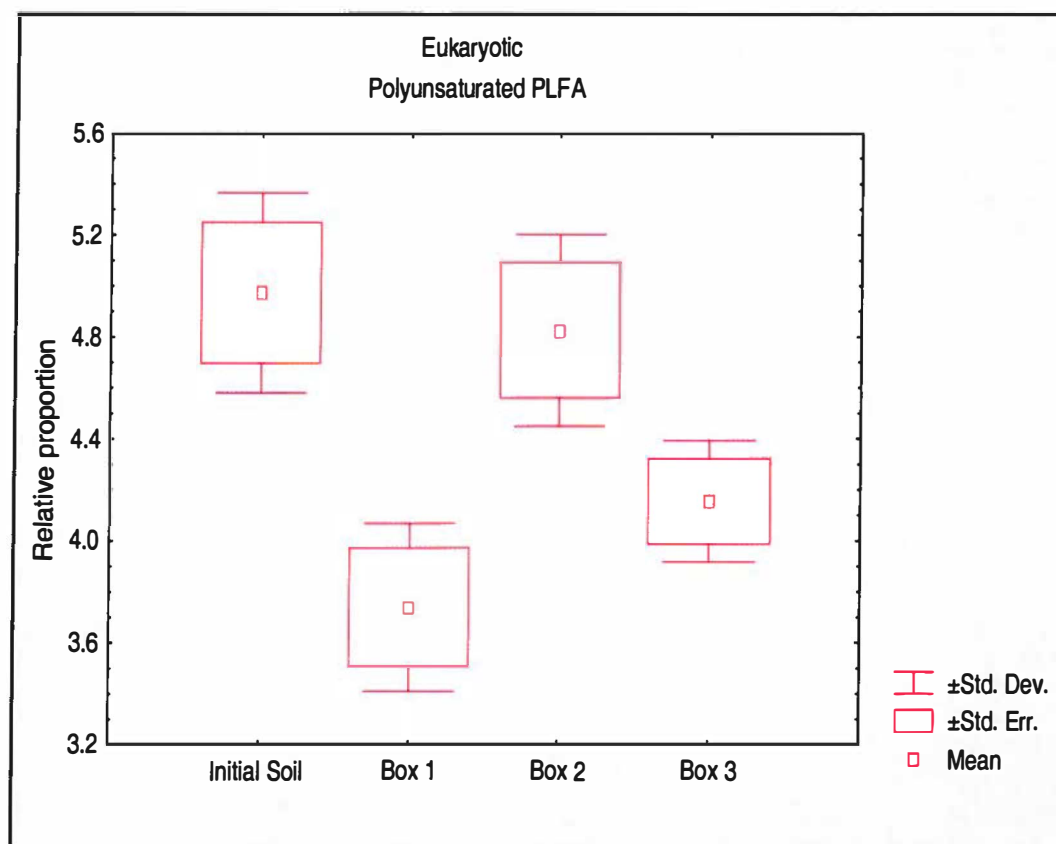


Figure A.2. Relative Proportion of Eukaryotic Organisms After Resistive Heating and Nutrient Addition

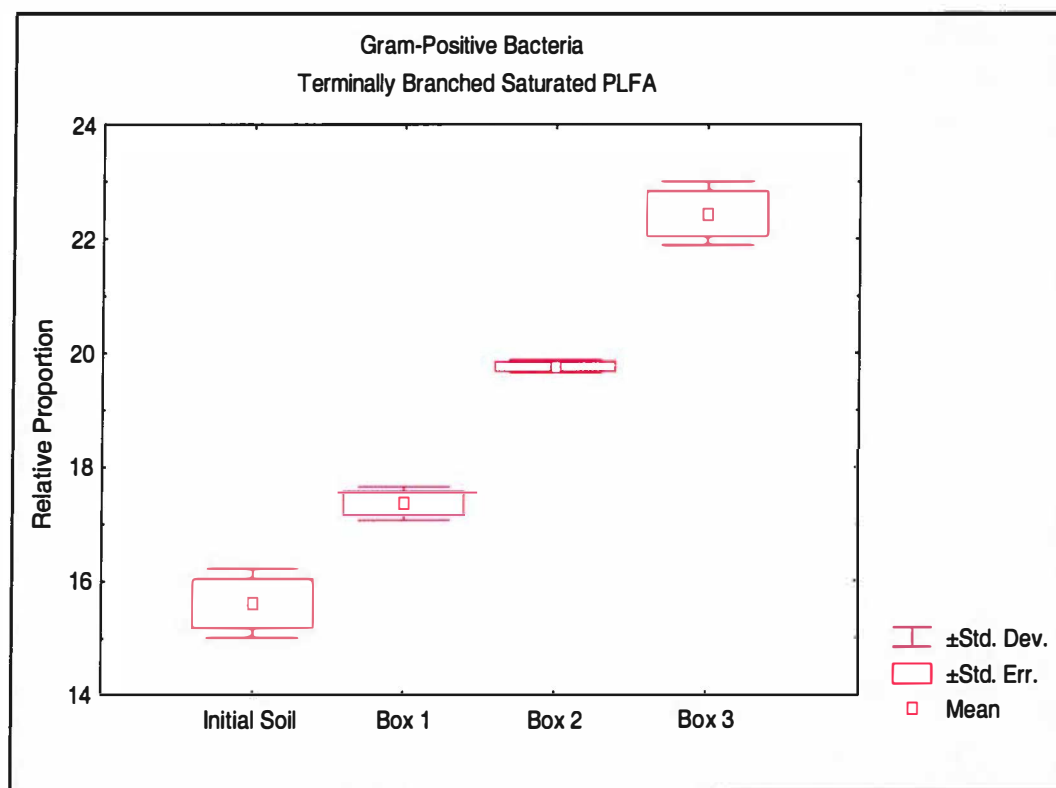


Figure A.3. Relative Proportion of Gram Positive Bacteria After Resistive Heating and Nutrient Addition

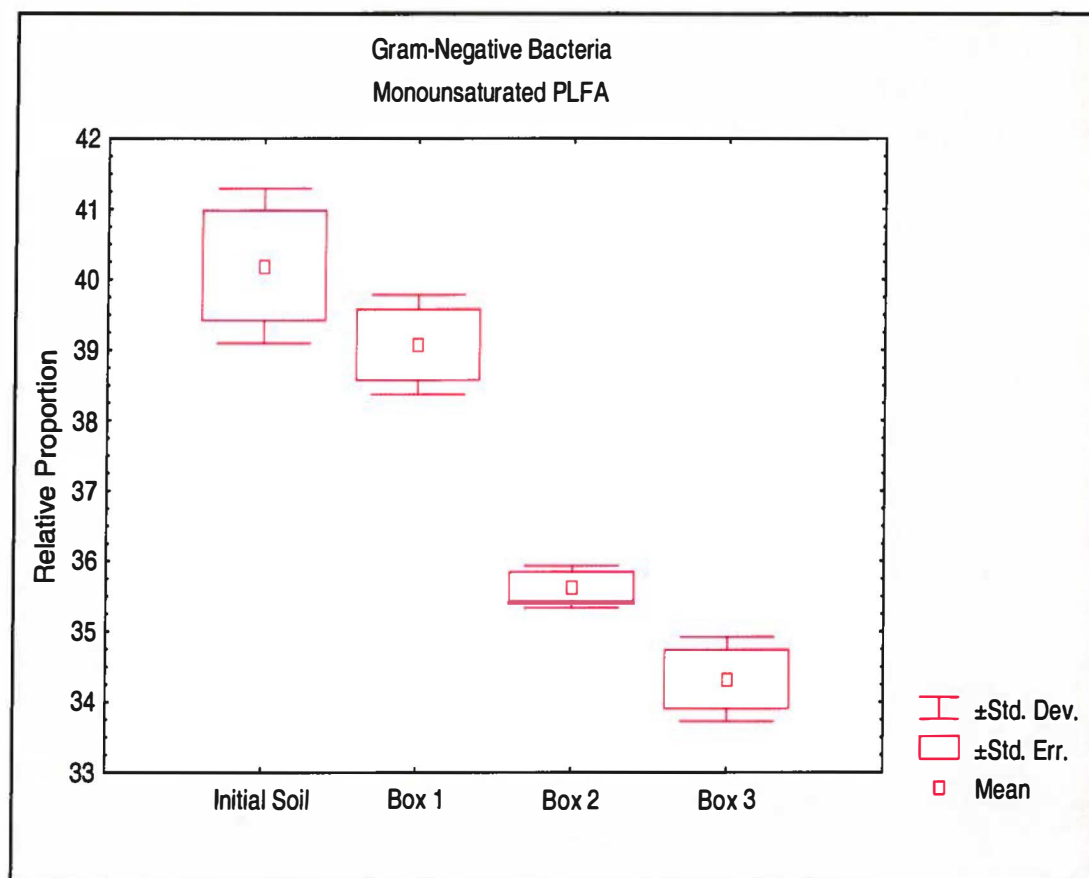


Figure A.4. Relative Proportion of Gram Negative Bacteria After Resistive Heating and Nutrient Addition

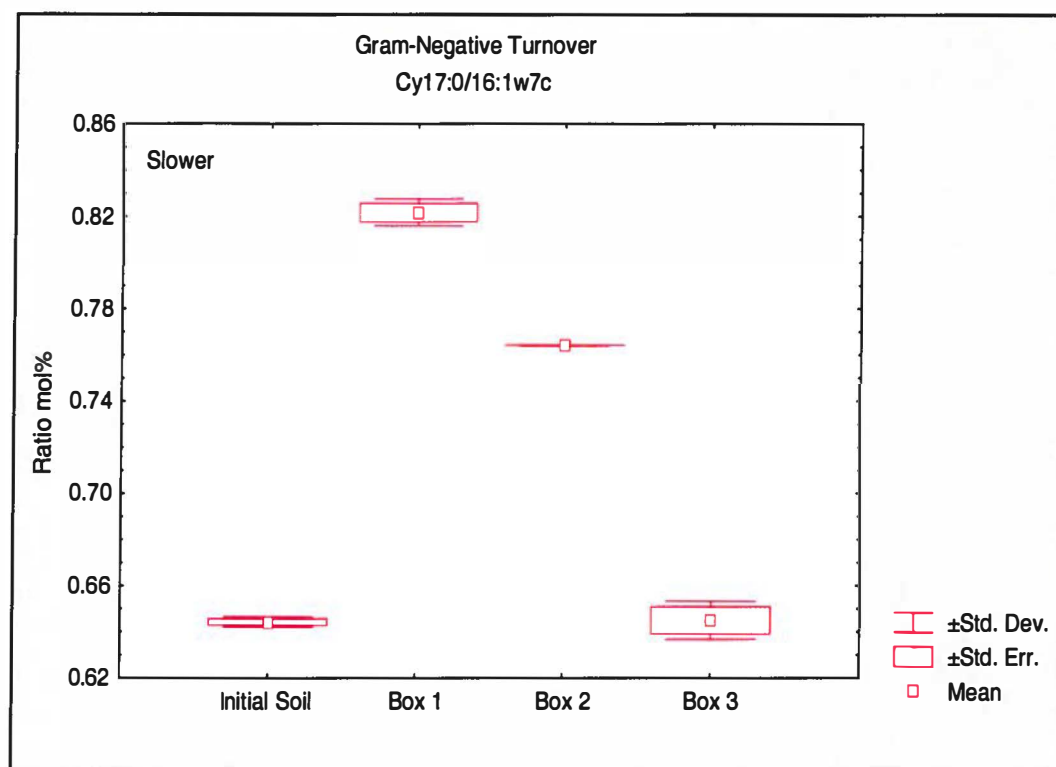


Figure A.5. Cy 17:0/ 16:1 w 7c Turnover in Gram Negative Bacteria After Resistive Heating and Nutrient Addition

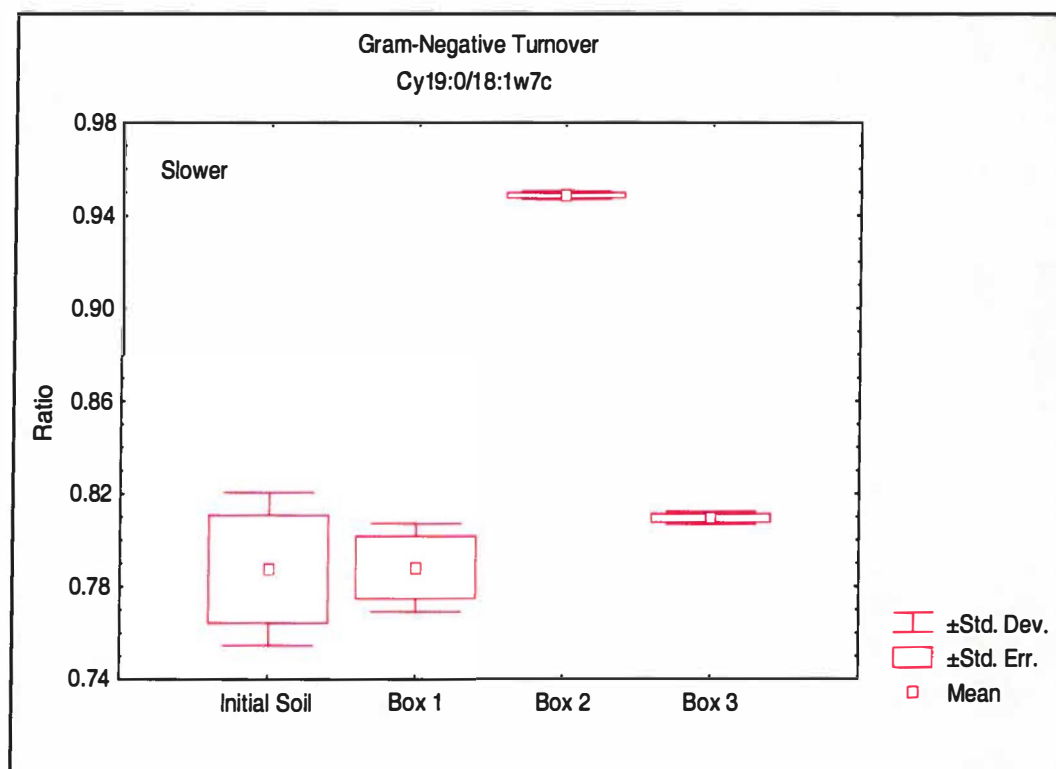


Figure A.6. Cy 19:0/ 18:1 w 7c Turnover in Gram Negative Bacteria After Resistive Heating and Nutrient Addition